AN INVESTIGATION OF THE KEROGEN-MINERAL INTERACTIONS

IN GREEN RIVER OIL SHALE

A Thesis
Submitted to the Graduate Faculty
of the
North Dakota State University
of Agriculture and Applied Science

By

Kristin Nadiene Alstadt

In Partial Fulfillment of the Requirements
for the Degree of
MASTER OF SCIENCE

Major Department:
Civil Engineering

October 2010

Fargo, North Dakota

North Dakota State University
Graduate School

Title

An Investigation of the Kerogen-Mineral Interactions in Green River Oil Shale

By

Kristin Nadiene Alstadt

The Supervisory Committee certifies that this *disquisition* complies with North Dakota State University's regulations and meets the accepted standards for the degree of

MASTER OF SCIENCE

ABSTRACT

Alstadt, Kristin Nadiene, M.S., Department of Civil Engineering, College of
Engineering and Architecture, North Dakota State University, October 2010.
An Investigation of the Kerogen-Mineral Interactions in Green River Oil Shale.
Major Professors: Dr. Dinesh R. Katti & Kalpana S. Katti.

Green River oil shale contains minerals, kerogen, and bitumen and
yields a significant amount of oil upon heating. Kerogen is the insoluble
organic remains found in sedimentary materials. It is a precursor to crude oil
and is one of the most abundant forms of carbonaceous materials on earth. The
richest oil shale deposits in the world are found in the Green River Formation
located in the states of Utah, Wyoming and Colorado in the United States with
the potential to be a major national resource. Current extraction methods
involve heating the shale to high temperatures in order to decompose and
evaporate the shale oil. This method is very inefficient due to tremendous
energy requirements and is environmentally unfriendly. Thus, the extraction
of kerogen is commercially not viable in the United States at this time.

My research at North Dakota State University has been focused on
understanding how the kerogen is "locked" in the surrounding mineral matrix.
The research involves experimental and modeling studies aimed at evaluating
the molecular interactions in the oil shale. The focus of my study has been on
the in situ chemical composition, mechanical properties, and the physical
location of kerogen in Green River oil shale. Fourier Transform Infrared (FTIR)
studies have been conducted using the photoacoustic step-scan method to

investigate the molecular nature of light and dark colored areas of the oil shale core. This technique provided the means for in situ investigation of kerogen-mineral interactions. Results show that light colored oil shale has a high kerogen content with spectra similar to that of isolated kerogen while dark colored oil shale has more mineral components. Kerogen band shifts occurred indicating interactions on the molecular scale between kerogen and the surrounding minerals. Scanning Electron Microscope (SEM) studies were performed in order to obtain information on the size and layout of pores, minerals, and kerogen in the shale. Energy Dispersive Spectroscopy (EDS) performed on light and dark colored samples indicate that the light colored oil shale contains more kerogen associated with the minerals quartz, clay, and potassium-feldspar. Dark oil shale samples contained kerogen, clay, dolomite, calcite, pyrite, and analcite. SEM images perpendicular to the bedding plane of cross-sectional polished oil shale samples showed orientated layers and elongation consistent with compression over time. The absence of large kerogen regions in SEM images and nanoindentation results suggest that Green River kerogen is on the scale of tens of nanometers and is in close proximity to oil shale minerals. The mechanical properties of kerogen and oil shale minerals were found using nanoindentation techniques. Green River kerogen was found to have an elastic modulus of 9 GPa and hardness of 1 GPa.

ACKNOWLEDGMENTS

TABLE OF CONTENTS

TABLE OF CONTENTS (Continued)

LIST OF TABLES

LIST OF FIGURES

LIST OF FIGURES (Continued)

LIST OF ACRONYMS AND ABBREVIATIONS

AFM - Atomic Force Microscope

CT – X-ray computed tomography

EDS - Energy Dispersive Spectroscopy

EPACT – Energy Policy Act of 2005

FTIR - Fourier Transform Infrared

MD – Molecular Dynamics

MMT - Montmorillonite

SEM - Scanning Electron Microscope

SPM - Scanning Probe Microscopy

TEM - Transmission Electron Microscope

TOC – Total Organic Content

CHAPTER 1. INTRODUCTION

1.1. Background

The world demand for oil is steadily increasing, but new resources for this product have had very few recent discoveries. Alternative fuel sources are, therefore, becoming increasingly popular. These alternative fuels include coal, oil shale, tar sand, heavy oil, and oil producible by carbon dioxide enhanced recovery. Out of concern for the country's oil supply and the amount of oil being imported into the country, the United States Task Force on Strategic Unconventional Fuels passed an Energy Policy Act of 2005 (EPACT) to increase the development of fuels from unconventional fuel resources. These alternative resources have gone undeveloped due to their high production costs compared to conventional light crude oil, as well as limited access to public lands, technology performance, market risks, infrastructure and water requirements, capital investments, and operating costs. Many countries are aware of the world decline of oil and have taken action. China has invested in a syncrude pipeline in Canada. India is offering technical assistance, investment financing, and field service to oil developers in return for guaranteed oil supply. The United States has taken the approach of an aggressive means to develop the increased production and supply of oil shale, tar sands, and coal liquids by the year 2035.

Oil shale has thus recently become a great interest since it is located in twenty-seven countries around the world. It is estimated that the United

State's oil shale has a supply of over 2 trillion barrels of shale with the majority of the shale oil, about 1.5 trillion barrels, coming from the Green River Formation located in the regions of Colorado, Utah, and Wyoming. Currently oil shale can be mined, crushed and sized before retorting, liquids recovered, and refined into a usable products for Air Force airplanes and Navy ship and land vehicles. The only step not proven on a commercial scale is the surface retorting or in situ operations. To create usable fuel, the kerogen in oil shale will need to be converted from a solid to a liquid state requiring a heat of 500 °C in the absence of oxygen (Hascakir, 2008). This converts the kerogen to a condensable vapor which becomes liquid shale oil when cooled through a process called retorting. The recovered shale oil will then need to be upgraded or rid of residue (nitrogen and sulfur) in order to be a marketable product.

According to the Department of America's Strategic Unconventional Fuels Resources report written in 2007 there was no shale oil production in the United States at this time (Huntsman, 2007). As of today, the United States has the largest known deposit of oil shale in the world with the richest location being the Green River Formation covering portions of Colorado, Utah, and Wyoming. There is an estimated 1.2 to 1.8 trillion barrels of shale oil, but a conservative estimate of 800 billion barrels of oil is recoverable. This recoverable amount is three time greater than the proven oil reserves of Saudi Arabia. In 2007 the U.S. oil demand was 20 million barrels per day. If the 800 billion barrels of oil met a quarter of that demand (5 million barrels per day),

the Green River Formation would supply the U.S. with shale oil for 400 years (Decora, 1979).

1.2. Problem Statement

An efficient way of extracting the kerogen from the surrounding minerals is needed for future competitive production of shale oil. Currently it is economically inefficient at about 0.3 efficiency when light crude oil is 0.7 efficient. Efficiency is described as the recoverable amount of original or residual hydrocarbons in a reservoir, expressed as a percentage of total hydrocarbons in place. After-product concerns include environmental standards and the use of spent shale or oil shale that has been heated and all organic matter removed. The spent shale can be 13-16% greater in volume than when in the ground. A need for an economical in situ oil extraction method from oil shale is needed to provide the United States with an important abundant natural resource. A better understanding of the interactions between the minerals and kerogen can lead to a better method of shale oil extraction and increased efficiency in the future.

1.3. Objectives

The primary objective of this research is to provide information on the interactions that occur between the oil shale minerals and the organic kerogen phase. This requires an in situ study of the kerogen, allowing the organic matter to be analyzed in its original environment since the isolation of kerogen would destroy some important properties, particularly the significance of

3

orientation parallel and perpendicular to the bedding plane. Currently, little information is known about oil shale and kerogen except the macro-scale or physically visible properties. The research on oil shale is focused on the micro and nano scale properties of kerogen in oil shale. Only a handful of research using EDS and nanoindentation of oil shale has been performed (Moreau, 2004) (Ahmadov, 2009) (Zeszotarski, 2004) and never on Green River oil shale. Photoacoustic step-scan FTIR has never before been performed on any type of oil shale. To fulfill the main objective, three subsidiary objectives were pursued, each having a set of experiments to aid in obtaining the primary objective. These three subsidiary objectives are:

1) Obtain information of how kerogen is "locked" in the Green River mineral matrix by performing SEM, nanoindenation, and AFM experiments.

2) Determine with what minerals kerogen interacts through tests involving FTIR, SEM, and TEM.

3) Obtain data on the in situ mechanical properties of Green River kerogen through nanoindentation tests.

4) Show how and why these interactions occur using FTIR analysis and Molecular Dynamics (MD)

1.4. Scope of Research

The scope of this research includes collecting data from a Colorado oil shale core, allowing information to be obtained about kerogen in its natural

4

state. The chemical composition and kerogen-mineral interactions were determined from in situ FTIR spectroscopic and EDS studies. Data on the physical surface features of the oil shale samples on a scale of nanometers were obtained using SEM and AFM imaging. The mechanical properties (elastic modulus and hardness) and load deformation behavior of in situ kerogen were found using nanoindenation tests.

1.5. Green River Oil Shale Samples

The first and most important task of our research was to obtain samples of kerogen-rich oil shale. The Core Research Center in Colorado provided us with eighteen pounds or seven feet of Piceance Basin oil shale core. The core is assumed to be from Township 4 South, Range 95 West near Rifle, Colorado on the border of Garfield and Rio Blanco counties. A map of the Green River Formation is shown in Figure 1.1 and the Piceance Basin is shown in Figure 1.2, showing the location from which our oil shale core was obtained. The core is from a depth of 567 ft to 572 ft below ground, is two inches wide and was broken into sections about twelve inches in length. Photos of each section are shown in Figure 1.3 and exact locations were determined by ruler measurements to provide a precise sample location for experimental purposes.

Samples used in the experiments are from various regions of the seven foot core. The samples are light and dark in color with no particular pattern to the location. The oil shale samples are kept in an air tight container at room temperature and were handled with gloves so as to not contaminate the core.

Through out the experiments two sampling views were examined and tests

were performed parallel and perpendicular to the bedding plane. A

representation of the parallel and perpendicular views are shown in Figure 1.4.
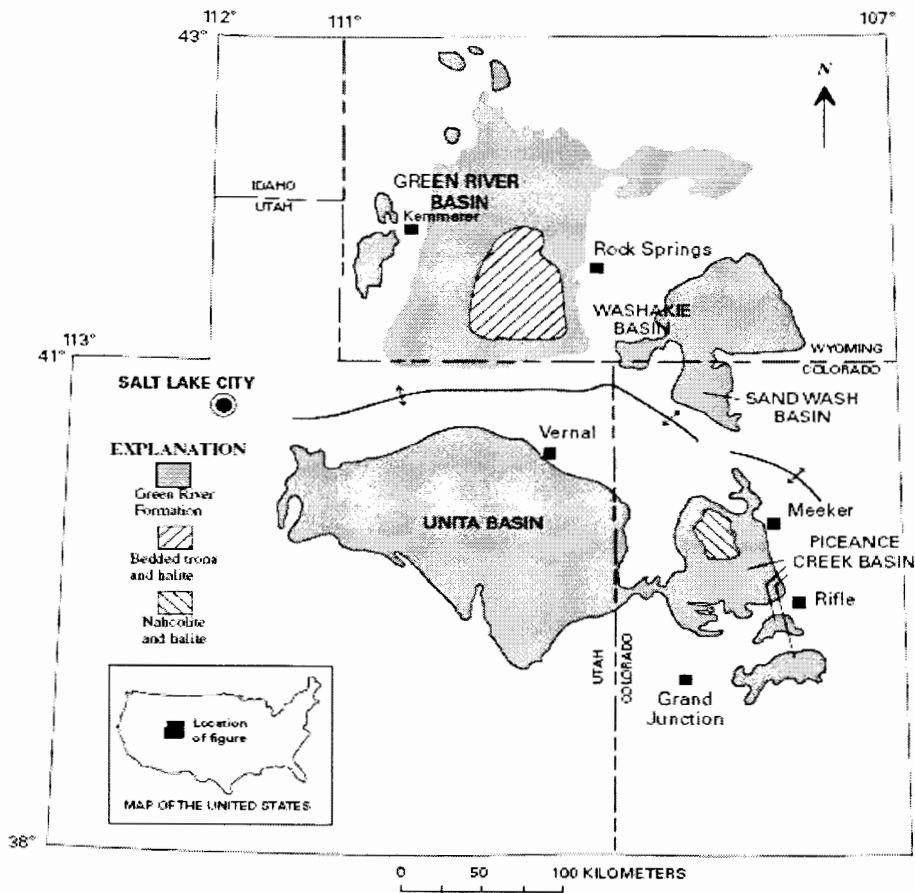
Figure 1.1. The Green River Formation in Colorado,
Utah, and Wyoming (Thompson, 2010).
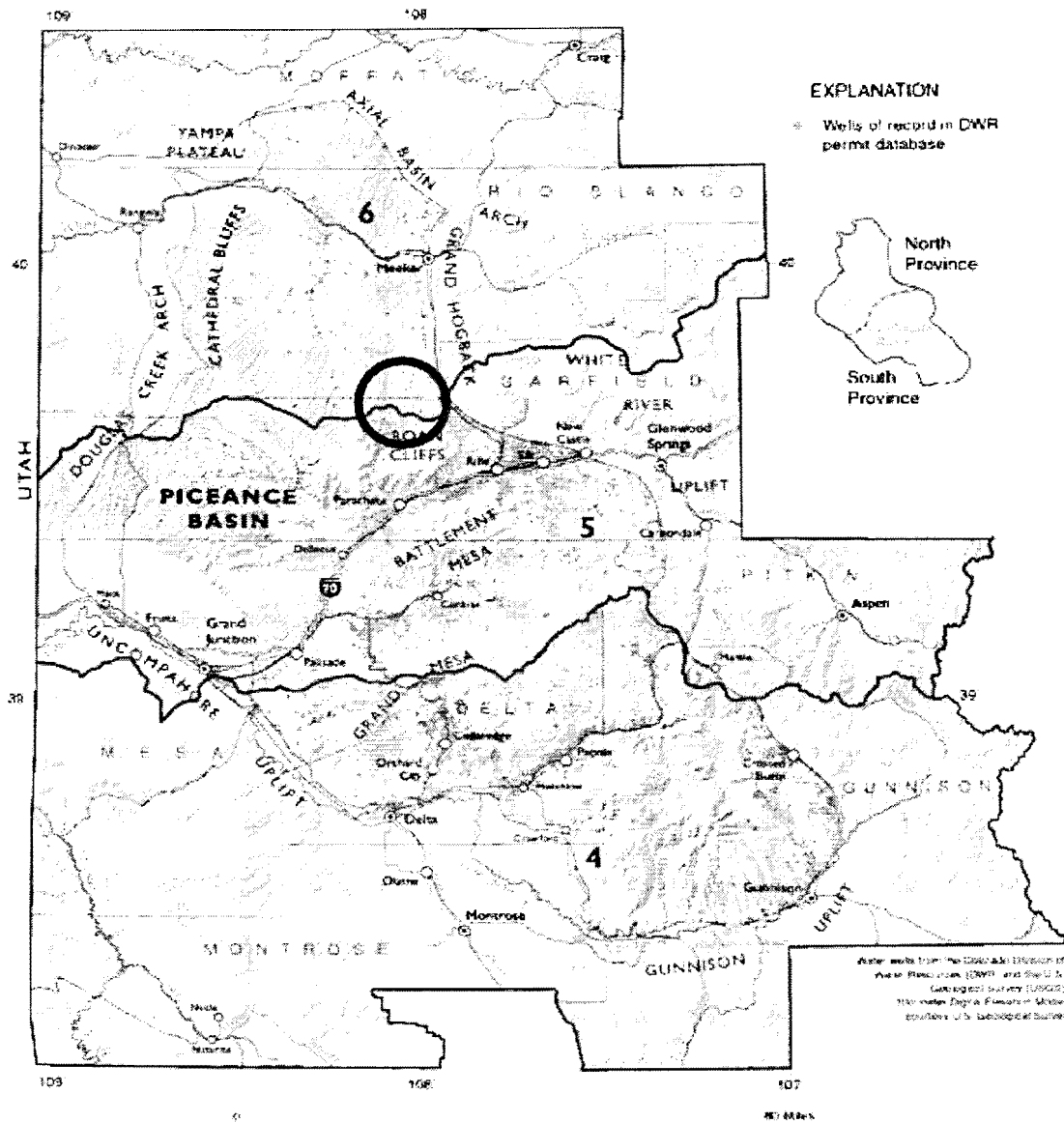
Figure 1.2. Piceance Basin of the Green River Formation in Colorado, United States. The circle indicates the location of the core from Township 4 South, Range 95 West near Rifle, Colorado on the border of Garfield and Rio Blanco counties (Natural Resources Conservation Services - United States Department of Agriculture, 2010).
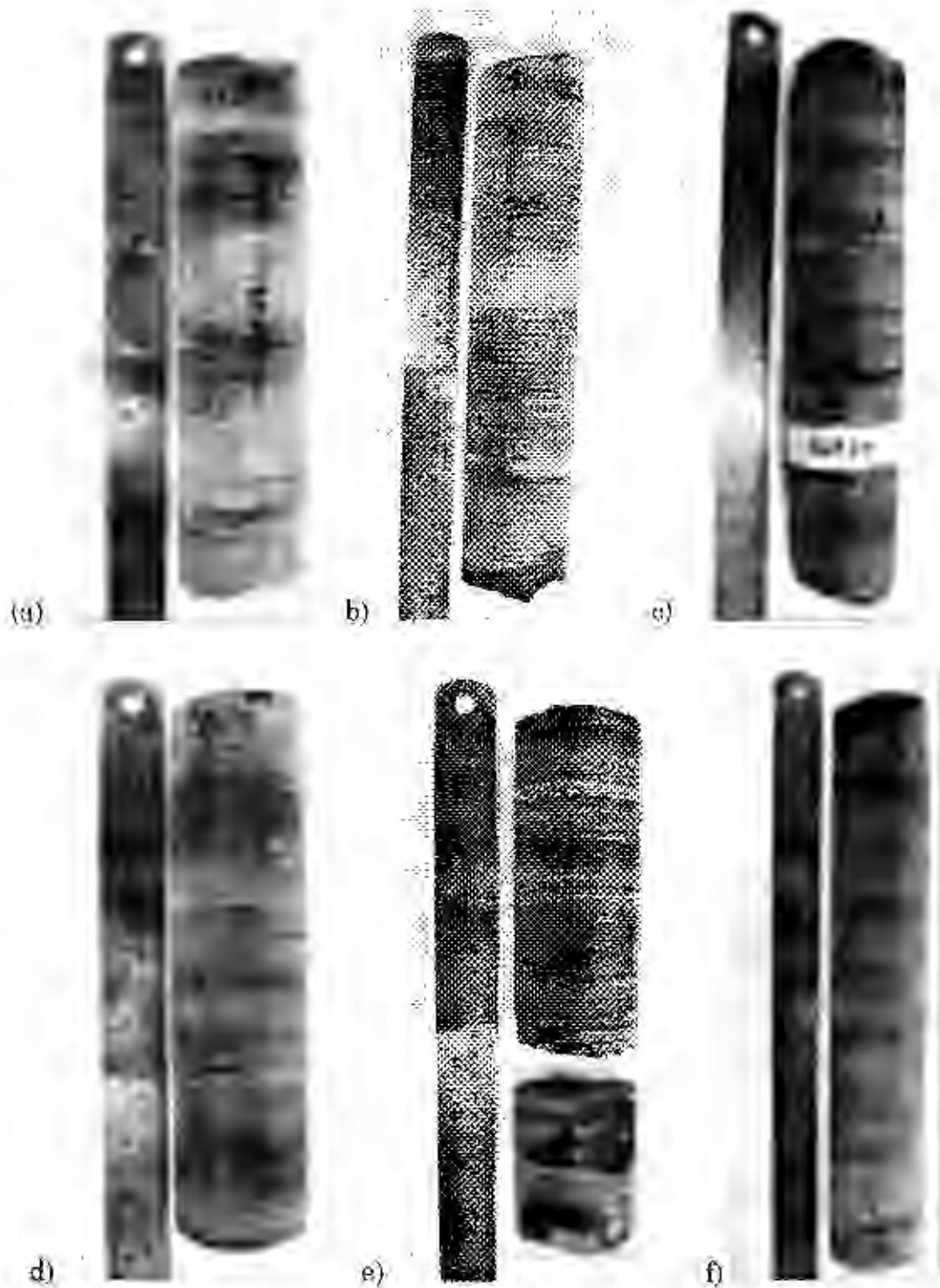
Figure 1.3. Photos taken of the Green River oil shale core used in our experiments. The core is from a depth of (a) 567 ft., (b) 568 ft., (c) 569 ft., (d) 570 ft., (e) 571 ft., and (f) 572 ft.
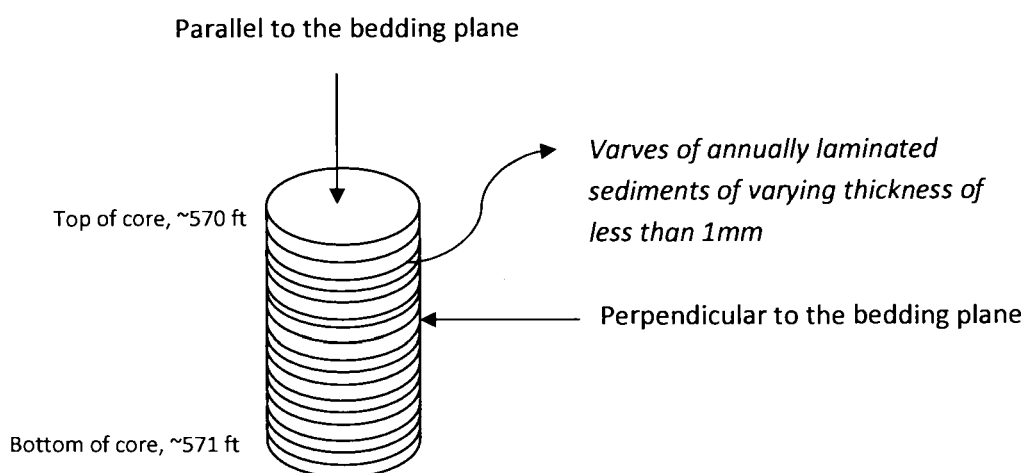
Figure 1.4. Schematic of a two inch oil shale core. The image is suggested to be from a depth of 570 ft showing sampling directions parallel and perpendicular to bedding plane.

1.6. Outline

Chapter 1 consists of the introduction, explaining the economical need for the research that has been performed on oil shale. This chapter introduces the purpose for the work discussed in the following chapters. It includes the background, problem statement, objectives, scope of research, and basic outline. Chapter 1 defines the overall purpose for the work on Green River oil shale.

Chapter 2 consists of the literature review. This chapter includes the definition of kerogen, the physical properties of an oil shale core, and the origin and classification of Green River kerogen. There is also a discussion on previous work that has been performed on the investigation of the interactions between kerogen, clay, and water and the pore sizes in oil shale. For the purpose of further work involving molecular modeling, a section dedicated to

the chemical composition, structure of kerogen, and three dimensional modeling literature review is included. The intent of this chapter was to provide background information on the current knowledge known about kerogen and oil shales.

Chapter 3 consists of the data obtained from fourier transform infrared experiments. The photoacoustic step-scan FTIR method was used to obtain in situ results providing information on the chemical composition of Green River oil shale. This chapter provides a review of literature, oil shale sample preparations and experimental procedures. The results of all tests performed are provided and summarized into a conclusion of major contributions from this work.

Chapter 4 consists of images and results obtained from Scanning Electron Microscope studies. This chapter provides experimental sample preparations and procedures used to obtain informational SEM images of oil shale samples parallel and perpendicular to the bedding plane. Images, results, and conclusions of SEM analysis are the highlights of this chapter.

Chapter 5 consists of nanoindentation analysis in determining the mechanical properties of oil shale and kerogen. This chapter contains a review of literature, sample preparations, and the methods used to perform experiments. The nanoindentation study provides information on the elastic modulus and hardness of oil shale components, most importantly kerogen, at

varying depths of indentation. The results and conclusion are further discussed in this chapter.

Chapter 6 consists of less relevant tests that were performed on kerogen. These tests include CT scanning, AFM images, modulus mapping data, and TEM sample preparation technique. The information collected from these experiments provide minor information to our research including physical and mechanical data on oil shale.

Chapter 7 summarizes all of the conclusions that were determined in the previous chapters. The conclusions are a result of quantitative and qualitative analysis performed on data from FTIR experiments, SEM images, and nanoindentation findings. This final chapter brings together all previous results and evaluates the objectives obtained as well as recommendations for future work.

CHAPTER 2. REVIEW OF LITERATURE

2.1. Definition of Kerogen

Oil shale is defined as a sedimentary rock which contains minerals, kerogen, and bitumen yielding a significant amount of oil through pyrolysis, or the chemical decomposition of a condensed substance by heating (Hascakir, 2008). The shale oil is produced by thermal or primary cracking of kerogen. Secondary cracking leads to the formation of gaseous compounds (Behar, 1997). Shale oil is similar to petroleum except for its high nitrogen content which can be removed by an upgrade to a solution with no heavy residual, ideal for diesel and jet fuels. On a dry weight basis, oil shales can contain 10-60% organic matter, 20-70% carbonate minerals and 15-60% sandy-clay minerals (Razvigorova, 2008). Oil shale consists of bitumen, the soluble portion that may exist in kerogen and occurs as a black, oily, viscous material that is a naturally-occurring organic byproduct of decomposed organic materials. Upon heating, the kerogen in converted to bitumen, which then converts to shale oil with increasing heat (Cummins, 1929).

Kerogen represents one of the most abundant forms of carbonaceous materials on earth and could be considered the most valuable and important component of oil shale (Robinson, 1969) (Bajc, 2008). It is a large macromolecule from the insoluble organic remains of small sea plants, such as algae, and belongs to the multipolymer class (Yen, 1975). Kerogen is only partly soluble due to the very strong bonding forces within. It is believed to

have a linear –type structure that is difficult to oxidize and is a hetero material, meaning highly unsaturated and only partly soluble, due to very strong bonding forces (Robinson, 1969b).

The origin of the word kerogen was used by Crum-Brown who gave this name to the organic matter of a Scottish oil shale that produced a waxy oil upon distillation (Robinson, 1971), hence the word *keros* = wax (Vandenbroucke, 2003). Kerogen has also been defined as the "organic constituent of the sedimentary rocks that is neither soluble in aqueous alkaline solvent nor in the common organic solvents" (Tissot, 1984). In 1980, B. Durand contributed to the definition of kerogen by including sediments in general, like the materials of humic coals, boghead coal, cannel coal, asphaltoid substances, and organic matter (Ikan, 2003). The current definition of kerogen has been extended to all insoluble sedimentary organic materials in sedimentary rocks and also as "pure" organic deposits like humic and algal coals (Dyni, 2003) (Vandenbroucke, 2003). Humin is an alkali-insoluble fraction of soil organic matter and differs from kerogen in that it has hydrolyzable and non-hydrolyzable fractions (Tissot, 1984). Hydrolyzable implies that it is able to undergo hydrolysis or a reaction with water in which a molecule is cleaved into two parts by the addition of a molecule of water.

Kerogen does not have a given chemical composition, but is a generic name like a lipid or protein (Vandenbroucke, 2003). The composition can vary greatly due to different organic precursors, geological burial of sediments,

earth temperatures ranging from 10 – 200 °C, time periods, and extraction procedure used for separation (Vandenbroucke, 2003). Its formation tends to take place in fine-grained sediments such as clays, marls, and carbonates since they have low permeabilities that seem to restrict the availability of oxygen found in water, causing the activity of aerobic organisms nearby to destruct the organic debris (Durand, 1985). Kerogen can vary between different regions in a country to different locations in a formation due to material variations, biological alterations, and ecological differences (Robinson, 1971). There are several oil shale regions in the United States with the richest formation, or formation with the most shale oil potential, being the Green River Formation located in Colorado, Utah, and Wyoming.

2.2. Physical Properties

The physical features of the oil shale core used in this study shows a distinct display of varves or annually laminated sediments ranging in thickness of 14 to 1000 μm. The richest grades have the thinnest lamina because the organic matter compresses easier than the mineral components of the rock when under pressure during burial. Some geologists have attributed the Green River Formation varves to indicate climate changes due to cool, moist winters and long, warm summers based on the area of the lake during the time of formation and its drainage basin. The varves also correlate with the 11-year sunspot cycle (Shastri, 1998) (Dyni, 2003) (Mahajan, 1997) and 21,000 year eccentric orbital cycle as well as the presence of glacier sheets (Dyni,

14

2003) (Bradley, 1929). Others conclude that the varves are due to non-seasonal storms, floods, turbidites, glacial melt water, and spontaneous segregation of dissimilar materials (Buchheim, 1988).

2.3. Formation of Oil Shale

The Green River Formation was developed over 54 million years ago in the Eocene Epoch, part of the Tertiary Period (Robinson, 1969b). During this time, the tectonic deformation and crustal compression was completed in the southern Rocky Mountains. A shift to crustal stretching took place during the Oligocene and Miocene Epoch in connection with the Rio Grande Rift system. Volcanic eruptions and shallow intrusions were widespread, particularly in the San Juan Mountains, San Luis Valley, and Raton Basin. Since the Miocene epoch, the southern Rocky Mountains and Colorado Plateau have undergone some vertical uplift of at least a mile (1.6 km). Deep erosion by streams and glaciers have carved the modern topography.

The Green River Formation is a very rich oil shale deposit due to the marine lakes that were formed in a time of subtropical climate. These lakes were shallow and permanently stratified. The Green River Formation is made up of four lakes that were formed on top of each other over time and became highly saline due to closed basins that existed for over ten million years in a warm-temperate to sub-tropical climate providing excellent conditions for the growth of blue-green algae. The formation and layering of the four creeks can be seen in Figure 2.1. Fluctuations of inflowing streams created very saline

15

and alkaline waters when the lakes contracted. During the driest periods, the

lake water was saline enough to precipitate disseminated crystals of nahcolite,

shortite, and dawsonite as well as carbonate and silicate minerals.
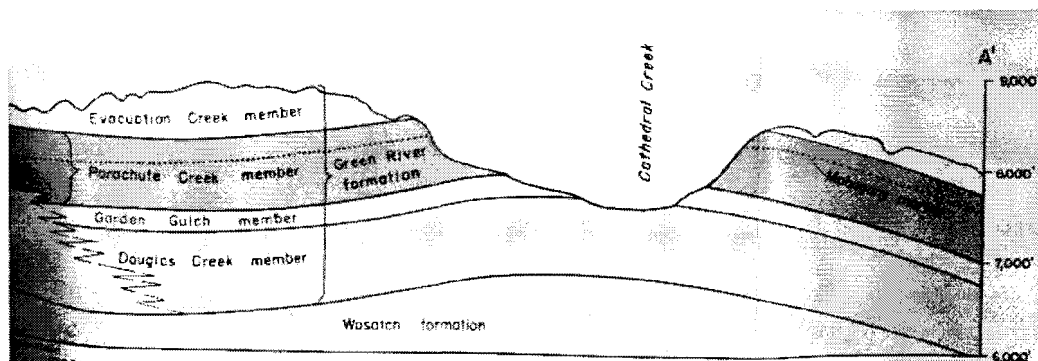
Figure 2.1. Green River Basin cross-sectional view. The image shows the four creeks that were formed on top of each other (Donnell, 1953) (Duncan, 1950).

The shale oil or kerogen from the Green River Basin is usually

"indigenous to the formation and has little opportunity for migration due to the

low porosity and low permeability of the surrounding minerals" (Robinson,

1969b). The Mahogany bed is considered to be the thickest and richest oil-shale

bed in the Green River Formation. An empirical formula for kerogen from the

Mahogany zone level is $C_{214}H_{330}O_{12}N_5S$ with a formula weight of 3,200 daltons.

(Robinson, 1969b).

2.4. Origin of Kerogen

Kerogen from the Green River Formation is considered to be from

cyanobacteria or microalgae, also known as blue-green algae (Lille,

2003)(Vandenbroucke, 2003). This organism is similar to algae in that it can live in water and manufacture its own food through photosynthesis. It uses the water as the source of electrons to reduce CO_2 to carbohydrates. The pigment phycocyanin is what gives them their blue appearance. Cyanobacteria are similar to bacteria in their unicellular structure and they contain no nucleus of chloroplasts like true algae. They also have similar biochemical and structural characteristics like prokaryotic (instead of eukaryotic) cells and the cell walls contain peptidoglycan. Scientists claim that Green River kerogen is from cyanobacteria because of its long polymethylenic chains due to algal contribution and the medium even-carbon-numbered fatty acids from microalgal input (Razvigorova, 2008) (Mongenot, 1999).

2.5. Classification

The "Maillard Reaction" is one of the leading pathways for describing the formation of kerogen (Tissot, 1984). The formation of kerogen starts as a microbial breakdown of proteins, polysaccharides and lignin forming into biomonomers like amino acids, simple sugars and phenols, followed by abiotic repolymerization or recondensation leading to melanoidin formation (high molecular weight heterogeneous polymers that are formed from sugars and amino acids through the Maillard reaction at high temperatures and low water activity (Carr, 2009)). There are three different stages that kerogen will undergo as it matures. The first stage of sedimentation and consolidation is diagenesis, usually occuring above a depth of 1500 meters and is the stage

17

where kerogen loses large amounts of oxygen in the form of CO_2 and H_2O (Durand, 1985). This is a dynamic process in which sediments are attempting to reach equilibrium with a constantly changing geologic environment. Pore water is reacted with and expelled out of sediments as burial pressure increases and is believed to occur at a temperature below 50 °C (Riddle, 2009). When there are negligible amounts of humic and fulvic acid (a water-soluble, natural organic substance of low molecular weight which is derived from humus), this signifies the end of diagenesis.

The second maturation stage is called catagenesis and will occur above a depth of 3000 meters at a temperature below 200 °C over millions of years in a naturally aqueous environment at a pressure of around 61 MPa (Siskin, 1991). Bradley suggests the static pressure of the Green River Formation may have been as high as 210 kg/cm² at temperatures from 90 – 125 ° C (Robinson, 1971). There is significant hydrogen and carbon loss as well as further oxygen loss through CO and CO_2, creating lower molecular weight compounds with an increase in aromatization. This is the stage of maturation of organic carbon when temperature and pressure increases and organic and inorganic components adjust their phase or form to compensate. Lithification occurs at this stage and is the process in which sediments compact under pressure, expel fluids that were present in the sediments at the time of deposition, and gradually become solid rock (Riddle, 2009).

The third and final maturation stage is metagenesis which consists of

very mature kerogen with a low hydrogen/carbon ratio and a parallelization

between existing aromatic structures and pi bonds (Vandenbroucke, 2003). As

kerogen matures, it changes from a very amorphous random molecule, to one

with more structure and rings, although it is still amorphous in nature as

shown in Figure 2.2 (Riddle, 2009) (Vandenbroucke, 2007).

(a)   (b)
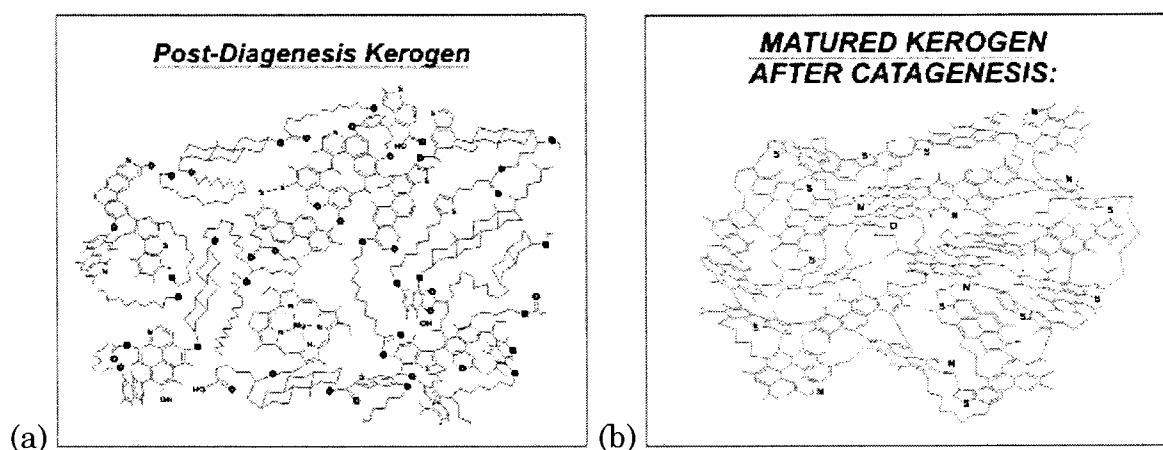
Figure 2.2. Kerogen chemical structure during diagenesis and catagenesis.
These figures show a high molecular weight kerogen structure during the (a)
early stages of maturation known as diagenesis where there are few rings and
amorphous structure while, (b) shows a mature kerogen molecule after
catagenesis with more structure and stable groups. (Riddle, 2009).

Kerogen can be classified by its stage of maturation (diagenesis,

catagenesis, or metagenesis), but also by its insolubility in organic solvents as

a function of hydrogen, carbon, and oxygen content identified as Type I, II, and

III (Razvigorova, 2008) (Kelemen, 2007). Green River oil shale is considered to

be Type I indicating immature kerogen that is able to produce a significant

19

amount of oil. Type I oil shales contain kerogen that is typically derived from algal material, have low maturity, and are considered to be in the diagenesis stage. They have a high H/C ratio of greater than 1.5% and a low O/C ratio of less than 0.1% (Killops, 2005). Type II kerogens are associated with moderately deep marine environment with the organic matter origin from phytoplankton. Type III kerogen is derived from higher vascular plants (Killops, 2005). A Type IV kerogen has no hydrocarbon generation potential and is usually not considered true kerogen, with an origin from high plant matter that was severely oxidized on land and was transported to the deposition area. The Van Krevelen diagram, shown in Figure 2.3, is used to interpret the kerogen type within its thermal evolution paths as a function of burial depths relating H/C to O/C atomic ratios (Razvigorova, 2008).

2.6. Pores in Oil Shale

Oil shale not only consists of kerogen, bitumen, and minerals, but there is the presence of pores between these phases. The organic material gives oil shale its resilience so that oil shale is tougher than pure mineral substances. Eseme et al.(2007) describe oil shale as a sort of concrete as shown in Figure 2.4 with the sizes of minerals and sand to be $2 - 60$ μm, the organics acting as the binding component, and the porosity to be about 30% with the size of pores in the range of $2 - 85$ nm (Eseme, 2007). The pore shapes were little slits with a pore volume of 0.048916 cm³/g and pore diameter of 2 - 85 nm.
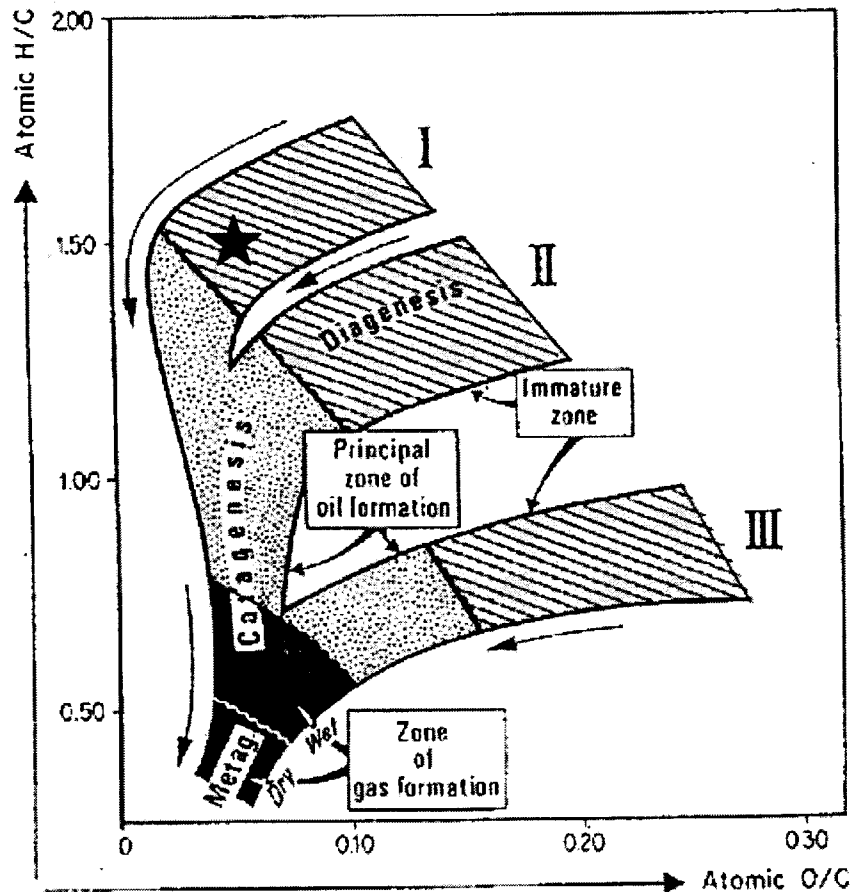
Figure 2.3. Van Krevelen diagram for kerogen (Tissot, 1984). The star indicates the placement of Green River oil shale as Type I in the late stage of Diagenesis.

Nitrogen vapor confined in the pore of sample particles condenses at a pressure lower than its saturation pressure called "capillary condensation". The mass loss rate of oil shale increases with increasing heating rate resulted in a large amount of volatile matter that can quickly be emitted from the particles (Xiangxin, 2008). The TOC or Total Organic Content increases when grain size decreases. Clay minerals protect the organic matter by physicochemical adsorption and also increase water pressure in the porosity,

preventing water input during further compaction on burial protecting against

microbial degradation due to the very small size of the pores (Vandenbroucke,

2003).
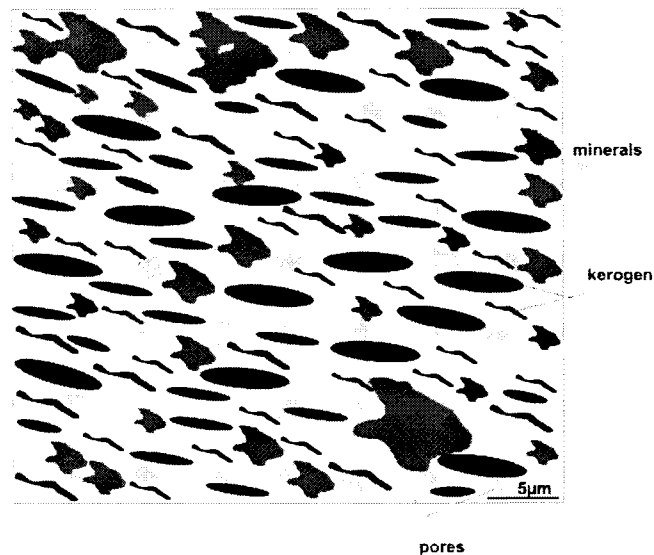
Figure 2.4. A schematic of oil shale showing the minerals, pores, and
kerogen. The kerogen is sitting in round pockets and elongated regions (Eseme,
2007).

Fluids in the pore volume support part of the overburden charge during

burial. Pressure inside a pore will depend on the relative burial rate and can

vary with geological time, even at a constant depth. Pressure applied to

kerogen can range from hydrostatic to lithostatic pressure of 300-800 bar at

3000 m. Kerogen is embedded in the mineral matrix of the source rock,

whereas water is contained in the pores. Water could have more influence on

secondary cracking reactions because the products generated as a result of

kerogen maturation are stored in source rock pores before expulsion.

2.7. Clay and Water Interactions

There seems to be a connection between the organic and inorganic phases of the oil shale since "it is impossible to separate the two phases by physical means and there is a direct proportionality between the organic matter concentration and sediment surface area" (Pan, 2009). Due to the apparent connection between kerogen and minerals, several authors have provided information on kerogen interactions with clay and water. One author reports that the effect of water did not seem to be a great influence in oil shale since the maturation of kerogen was unaffected with a small amount present and there was no pattern to the amount of water. However, with increased mineral acidity there was an increase in naphalene, methylnaphalenes, phenanthrene and methylphenanthrenes as well as a decrease in isoalkanes, cycloalkanes and light alkylbenzenes (Pan, 2009).

Hot water hydrous pyrolysis of kerogen at 200 – 300 °C performed by Siskin and Katritzky (1991) showed results on the influence of clay minerals on organic matter. The authors saw an increase in production of aliphatic hydrocarbons and normal alkanes of twelve or more carbon atoms that were almost completely destroyed by montmorillonite (MMT). The components of bitumen were found to fractionate according to their polarity in the presence of clay minerals, especially when dry. The clay influenced the amount of acetic acid produced, suggesting ester hydrolysis as a key route. Clay minerals

concentrate organic substituents by absorption and then act as acid catalysts in converting kerogen into petroleum (Siskin, 1991).

The chemical composition of kerogen was found to contain alkane chains, cyclohexane chairs, saccaride units, porphyrin structures, aromatic ring structures, and cyclic alkanes (Riddle, 2009). Pyrite is extremely difficult to separate from the organic material because of an apparent attraction for the kerogen (Robinson, 1969). Another author suggests that isoprenoid acids are bound to kerogen and were incorporated at the time of burial (Burlingame, 1968).

2.8. Kerogen Structure and Composition

Knowledge of the kerogen structure and chemical composition will be useful when determining a three dimensional model of Green River Kerogen. Tests performed on an oil shale core from the Green River Formation using chemical analysis, X-ray analysis, and infrared analysis suggest that the kerogen becomes more aromatic with the increase in depth of burial. The types of structures present in the oil-producing portion of the kerogen can be determined from the specific gravity of the assay oil. Since the Green River Formation is very young, the shallow depths are not deep enough for high thermal activity. The organic carbon weight-percent of alkanes was found to increase linearly with increasing burial depth due to increased temperature and pressure (Robinson, 1971). Green River kerogen was found to be a nonbenzenoid and is highly unsaturated. Hydrocarbons are the dominant

24

structural unit with straight-chains, rings, and heterocyclic structures. Oxygen is in the form of acid or ester groups while the other half is in ether or "oxygen bridges" as linkages (Petersen, 2008). Nitrogen and sulfur are assumed to be present in the heterocylic ring systems (Robinson, 1969b).

Kerogen usually accumulates in fine-grained sediments because of the low permeabilities that restrict the oxygen that is dissolved in water. Thus the aerobic destruction of organic matter is more complete than anaerobic conditions (Durand, 1985). The bulk of the carbon structure is naphthenic containing 3-4 rings. They could be linked by heterocyclic atoms and short-chain bridges. Oxygen functional groups are ether and ester type and are suggested to be crosslink sites (Yen, 1975). Razvigorova et al. assumed that the Green River kerogen had not been transformed because of temperature or pressure due to the high amount of unbranched, even number, aliphatic acids (Razvigorova, 2008). Free carboxylic groups in kerogen suggest that the bonds between kerogen and minerals can be fulfilled with carboxylic and complicated ether bonds.

2.9. Molecular Modeling Literature Review

Philip J. Smith is a professor at the University of Utah who is working with a group to develop a three dimensional structure of kerogen. The conclusion of their literature search resulted in finding the Sisken Model to be the best Green River kerogen representation, shown in Figure 2.5. The group created a roadmap, Figure 2.6, of their process and procedure for creating the

3-D kerogen model. The structure obtained from Hyperchem was minimized using the RHF/STO-3G level of theory in GAMESS. Their 3-D kerogen structure was compared with experimental kerogen structure data using x-ray scattering by calculating the atomic pair distribution functions (PDFs) of the model in the DISCUS program and plotted using KUPLOT. The largest kerogen molecule that the University of Utah group created was a 20-unit model with 20,402 atoms fitting a rectangular box and is shown in Figure 2.7. They found the density of isolated Green River kerogen to be 0.98 g/cm^3 and the density of the 3-D model to be 0.80 g/cm^3 after a volume correction was added to address "dead" spaces around the corners of the box.

Oil Shale Kerogen Model
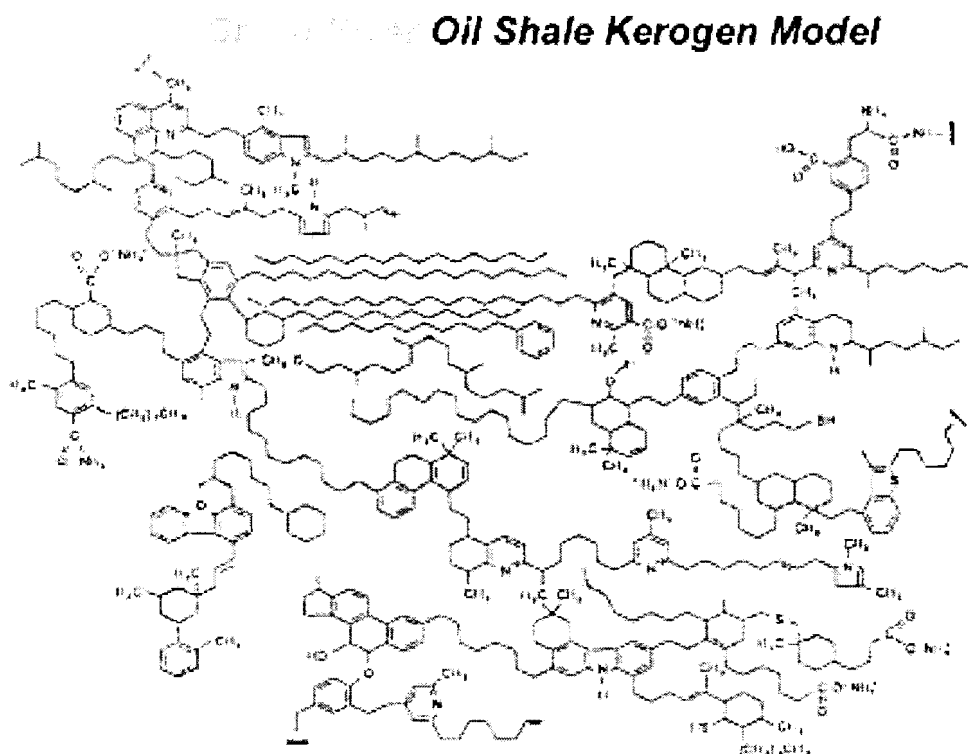
Figure 2.5. Most complete model of the Green River kerogen molecule (Snape, 1995).

The percent of elements in a Green River Kerogen molecule is about 2%

normal alkanes, 2% branched alkanes, 34% cycloalkanes (1-6 rings), 15%

aromatic compounds (1-2 rings), and 47% heterocyclic compounds (Yen, 1975).

Several three dimensional type models have been created to represent a Green

River oil shale kerogen molecule. Figure 2.8 shows the building blocks of a

kerogen structure and a 3-D model of Type III kerogen. Figure 2.9 shows two

models of kerogen originating from cyanobacteria, the precursor to Green River

kerogen.
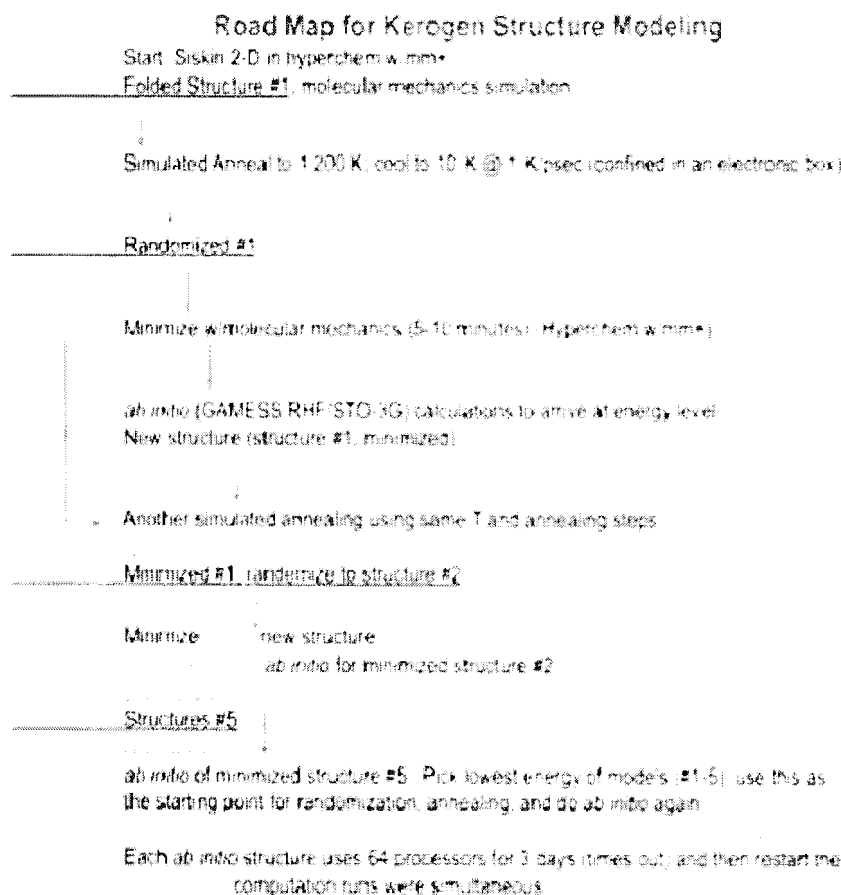
Figure 2.6. Road map for kerogen structure modeling (Smith, 2008-2009)

(a)

(b)
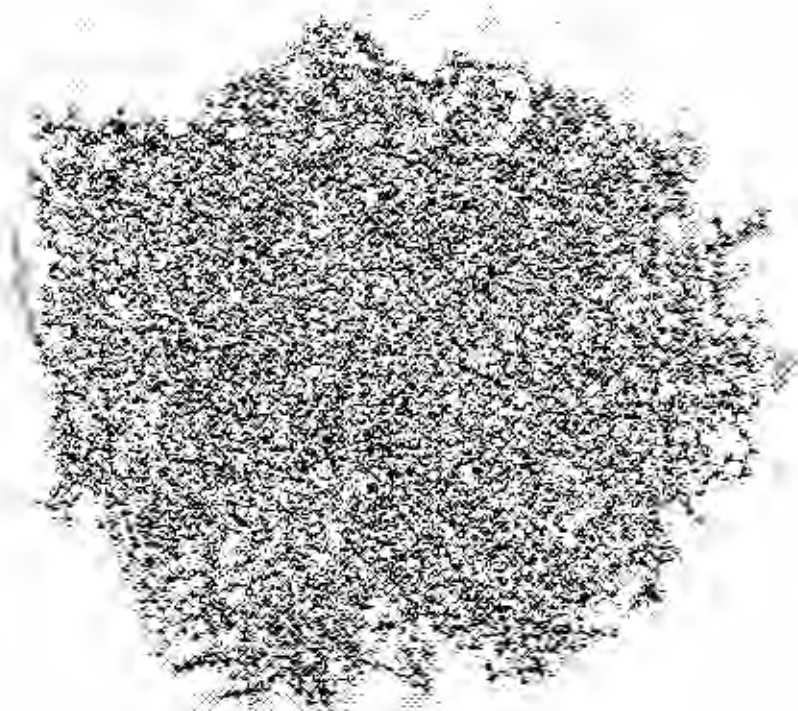
Figure 2.7: Three dimensional Green River kerogen molecule. (a) Three dimensional representation of a folded Siskin Green River Oil Shale Model and (b) 20 unit model with more than 20,000 atoms (Smith, 2008-2009).

(a)
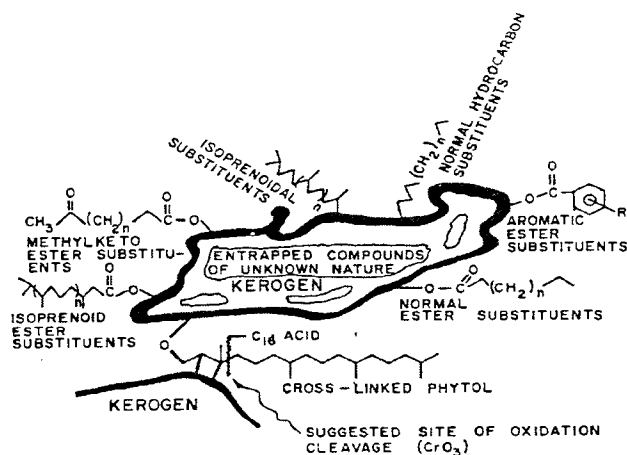
(b)
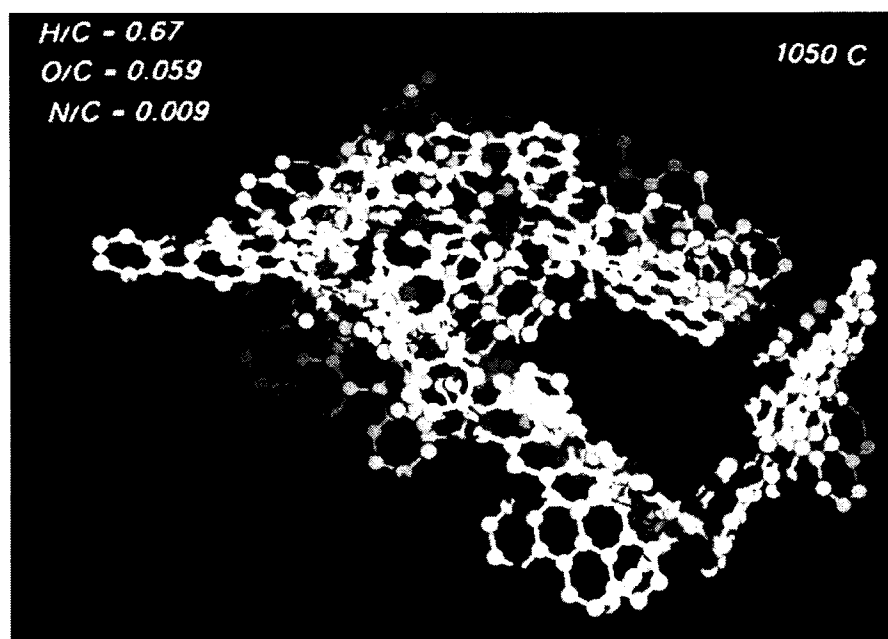
Figure 2.8. Representative kerogen three dimensional structure. The figure in
part (a) represents building blocks of kerogen structure in Green River shale
from oxidative cleavage using CrO_3 and (b) is a 3-D representation of Type III
kerogen at the end of catagenesis using XMol software (Vandenbroucke, 2007).

29
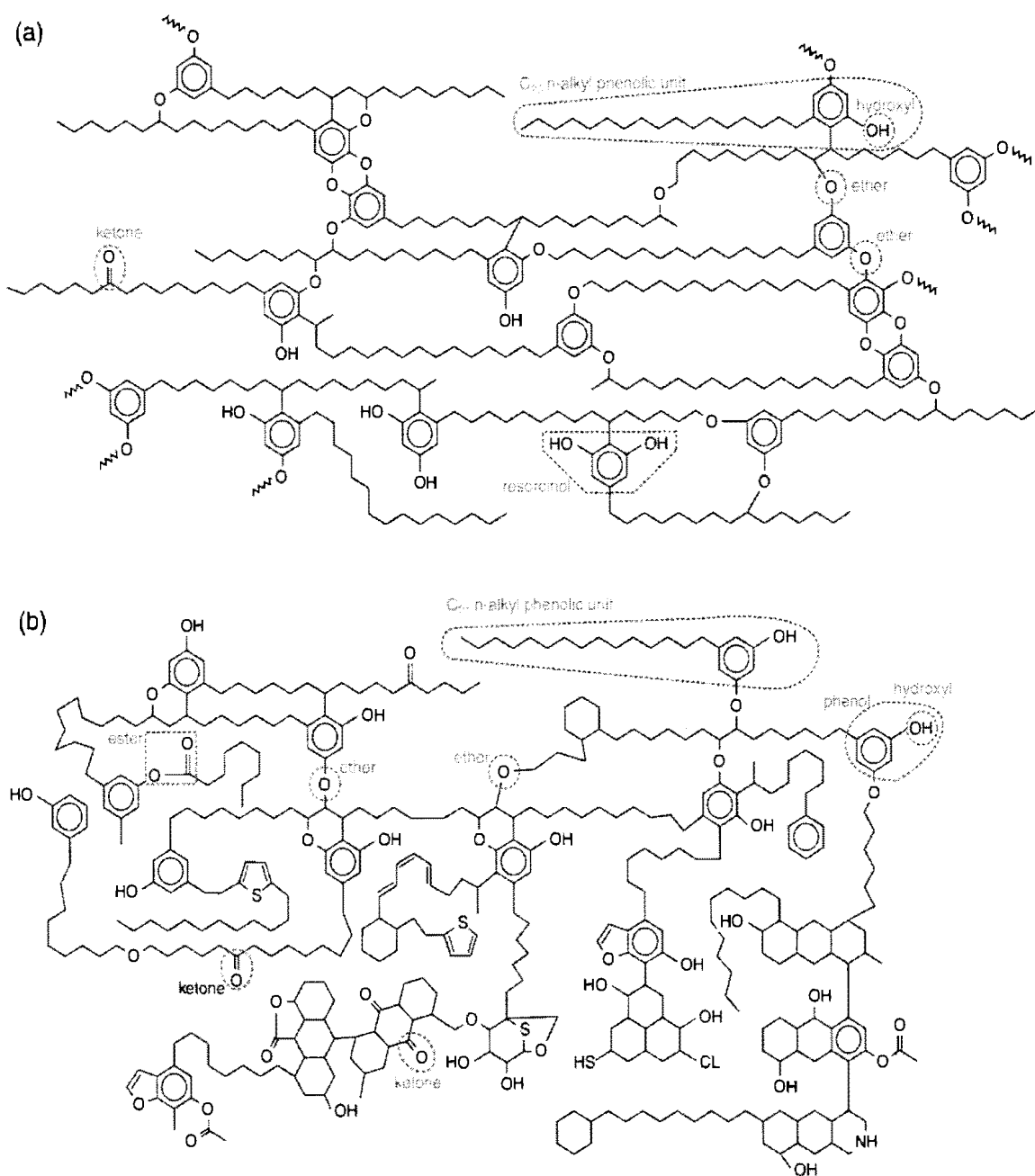
Figure 2.9. Two models of cyanobacteria kukersite. They show oxygen in kerogen bound as ether, carbonyl (C=O), and hydroxyl (OH) and high absorption of ether n-alkane chains (Petersen, 2008).

30

2.10. Mineralogy of the Green River Formation

Studies performed by D.C Duncan, Carl Belser, and J.R. Donnell confirm the geology of the Northwestern corner of the state of Colorado, the location of the Piceance Basin. This region is made up of marlstone as shown in Figure 2.10. Marlstone consists of about 60% clay minerals, 30% quartz, 5% feldspar, 4% carbonates, 1% organic matter, and 1% iron oxides (Donnell, 1953) (Duncan, 1950).
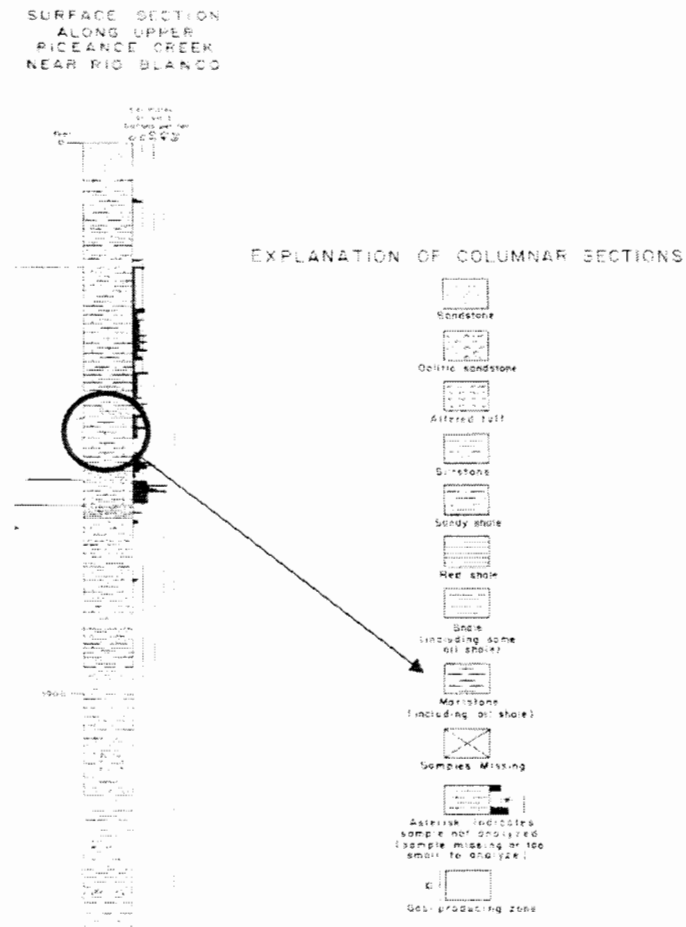
Figure 2.10. Geology of the Piceance Creek near Rio Blanco county in Colorado. At 570 ft below ground the region consists of Marlstone.

There are important resource minerals in the Green River Formation such as nahcolite, trona, and dawsonite (Brownfield, 2009). Nahcolite ($NaHCO_3$) is used as baking soda. Trona is currently being mined as sodium carbonate and the mineral dawsonite occurs in oil shale of the Green River formation in extensive beds that constitute a source of aluminum. The overall oil shale wt % composition from the Green River Formation Piceance Basin can be seen in Table 2.1. The mineral matter in oil shale plays an important role in the formation and interaction of kerogen in its environment.

Table 2.1. The composition of Green River oil shale by weight (Yen, 1975).

Mineral matter 86.2%	Pyrite (FeS_2)		0.86%
	Analcite ($NaAlSi_2O_6*H_2O$)		4.30%
	Quartz (SiO_2)		8.60%
	Montmorillonite [$Na_{0.2}Ca_{0.1}Al_2Si_4O_{10}(OH)_2(H_2O)_{10}$]		12.90%
	K-feldspar ($KAlSi_3O_8$)		16.40%
	Dolomite and Calcite ($CaMg(CO_3)_2$) 43.1%	O	22.20%
		Ca	9.50%
		Mg	5.80%
		C	5.60%
Organic matter 13.80%	Bitumen 2.76%	S,N,O	1.28%
		H	1.42%
	Kerogen 11.04%	C	11.10%

2.11. Isolation of Kerogen

Isolation is a technique that "strips" away all oil shale components, leaving behind kerogen (Goklen, 1984). Isolation is peformed in order to obtain an independent kerogen without changing the chemical structure, although minor degradation of the organic material in the kerogen rock can occur (Robinson, 1969). The first procedure that must occur is the crushing of oil shale samples. The oil shale is crushed to 1-2 inches by a large jaw crusher, then crushed to eight mesh or smaller with a small jaw crusher. The last crush is to 100 mesh or smaller in a hammer mill or disc mill. The next step is to perform a carbonate mineral removal using the following steps; (1) Place oil shale in 4 liter beaker. (2) Add 1 liter of 3M HCL. (3) Heat with stirring to 65-70 °C. (4) Continue heating and stirring for 1 hour. (5) Vacuum filter, rinsing with distilled water until pH of water exiting filter is same as water used for rinse. (6) Repeat steps 1,2,3,4, and 5. (7) Dry filter cake in vacuum oven at 65 °C. (8) Re-sieve through 100 mesh. After that a Bitumen removal occurs; (9) Place in extraction thimble rinsed with 3:1 toluene to methanol (10) Insert thimble in Soxhlet extractor which is charged with 800 mL of 3:1 toluene to methanol mixture. (Make sure to use boiling chips.) (11) Turn heating mantel ON, and adjust powerstat so that cycle time in extractor is roughly 5 min. (12) Run Soxhlet extractor for 24 hours. (13) Turn heating mantel OFF (14) Remove thimble from extractor and dry at 65 °C in vacuum oven. This is followed by a Silicate removal; (15) Transfer contents of thimble to 1 liter *plastic beaker(16)*

With extreme caution, add 1 liter of 1:1:1 20:HCL:HF solution (17) Heat with stirring to 65 °C and maintain for 1 hour (18) Vacuum filter, quickly, and dilute filtrate with water to prevent etching of flask. (19) Repeat steps 15, 16, 17, and 18. (20) Rinse with several liters of distilled water and filter. (21) Dry at 65 °C in vacuum oven. The next step is the removal of Pyrite; (22) Transfer dried solid to 1000-mL 3-neck flask, with roughly 7 g of lithium aluminum hydride (LAH). (23) Fit with refluxing condenser and filling funnel. (24) Slowly add 500 mL of tetrahydrofuran (THF), and reflux 30 min. (25) Vacuum filter. This is a tricky step; the mixture is quite messy and gives off disagreeable gases. The process is finished with a final washing; (26) Transfer to 1 liter beaker and add 500 mL of 3:1 H_2O to HCL solution (27) Heat to 65 °C with stirring and maintain 1 hour. (28) Vacuum filter, rinsing with several liters of distilled water. (29) Vacuum dry at 65 °C. There are several isolation methods and treatments that have been performed on Green River oil shale (Robinson, 1969).

2.11.1. Isolation Techniques:

1) Modified Quass Method is the differential wetting of organic kerogen (wet by liquid phase) and inorganic mineral (wet by waterphase) by two immiscible liquids (oil and water) to reduce ash content. The advantages of this technique is the chemically unaltered kerogen concentrate. The disadvantages are; 1) fractionating of the kerogen

does exist, 2) time requirement prepare concentrate, and 3) Some mineral reduction is not complete.

2) Sink-float method is when centrifugation separates the dense liquid medium since lightweight kerogen floats and minerals sink. The advantages are a chemically unaltered kerogen, a concentrate of less than 10% mineral can be obtained. Disadvantages include low yield of good concentrate and some kerogen may be fractionated.

3) Acid treatment uses hydrochloric acid and has an advantage in that most minerals (except pyrite) are removed from the kerogen rock. There is little opportunity for fractionation or organic material, and it is a rapid process. A disadvantage is the possible alteration of organic kerogen by strong mineral acids

4) Pyrite Removal uses lithium aluminum hydride treatment to obtain a carbonate-free kerogen rock, but the functional groups are altered. There is also the use with zinc and hydrochloric acid that is a slow process and the reduction of functional groups in kerogen has not been predicted. Nitric acid digestion is also used which oxidizes and nitrates the kerogen.

5) Reduction of oil shale is a catalytically hydrogenated process using hydrogen at 4200 psig (pound-force per square inch gauge) of hot pressure at 355 °C for 4 hours in presence of stannous chloride catalyst.

6) Hydrolysis on oil shale resulted in fatty acids showing an even over odd carbon number of 1.41 in the C_{16} to C_{20} range and 2.05 in the C_{26} to C_{30} range. Even number fatty acids seen to convert to odd number n-alkanes or odd carbon fatty acids by carbon loss further confirming the origin of Green River kerogen from cyanobacteria.

7) Pyrolysis is used as a degradation technique that allows breaking a complex substance into fragments by heating it under an inert gas atmosphere. The small compounds obtained are building blocks of the complex substance but can be analyzed to a molecular level and quantified. There is an Open Systems pyrolysis where effluents are swept away from the hot zone by inert gas flow or vacuum extraction and monitors the formation of molecular building blocks since secondary reactions between generated products should not occur. A qualitative Analytical pyrolysis is coupling the pyrolysis chamber in a graduated cylinder column. Recovery depends on the molecular weight and the chemical structure. Chemical fractions can be recovered in a cold trap or as carbon weight with a flame ionization detector.

8) Isolation of Bitumen is a Benzene Extraction technique where oil shale is crushed to pass a 100-mesh then placed in a soxhlet extractor with a mixture of methyl alcohol and toluene for 200 hours. The Fractionation Technique is where crude extract is dissolved in

40:1 volume ratio of n-pentane to sample at 0 °C and then filtered, washed, and dried. It is then placed on a prewetted column of 25 parts of alumina and eluted with purified solvents. The column is eluted with pentane, then benzene, then a mixture of 10% methanol and 90% benzene.

9) Isolation of Porphyrins occurs since Porphyrins are regarded as remnants of biological precursors like chlorophyll and hemin. The extraction reagent is a saturated solution of hydrogen bromide in glacial acetic acid. This allows the extraction of the soluble material from the rock prior to treatment or directly with the porphyrin extraction reagent

10) Isolation of amino acids uses extraction with a ground, air-dried sample that is refluxed with 150 mL of 6 M HCL for 24 hours then filtered through a Buchner funnel. HCL is removed by evaporation under reduced pressure and any humin is centrifuged. The Fractionation technique is an amino acid solution passed through a column of cation exchange resin in hydrogen form and washed with 1.5 M, 2 M, and then 4 M HCL.

11) Isolation of Carbohydrates uses Extraction methods on crushed samples treated with 50% sulfuric acid. Monosaccharides are extracted and separated by acid hydrolysis. 0.5 M H_2SO_4 acid

neutralizes the alkaline constituents. Fractionation methods use uni-dimensional paper chromatography to separate sugars.

12) Oxidation tests show differences in structure due to the aromatic portion of the structure. The process degrades kerogen to a lower-molecular-weight by boiling in alkaline potassium permanganate. Green River kerogen was completely oxidized to oxalic acid, volatile acids, and CO_2 showing absence of significant amount of fatty or condensed aromatic structures. Thus, Green River kerogen is nonbenzenoid and contains little or no fatty or algal remains resistant to oxidation. Filtrate-soluble acids were predominately decarboxylic and linear

13) Thermal Degradation occurs at 325°C when kerogen softens, swells slightly and becomes darkened. Water is formed at 300-405°C with ammonia and other volatile nitrogen compounds and hydrogen sulfide. Heavy oil vapors form about 390°C and continue to 500 or 600° C. At 500 °C, 66% oil, 9% gas, 5% water, and 20% carbon residue is formed. Oxygen structures are unstable and were degraded with loss of CO_2, CO, and water. Nitrogen structures were stable and higher temp was needed for degradation indicating the presence of double-bonded nitrogen. Nuclear magnetic resonance at 350°C indicated 32% aromatic and 68% alkyl and cycloalkyl structures. Test results show that kerogen is predominantly a heterocyclic material

connected to or associated with smaller amount of hydrocarbon material consisting of straight-chain alkyl, cycloalkyl, and aryl groups.

2.12. Conclusions on the Literature Review

Green River oil shale is a fine-grained sedimentary rock located in northwest corner of Colorado, Utah, and Wyoming. Information is known about the origin and chemical composition of kerogen, but the exact chemical structure and interactions between the minerals and kerogen is yet to be confirmed. Obtaining information on the kerogen structure and interactions with its surroundings would be beneficial in finding a more efficient and economical means of shale oil extraction. To increase the efficiency of extracting shale oil from the mineral matrix, the thermal conductivity and reduction of oil viscosity should be increased (usually done by heating to 500 °C) (Hascakir, 2008). For this reason a better understanding of the Green River kerogen chemical composition, physical locations, and mechanical properties would provided the needed understanding of in situ Green River kerogen.

CHAPTER 3. THE PRESENCE OF KEROGEN AND MINERALS IN OIL SHALE: AN IN SITU FTIR SPECTROSCOPIC STUDY

3.1. Introduction

Fourier Transform Infrared spectrometers subject a sample material to infrared radiation, then measure the frequencies and intensities of radiation that is emitted, reflected, or absorbed by the sample. This technique can be used for solids, liquids and gases and is a powerful tool in identifying chemical bonds (by interpreting the absorption spectrum). Information on molecular vibrations is directly related to molecular structure providing us with information on a sample's structure, symmetry, functional groups, purity, and hydrogen-bonding.

The chemical composition of the Green River oil shale samples was determined through light spectroscopy experiments. The photoacoustic FTIR method provided the means to perform an in situ study of Green River oil shale kerogen and minerals. Photoacoustic results on oil shale have never before been reported in literature. The major objective for this experiment was to perform an in situ oil shale study that would identify structural changes to kerogen due to kerogen-mineral interactions found by band shifts. The second objective for this study was to distinguish any differences between light and dark colored regions located in the oil shale core as well as any differences in various depth locations of the oil shale core. The third objective was to observe

40

any depth changes on a micron level within the sample. The last objective was to distinguish between any changes in orientation perpendicular or parallel relative to the bedding plane.

3.2. Literature Review

In previous studies of light spectroscopy from literature, kerogen was isolated from the oil shale through chemical and physical isolation methods since it is "trapped" in, or adsorbed on, the inorganic mineral matter that surrounds it. Isolation is a technique to produce a material in a pure form by stripping all other oil shale components away, leaving behind the kerogen without changing the chemical structure (Dyni, 2003) (Goklen, 1984). There is only one current spectrum of isolated Green River kerogen shown in Figure 3.1 (Robinson, 1969b). Figure 3.1 shows a Green River kerogen spectrum in the range of $4000 - 400$ cm^{-1} performed by Robinson on isolated kerogen crushed into KBr pellets. Kerogen is represented by the 3400 cm^{-1} OH stretching band, the ~2900 cm^{-1} CH$_2$/CH$_3$ stretching band, the 1700 cm^{-1} C-O stretching band, the 1500 cm^{-1} C-C band, and the C=C stretching band at 1000 cm^{-1}.

3.3. Materials and Methods

3.3.1. Sample Preparation

The oil shale samples used to perform FTIR experiments were taken from the core obtained from the Core Research Center located in Colorado.
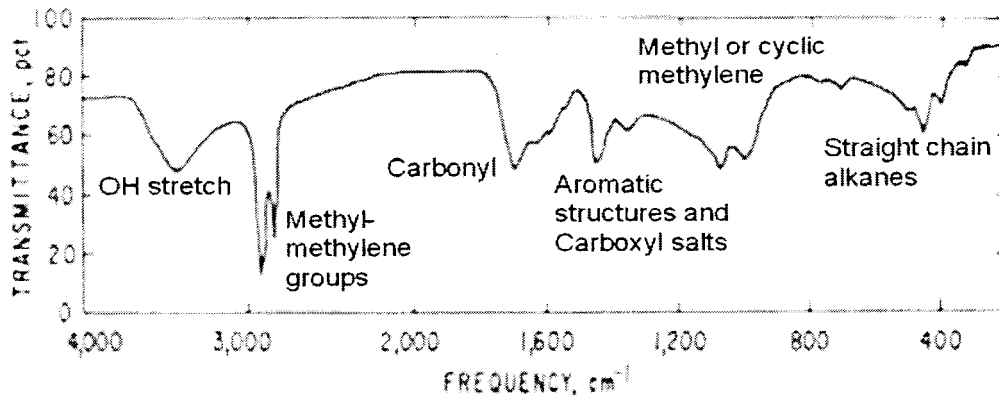
Figure 3.1. FTIR transmission spectrum of Green River kerogen (Robinson, 1969b).

Samples were taken from the core at a location of 571 ft @ 15 cm, 571 ft at 8 cm, and 569 ft at 2 cm. The two inch diameter core was cut with a tile cutter into semi-circles of about 1 inch thick. These pieces were then cut with a diamond cutter at a speed of 2 Hp into 5 x 5 x 3 mm pieces for the parallel to the bedding plane samples and 6 x 4 x 3 mm pieces for perpendicular to the bedding plane samples. Cut pieces were kept in an air-tight container. Oil shale samples were made from dark and light colored sections of the core. Refer to Appendix B.1 for additional sample preparation details.

3.3.2. Methods and Technique

Alexander Graham Bell stumbled upon acoustic frequency in 1880 when he discovered that a beam of light focused on a sample produced an audible sound in the air around the sample if the beam was turned on and off at an acoustic frequency (Chalmers, 2002). He also observed that strongly absorbing

42

materials produced louder sound or photoacoustic signal compared to weakly absorbing materials (Mirabella, 1998). Results from his work enable the performance of the FTIR photoacoustic step-scan method to analyze bond interactions in an oil shale sample while in its solid natural form.

For the infrared photoacoustic spectroscopic experiments, a Nicolet 850 FT-IR spectrometer was utilized with MTEC Model 300 photoacoustic detector in the range of 4000 – 400 cm^{-1} at a spectral resolution of 4 cm^{-1} for 32 scans. In-phase (0°) and quadrature (90°) signals were collected at modulation frequencies of 800, 500, 200, and 50 Hz. Background spectra using a carbon black filled elastomer were collected at each of these frequencies. For both dark and light-colored areas in the oil shale core, samples were taken from various depth locations and were evaluated parallel and perpendicular to the bedding plane. All spectra were normalized to the C-H stretching band at 2900 cm^{-1}. This band was chosen due to its sharpness, consistent location, intensity, and presence in all the spectra taken of light and dark-colored samples.

Fourier Transform Infrared (FTIR) experiments have been performed on oil shales from around the world, but has never before seen results using the photoacoustic technique. The method of photoacoustic step-scan spectroscopy was chosen since it is non-destructive to the sample and allowed spectra to be taken of the kerogen within its original environment or, in this case, the kerogen surrounded by the mineral matrix. Photoacoustic step-scan spectroscopy is a non-contact method that is insensitive to surface morphology,

ideal for materials that are too opaque for direct transmission in the mid-infrared spectral region, and does not expose samples to air or moisture. An advantage of this technique is depth profiling which can be controlled as a function of time or by the frequency intensity. The depth layer that is penetrated by the infrared beam produces most of the resulting data spectrum. The penetrated layer depends on the frequency and the thermal diffusivity of the sample which can result in sampling depth variations within the sample making interpretation of results more complicated. The frequency and sampling depths for our study is given in Table 3.1. The sampling depth (L) depends on the thermal properties of Green River oil shale.

The sampling depth (L) is determined by:

$$L = (D \: / \: \pi * f)^{1/2} \tag{1}$$

where D is the thermal diffusivity, and f is the modulation frequency. The thermal diffusivity (D) of the sample is given by:

$$D = K \: / \: \rho * C \tag{2}$$

where K is the thermal conductivity, ρ is density and C is specific heat of the sample material (Chalmers, 2002) (McClelland, 2002).

The thermal properties of Green River oil shale, shale, and isolated kerogen were found in literature and are displayed in Table 3.2.

Table 3.1. Sampling depths of Colorado oil shale for varying photoacoustic FTIR frequencies (McClelland, 2002)

Frequency (Hz)	Depth (μm)
50	48
100	33.85
200	24
300	19.54
500	15.14
800	11.97

3.4. Results

3.4.1. Mineral Bands in Green River Oil Shale

Green River oil shale is composed of marlstone, consisting of clay minerals, quartz, feldspar, carbonates, organic matter, and iron oxides (Donnell, 1953) (Duncan, 1950). The mineral matter in oil shale plays an important role in the formation and interaction of kerogen in its environment. Refer to Table 2.1 for the composition of Green River oil shale by weight. A photoacoustic FTIR spectrum in Figure 3.2 shows the bands characteristic of bonds in minerals. The Green River oil shale minerals include pyrite, analcite, quartz, montmorillonite, k-feldspar, dolomite, calcite, nahcolite, trona, and dawsonite. The bands attributed to pyrite is the hydrated FeOH band at 1395 cm^{-1}, 1184 cm^{-1}, 1075 cm^{-1}, 1000 cm^{-1}, 694 cm^{-1}, 670 cm^{-1}, 637 cm^{-1}, 615 cm^{-1}, 509 cm^{-1}, and

Table 3.2. Thermal properties of oil shale, kerogen, and shale rock

	Oil Shale	Kerogen	Shale rock
Density (ρ), g/cm³	2.06 - 2.47 (Yen, 1976) (Prats, 1975)	1.05 (Yen, 1976)	2.72 (Yen, 1976)
Heat Capacity (Cp), J/g/K	~ 0.95	1.5 - 1.82 (Waples, 2004)	0.8 (Waples, 2004)
Thermal conductivity (K), J / sec/cm/K	0.391411 – 0.707748 (Prats, 1975) (Rajeshwar, 1979)	*	0 .284151 (Prats, 1975)
Thermal diffusivity (α), cm²/s	0.0026 - 0.0098 (Lee, 2007)	*	*
Thermal capacity (Cp), J/ cm³/K	2.167 (Waples, 2004)	1.8 (Waples, 2004)	2.58 (Waples, 2004)

* Indicates information that was not available

462 cm^{-1} (Beutelspacher, 1976) (Farmer, 1974). Analcite bands are present at 1115 cm^{-1}, 1034 cm^{-1}, 785 cm^{-1}, 756 cm^{-1}, 637 cm^{-1}, 615 cm^{-1}, and 462 cm^{-1} (Beutelspacher, 1976) (Farmer, 1974). Quartz bands are represented at 1180 cm^{-1}, 1092 cm^{-1}, 868 cm^{-1}, 837 cm^{-1}, 785 cm^{-1}, 694 cm^{-1}, 509 cm^{-1}, and 462 cm^{-1} due to Si-O bonds (Beutelspacher, 1976) (Farmer, 1974). Montmorillonite

bands are located at 3649 cm⁻¹ and 3613 cm⁻¹ due to O-H stretch of structural hydroxyl, 3450 cm⁻¹ and 3294 cm⁻¹ from H-OH hydrogen bonded water, 1644 cm⁻¹ from O-H deformation, 1230 cm⁻¹ to Si-O orientation dependent band, 1154 cm⁻¹, 1115 cm⁻¹ and 1034 cm⁻¹ from Si-O inplane stretch, 1092 cm⁻¹ and 637 cm⁻¹ due to Si-O out of plane stretch, 919 cm⁻¹ due to Al-O/Al-OH stretch, 868 cm⁻¹ from Al-FeOH deformation, 785 cm⁻¹ because of Si-O bond, 725 cm⁻¹ Si-O deformation perpendicular to the optical axis, 694 cm⁻¹ Si-O deformation parallel to the optical axis, and 462 cm⁻¹ to Si-O-Fe vibration (Katti, 2006). K-feldspar bands are found at 1092 cm⁻¹, 785 cm⁻¹, 756 cm⁻¹, 670 cm⁻¹, 583 cm⁻¹, and 462 cm⁻¹ (Beutelspacher, 1976) (Farmer, 1974). Dolomite and calcite bands are very similar and can be found at 2514 cm⁻¹ from O-H stretch, 1808 cm⁻¹ due to C-O stretch, C=O stretch at 1606 cm⁻¹, CO_3^{-2} stretch at 1436 cm⁻¹, 1395 cm⁻¹, 1092 cm⁻¹, and 868 cm⁻¹, CO_3^{-2} bending at 725 cm⁻¹, and C-O stretch at 694 cm⁻¹ (Balmain, 1999) (Beutelspacher, 1976) (Farmer, 1974). Nahcolite signature bands are located at 2624 cm⁻¹ from O-H stretch, 1671 cm⁻¹, 1606 cm⁻¹, 1454 cm⁻¹, 1395 cm⁻¹, and 1092 cm⁻¹ due to C=O stretch, 1302 cm⁻¹ from O-H-O in-plane bending, 1000 cm⁻¹ from O-H-O stretch out of plane, 837 cm⁻¹ from CO_3 out of plane, and 694 cm⁻¹ due to O-H stretch. Dawsonite bands are found at 3360-3022 cm⁻¹ from H-OH hydrogen bonded water, 1550 cm⁻¹, 1092 cm⁻¹, 868 cm⁻¹, and 837 cm⁻¹ from CO_3^{-2}, 1395 cm⁻¹, and CO_3^{-2} bending at 725 cm⁻¹ (Beutelspacher, 1976) (Farmer, 1974). In summary, the bands for oil shale minerals include the ~3660 cm⁻¹ O-H stretch band of structural hydroxyl

indicating that there is some free water in the oil shale core. Water is present

during the formation of kerogen and is a natural component in oil shale. The

3600 cm^{-1} is also from Al-O-H stretching band attributed to montmorillonite.

There is a sharp band at 2515 cm^{-1} due to OH stretch of calcium carbonate

with its signature band at 1800 cm^{-1} characteristic of an unsaturated ester

(C=O) and occurs as a doublet, meaning two esters are close together. Mineral

bands present at 1600 cm^{-1} are contributed to dolomite, a 1436 cm^{-1} band is

present from dolomite and calcite, and strong bands in the 1230-1000 cm^{-1}

region are due to Si-O from montmorillonite, quartz, and Fe-S bands from

pyrite (Bozlee, 2005). Weaker bands due to montmorillonite, dolomite, calcite,

quartz, and pyrite are found in the 900 – 400 cm^{-1} region.
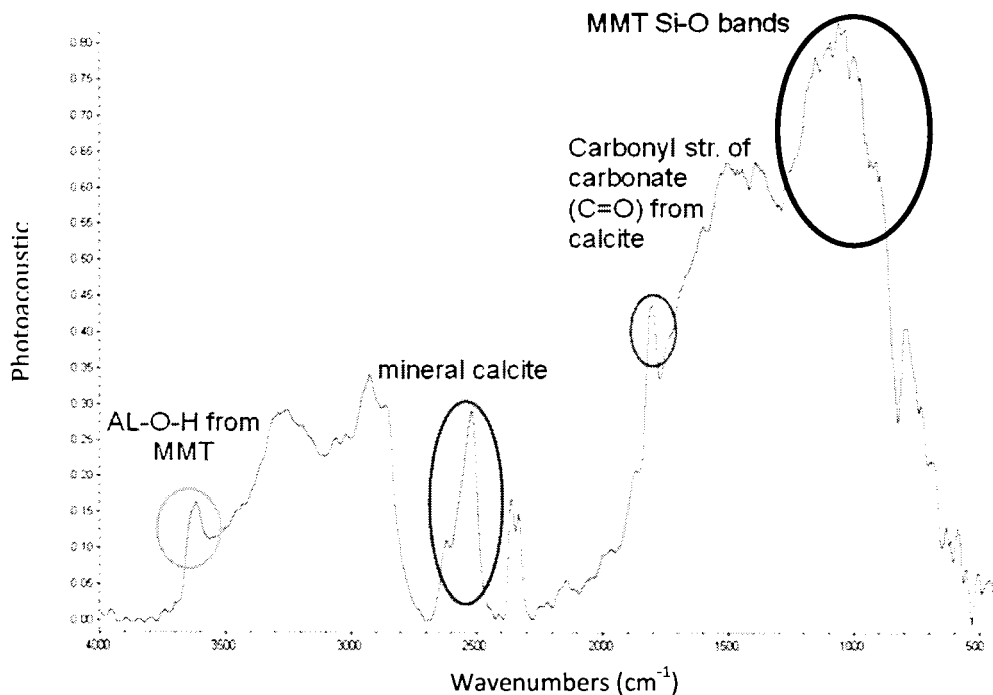
Figure 3.2. Spectrum of a dark parallel oil shale showing bands of
Green River minerals.

3.4.2. Kerogen Bands in Oil Shale

Photoacoustic step-scan experiments were performed on light and dark colored oil shale and analyzed parallel and perpendicular to the bedding plane. The light-colored areas of the oil shale can be found in groups of very thin layers (about 1-4 mm thick parallel to the bedding plane) throughout the core. There does not seem to be any particular pattern to the location of these regions. Spectra of light and dark colored samples prepared from different depths of the oil shale core exhibit bands that are very similar to that of isolated kerogen bands found in literature. Figure 3.3 shows a dark colored oil shale spectra taken parallel to the bedding plane where the kerogen bands have been circled.
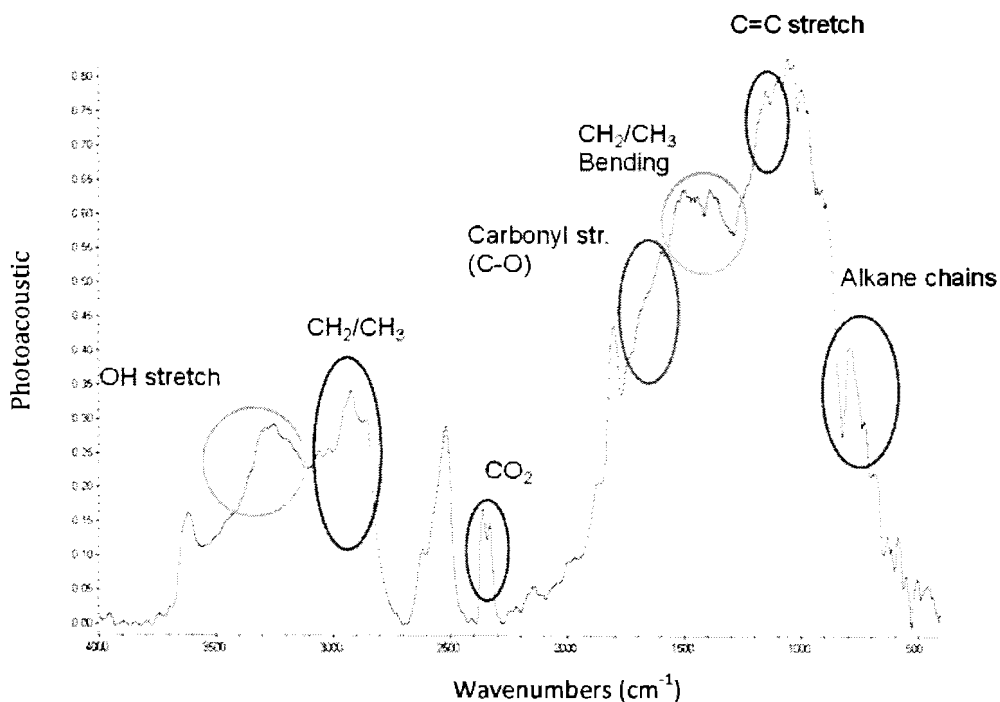
Figure 3.3. Spectrum of a dark colored oil shale parallel to the bedding plane showing the bands characteristic of Green River kerogen.

Important kerogen bands in our samples include the OH and NH$_2$ stretching bands in the region 3350 - 3250 cm^{-1}. There are characteristic aliphatic asymmetric and symmetric CH$_3$ and CH$_2$ stretching bands around 2950 – 2850 cm^{-1} as well as a band nearby at 3000 cm^{-1} representing aromatic CH stretch. The kerogen bands in the 1750 - 1500 cm^{-1} region are assigned to ester, ketone, and quinine components due to C=O and C=C stretching bonds. There are three strong distinct bands in the region 1637 cm^{-1} due to C=C stretch. Phenanthene bands are present in the 1550 - 1500 cm^{-1} region. A sharp, strong band at 1455 cm^{-1} is due to CH$_3$ asymmetrical deformation overlapped by CH$_2$ scissor vibration. Bands at 1400 – 1350 cm^{-1} are due to CH deformation as well as naphthalene and some mineral bands due to dolomite and calcite. In the region 1230 – 1150 cm^{-1} there are weaker C-O bands as well as bands of aliphatic ether (OCH$_3$) rocking vibration. Bands in the region of 1000 cm^{-1} are attributed to CCO stretching. There are two sharp, medium bands that are found at 870 cm^{-1} due to aromatic structures with isolated aromatic hydrogens and a 750 cm^{-1} band due to four adjacent aromatic hydrogens (Premovic, 2000). Lower bands around 756 cm^{-1}, 725 cm^{-1}, and 670 cm^{-1} are aromatic CH out-of-plane deformation vibrations and skeletal vibration of straight chain alkanes. All of these bands can be found in the light and dark colored regions. The bands that we have listed are all characteristic of kerogen, confirming that the kerogen molecule is present throughout the oil shale core, and is more dominantly present in the lighter-colored oil shale

samples. The light and dark colored oil shale bands, their intensities, and the kerogen and/or mineral bond assigned to certain bands were organized and are displayed in a table found in Appendix A.

Another band that was found in the oil shale spectra is the 2362 cm^{-1} and 2333 cm^{-1} bands characteristic of CO_2 which is not from the FTIR chamber. References found in literature comment that H_2O and CO_2 are major products in the effluent before and during the stage of hydrocarbon generation (Vandenbroucke, 2003). Other authors comment that decarboxylation results in formation of CO, H_2O, and CO_2 (Petersen, 2008) and kerogen gives off CO_2 and H_2S to produce a rubbery depolymer which gives off H_2S to form a tarry intermediate turning into bitumen leading to the formation of oil, coke, and gas (Yen, 1976).

3.4.3. Discussion of Results

Spectra from the dark and light colored locations throughout the core depth show characteristic bands of kerogen. Kerogen bands in the dark colored samples are overlapped with mineral bands from quartz, clay, pyrite, and calcite. Figure 3.4 shows the spectra of a light and dark colored oil shale sample, taken from the same location in the oil shale core, scanned parallel to the bedding plane at a frequency of 50 Hz. A comparison of the light and dark colored oil shale spectra show differences occurring in the 2000 – 800 cm^{-1} region. The dark colored samples parallel and perpendicular to the bedding plane have dominant mineral bands overlapping the kerogen bands due to

51

bonds from montmorillonite (MMT), analcite, dolomite, nahcolite, dawsonite,

and quartz. The light colored oil shale spectra is very similar to that of isolated

kerogen, displaying three distinct kerogen bands around 1600 cm^{-1}, 1455 cm^{-1},

and 1200 cm^{-1}. Results from comparing light and dark-colored depth regions of

the oil shale core suggest that the light-colored areas have a low mineral

content with a spectra similar to that of isolated kerogen and the dark-colored

samples have more mineral components which overlap some of the distinct

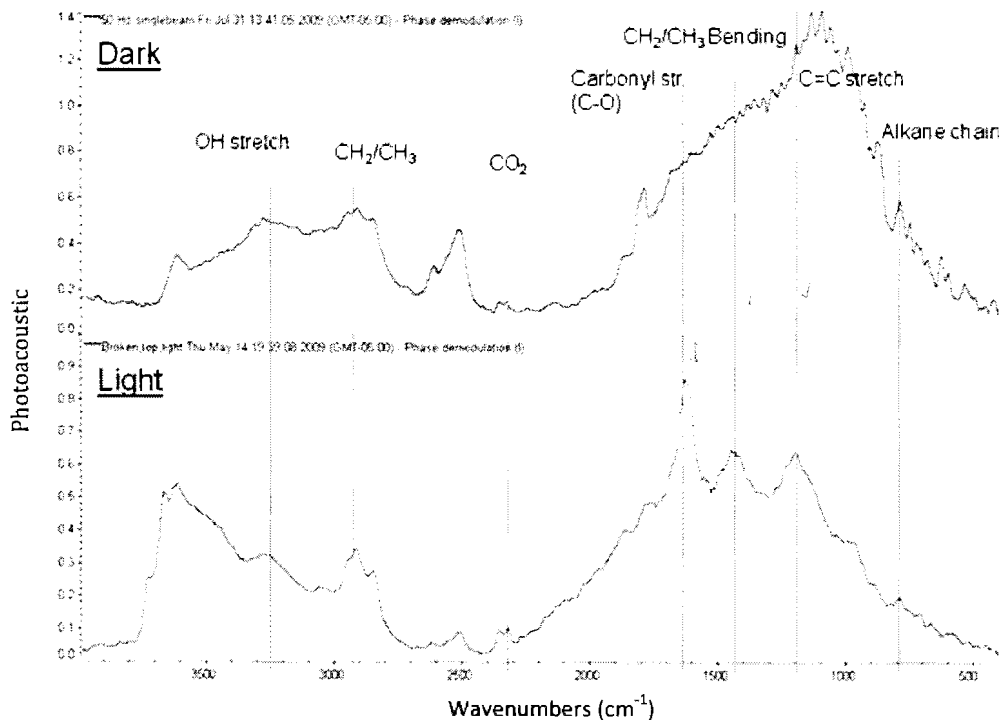kerogen bands.

Figure 3.4. Light and dark colored oil shale spectra parallel to the bedding plane at a frequency of 50 Hz. The kerogen bands are identified in the figure.

An advantage of the photoacoustic step-scan technique is that spectra

can be taken at different sampling depths of the same sample by changing the

scanning frequency. Depth sampling was performed on dark and light colored

52

oil shale parallel and perpendicular to the bedding plane in order to observe any depth changes occurring on a micron level in the samples. A representative spectra of depth sampling from a light and dark colored sample is shown in Figure 3.5. The samples were scanned at frequencies of 800, 500, 200, and 50 Hz resulting in a sampling depth of 12, 15, 24, and 48 μm. Results of sampling at different depths show that the lower frequency, or the deeper the sampling depth, a spectra will often have a stronger intensity in the region of 4000 to 1800 cm^{-1}, but a lower band intensity in the 1800 to 400 cm^{-1} region. As sampling depth decreases, or gets closer to the sample surface, the intensity tends to decrease in the 4000 to 1800 cm^{-1} and increases in the 1800 to 400 cm^{-1} region. Band intensity can be contributed to how many places the bonding group occurs in the sample, the phase of the sample, neighboring atoms/groups, and intra/inter – molecular bonds (Socrates, 2001). Similar results are seen in different light and dark regions as well as parallel and perpendicular to the bedding plane. Results indicate that some oil shale layers tend to have slightly more methyl-methylene bonds, hydroxyl groups, bicarbonate, and carbonyl (C=O). Other oil shale layers have more C=O, C=C, CH$_3$ and CH$_2$ deformation and scissor vibration, minerals, Si-O, C-O, CCO, and aromatic CH out of plane bonds. This suggests that kerogen is in small regions and is not uniform throughout the sample. At deeper sampling depths, the bulk characteristics of the sample are represented. Varying intensities at
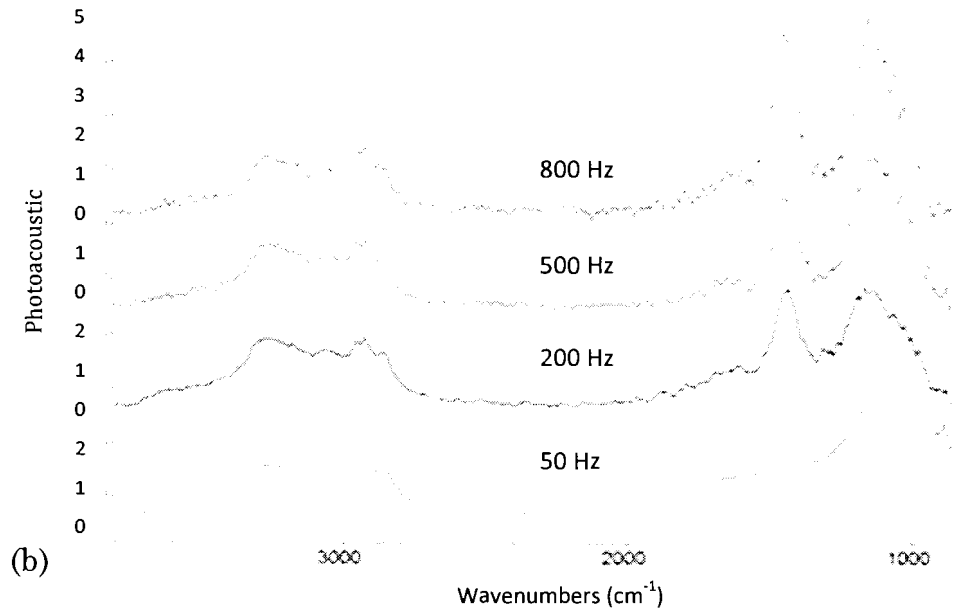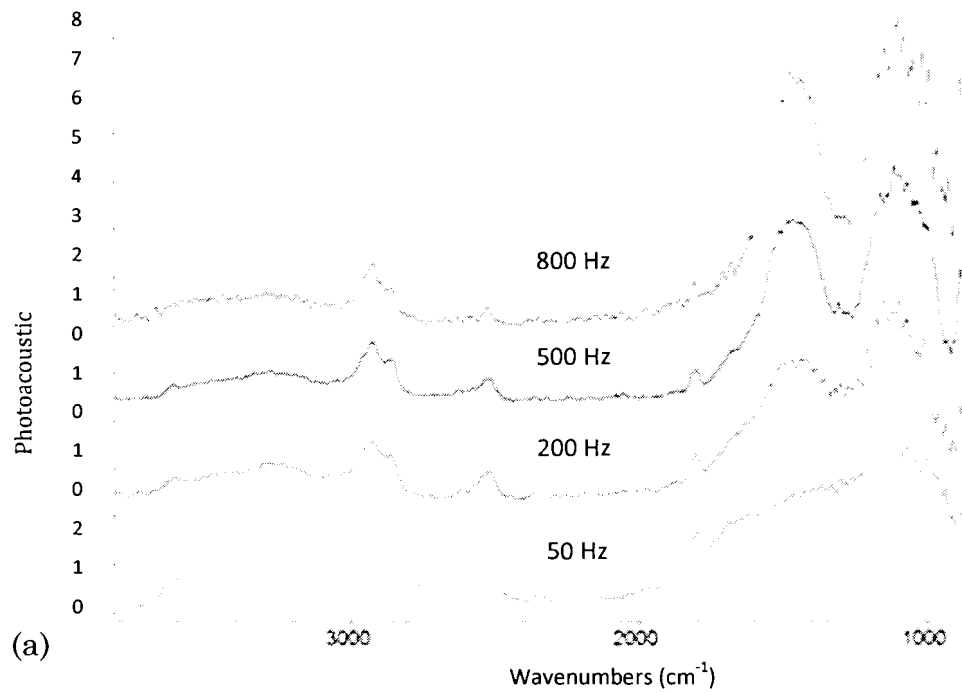
Figure 3.5. Spectra of sampling depth using the photoacoustic step scan method. The spectra shown is scanned parallel to the bedding plane on (a) dark colored oil shale and (b) light colored oil shale.

54

different frequencies suggest that there are compositional differences occurring in the oil shale indicating layering at the micron scale. The nature of the oil shale due to the environment from when it was formed and has undergone over time can contribute to varying oil shale composition as well as molecular interactions. Oil shale is a mixture of kerogen, bitumen, and minerals that may not be evenly distributed throughout the sample resulting in slightly different sampling depths than what have been calculated (Katti, 2003) (Rosencwaig, 1976).

Comparing spectra that was taken parallel and perpendicular to the bedding plane, there seems to be identical features independent of the sample orientation. An example of orientation similarities is shown in Figure 3.6 of a light and dark colored oil shale sample scanned at a frequency of 50 Hz parallel and perpendicular to the bedding plane. The parallel and perpendicular bands in any given sample are very similar in wavenumber and intensity, indicating uniformity throughout the sample. There were also no orientational differences parallel and perpendicular in spectra that was scanned at the same frequency of 50 to 800 Hz. To clarify, there are spectra changes occurring at different frequencies or sampling depths, but no noticeable differences between parallel and perpendicular spectra of the same frequency. These similarities support the similar depth changes which occur in both the light and dark-colored regions parallel and perpendicular to the bedding plane.
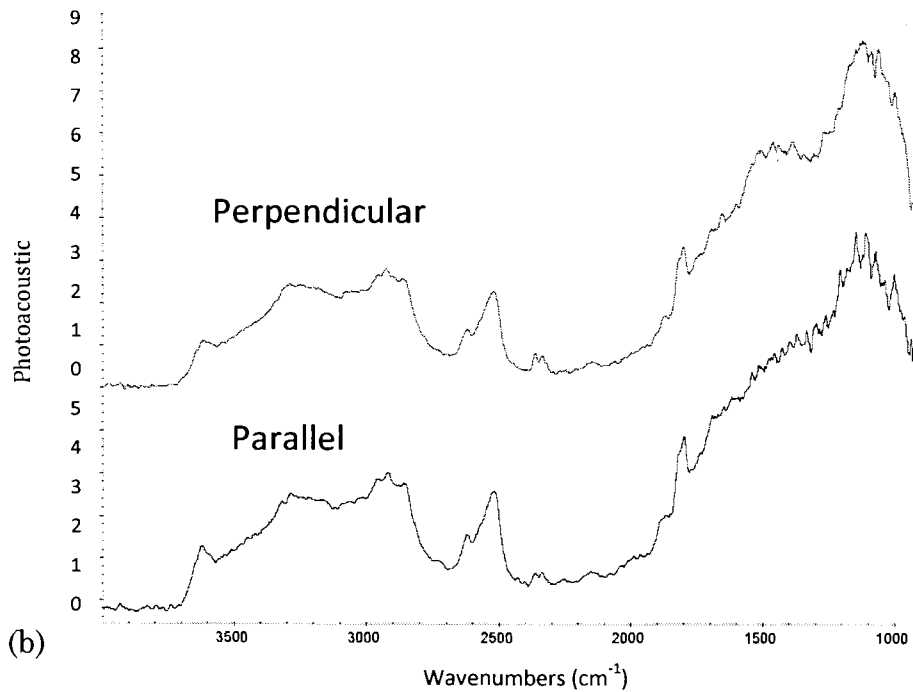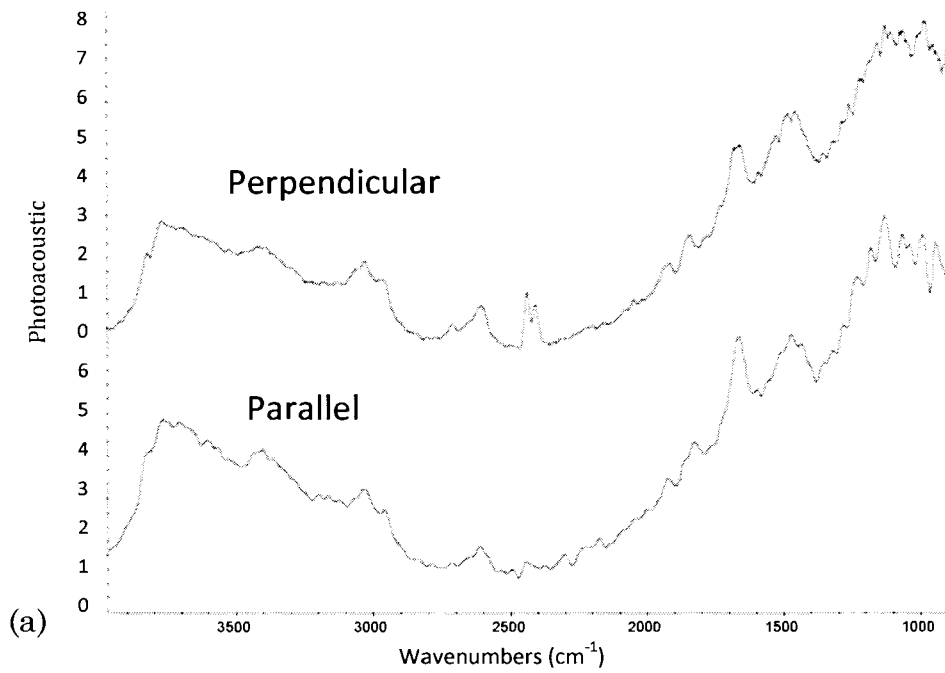
Figure 3.6. Oil shale scanned at 50 Hz parallel and perpendicular to the
bedding plane. The spectra is of (a) light colored oil shale and
(b) dark colored oil shale

56

The main objective for this experiment was to identify any structural changes to kerogen due to mineral interactions. In order to verify any structural changes of in situ oil shale the kerogen bands were analyzed and compared to isolated Green River kerogen from literature. Changes or band shifts were noticed in band assignments between isolated and in situ kerogen and is shown in Figure 3.7. Spectra of light and dark colored samples from photoacoustic analysis indicate a presence of aromatic structures with a band at 3065 cm^{-1} and also a band at 1600 cm^{-1} in the dark-colored samples which is not often seen in isolated kerogen. The C=O carbonyl stretch at 1700 cm^{-1} in

Figure 3.7. Spectrum of a light and dark colored oil shale scanned parallel to the bedding plane showing band shifts.

Robinson's Green River isolated kerogen sample was found at 1637 cm^{-1} in our Green River oil shale samples. This indicates a band that has shifted down about 50 cm^{-1}. There is another ~50 cm^{-1} band shift in the dark colored oil shale sample located at 1500 cm^{-1} which is attributed to CH_3 asym def and CH_2 scissor vibration. This band is found in literature and in our lig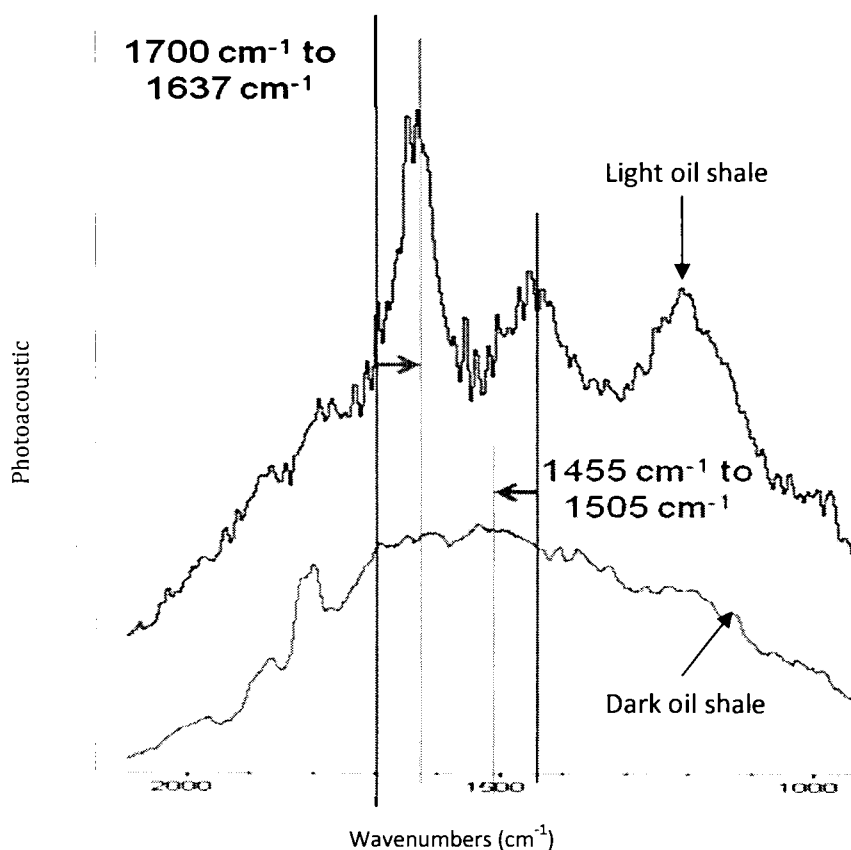ht colored sample at 1455 cm^{-1}. In situ kerogen also shows CH out-of-plane deformation shift from three adjacent hydrogen atoms on a ring from bands in the 1200 - 1000 cm^{-1} region which is higher than the C=C stretching bands of isolated kerogen from literature around 1000 cm^{-1}. Band changes would signify that there are interactions on the molecular scale occurring between the kerogen and mineral components. The band shifts that we have mentioned are related to bonds containing oxygen and the mineral bands signature of quartz and pyrite which is known to have a strong interaction with the kerogen.

3.5. Conclusion

1) Step Scan Photoacoustic FTIR results comparing light and dark colored regions of the oil shale core suggest that the light region of shale samples exhibit spectra similar to that of Green River isolated kerogen that was found in literature with distinct characteristic bands at 3450, 2900, 1700, 1450, and 1050 cm^{-1}. The dark colored sample spectra have more mineral components bands (sometimes overlapping kerogen bands) at 2500, 1800, and 1200 – 1000 cm^{-1} due to clay, quartz, dolomite, and calcite minerals all found in Colorado marlstone.

2) The band shifts observed in the spectra relating to bonding with oxygen and

   pyrite strongly suggest that the mineral components have a molecular

   interaction with the kerogen molecules.

3) Varying intensities at different frequencies suggest that there are

   compositional differences occurring in the oil shale on a micron scale

   indicating layers.

4) Parallel and perpendicular spectra at the same frequency indicate

   uniformity throughout the sample with no orientational properties.

CHAPTER 4. ELECTRON MICROSCOPY STUDY OF IN SITU GREEN RIVER KEROGEN

4.1. Introduction

The scanning electron microscope (SEM) images a sample's surface by scanning it with a high-energy beam of electrons. The electrons from the beam interact with the atoms on the surface of the sample which then produces a signal containing information about the surface topography and composition. Advantages of SEM images are that there are no image artifacts and it has a depth of field on the scale of millimeters, providing a three-dimensional image with details of about 1 – 5 nm in size. The objectives for performing SEM were to better understand the micro- and macro- structure of kerogen and minerals in oil shale. We are interested in determining the size and layout of pores, minerals, and kerogen as well as any compositional differences in various colored regions, depth locations, and orientation qualities. EDS data was used to show the relative amount of carbon present in certain areas for comparison of more carbon-rich regions, and is not used as an exact amount of carbon present.

4.2. Literature Review

SEM has been performed on oil shale in various regions of the United States. Oil shale samples from Kentucky and Mississippi were broken and examined perpendicular to the bedding plane. Images showed numerous open channels or micropores contributed to the open packing of particles. This is

60

caused by the presence of organics suggesting migration pathways (O'Brien, 1994). SEM has also been performed on oil shales around the world. Samples from the Messel Pit in Germany show clay minerals often covered by amorphous organic matter in layers of 10 μm long and 2 μm thick (Nix, 2003). Similar experiments have been performed on other oil shales from Germany showing minerals mixed with organic matter occuring in finely-dispersed, thin layers (Eseme, 2007). Vandenbroucke used the backscatter electron microscope to find organic matter appearing black due to the low atomic number and was found in elongated shapes, parallel to the bedding plane, in the size of 2 – 5 μm thick (Vandenbroucke, 2007).

The Gunflint Formation in Ontario, Canada, is made up of quartz chert. Microscope images show dense brown kerogen in a matrix of microquartz and in other location kerogen is located on the grain-boundary of the microquartz next to pores the size of 100 nm (Moreau, 2004). SEM images and EDS microanalysis show kerogen surrounding quartz grains having a high oxygen and sulfur content. The distribution of kerogen in the oil shale was varied and random.

4.3. Materials and Methods

4.3.1. Sample Preparation

Light and dark colored oil shale samples were prepared for SEM analysis from several locations in the seven foot core with known orientation parallel and perpendicular to the bedding. Broken oil shale samples used for

61

SEM imaging were about 3 mm thick with sampling area of 6 x 6 mm. Samples were attached to aluminum mounts using colloidal silver or carbon adhesive tabs, then coated with a conductive gold coating (about 20 nm thick) to provide an electrical ground from the sample to the plug. Cross-sectional polished samples were cut with a diamond-wafering blade into 1 x 10 x 11 mm. The 1 mm side was the surface that was cross-sectional polished for SEM examination. Refer to Appendix B.2 for additional sample preparation details.

4.3.2. Methods and Technique

The x-rays that are emitted are from the inner K, L and M electron shells of a sample having unique and identifiable wavelengths. We found the energy bands of each element to make sure the elements in the oil shale didn't overlap with each other or with the gold coating band. Table 4.1 shows a list of the elements and their corresponding energy band assignments. An energy discriminating system (EDS) sends the x-ray beam through a detector and divides the resulting signal by a multichannel pulse height analyser providing data on the chemical composition of a sample's surface.

A JEOL JSM-6490LV Scanning Electron Microscope [JEOL USA, Peabody MA] was used. An Oxford Isis Energy Dispersive System (EDS) was also performed on the oil shale samples. A beam current of 3 nA, and acceleration voltage of 15 keV. Energy Dispersive X-ray data was collected using a Nanotrace EDS detector equipped with a NORVAR light element

window [ThermoScientific, Madison WI] coupled with a Noran System Six

imaging system 202 [ThermoScientific, Madison WI].

Table 4.1. Energy bands of all the elements assumed to be in
Green River oil shale

Element	K-α (keV)	L-α (keV)	M-α (keV)
C	0.282		
N	0.392		
O	0.523	0.341	
Na	1.04	0.705	
Mg	1.254		
Al	1.487		
Si	1.74		
Au		9.712	2.122
K	3.313		
Ca	3.691		
Fe	6.403		

Cross-sectional polished samples were mounted to a molybdenum block

using Crystalbond™[Ted Pella, Redding CA]. Surfaces were exposed using a

JEOL IB-09010CP Cross Sectional Polisher [JEOL USA, Peabody MA]. Argon

milling conditions were 5kV accelerating voltage for 6 hours. The sample was

pivoted +/- 30° during polishing cycle.

63

4.4. Results

The first step was to determine what type of samples would provide us with the best information of in situ kerogen and oil shale minerals. Our first set of samples were from the dark colored region of the oil shale core at a depth of 571 ft @ 15 cm. The SEM images of these first samples examined parallel to the bedding can be seen in Figure 4.1. These images show a very rough surface with smooth flakes and crushed minerals. There were a lot of cavities present and the surface was too rough for proper EDS performance. The second set of samples were prepared by cutting the oil shale core into small sections with a diamond cutter parallel to the bedding plane Figure 4.2 shows the results of these images. We could see from these images that the oil shale samples cut with the diamond cutter were impacted by the blade since there are smooth regions, loose particles, and the original sample surface underneath. Since our objective was to view kerogen in its original in situ state without any alterations, the rest of our samples were broken parallel and perpendicular to the bedding plane and smoother surfaces were imaged. SEM images of light colored oil shale examined parallel to the bedding plane are shown in Figure 4.3. The images show minerals with flat smoother surfaces, minerals looking similar to that of quartz, and some lighter colored flaky sheets. A closer examination of the flaky sheets (Figure 4.3c) shows a complex matrix of solid minerals held together with a dark-phase material looking similar to cracks on the surface. An EDS analysis of this region would confirm the presence of

64

kerogen, represented by a carbon peak, and provide us with the mineral elements most closely associated with the organic phase.
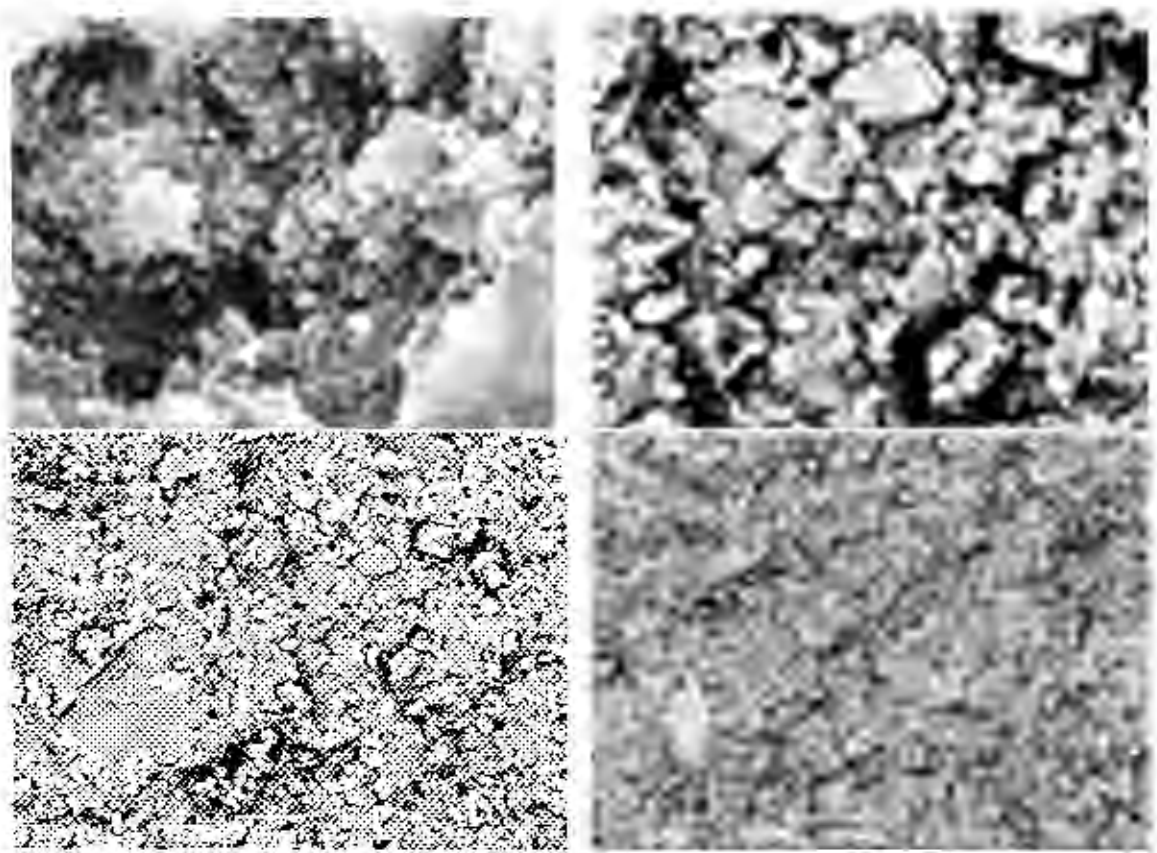

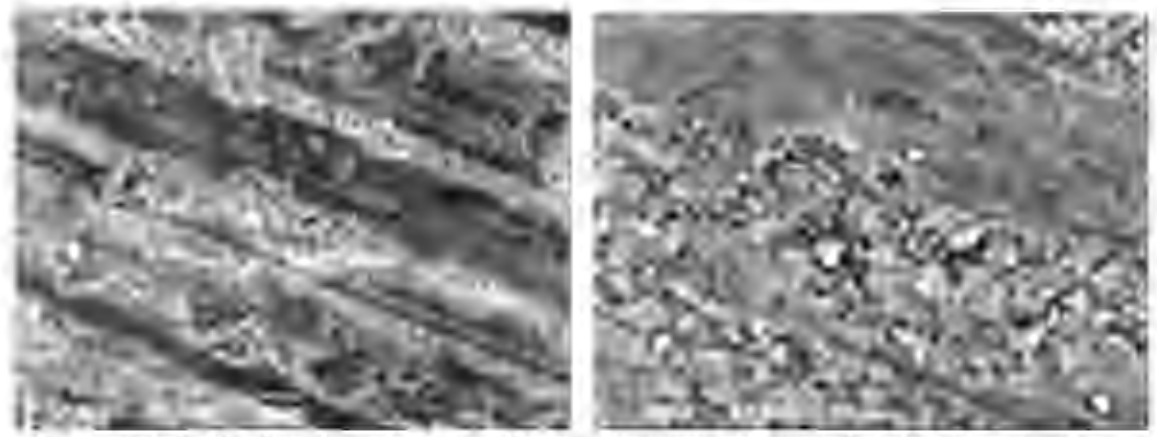Figure 4.1. Dark colored Green River oil shale broken and examined parallel to the bedding plane.

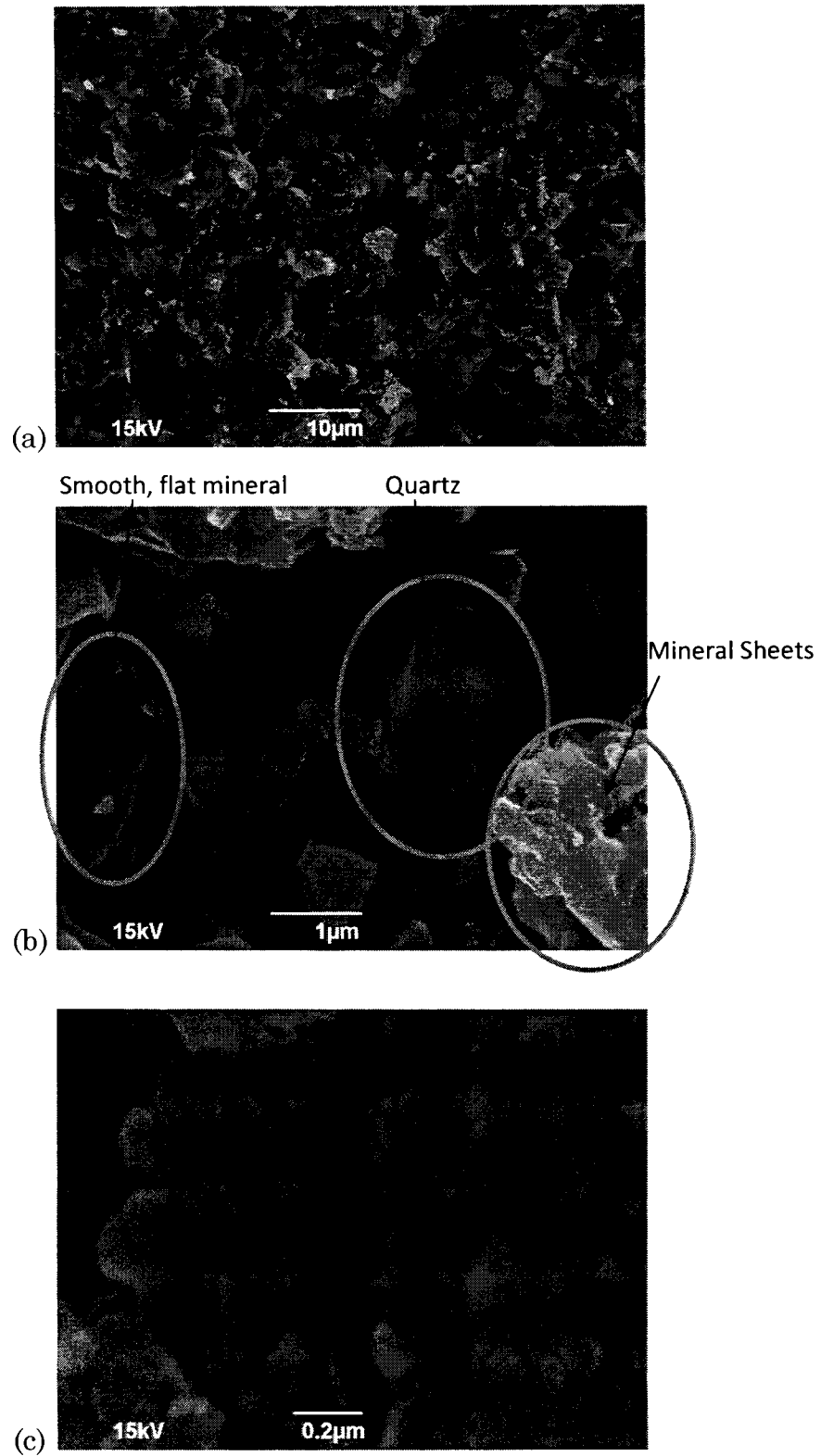Figure 4.2. Dark colored Green River oil shale diamond cut and examined parallel to the bedding plane.

(a)

Smooth, flat mineral   Quartz

Mineral Sheets

(b)

(c)

Figure 4.3. Light oil shale scanned parallel to the bedding plane. The scale is at (a) 10 µm, (b) 1 µm, and (c) 0.2 µm

An EDS analysis was performed on the light colored region shown in Figure 4.3.b. Six different locations were tested and the EDS data is shown in Figure 4.4. The elements present in this region of the light colored oil shale sample are carbon, silicon, aluminum, potassium, oxygen, a small amount of sodium and chlorine. The presence of these elements suggest that montmorillonite is present due to sodium, aluminum, silicon, and oxygen. Quartz is present due to silicon and oxygen. K-feldspar is present due to the potassium, silicon, oxygen, and a trace of aluminum. Kerogen is also confirmed to be present in this whole region due to the presence of a carbon band. All the carbon present belongs to kerogen since there is no carbon in any of the minerals present. All EDS spectra for light colored oil shale were very similar confirming these minerals of clay, quartz, and k-feldspar are present in the light colored oil shale. Additional EDS spectra taken of light colored oil shale samples can be seen in Appendix E. The results from the EDS analysis and SEM images show that kerogen is present in these regions and is most closely associated with quartz and clay minerals. The atom % for each EDS scan was given as a rough estimate of the amount of carbon present in that scan. According to the atom % data, the area with the most carbon was in the region of point 5 and 2. The second largest carbon content was found in area 3 on the flakey surface, most likely sheets of clay.
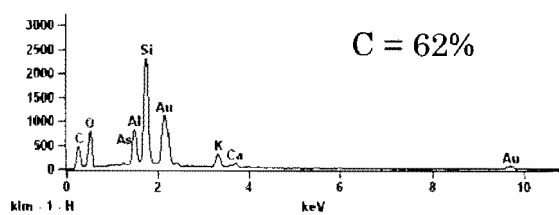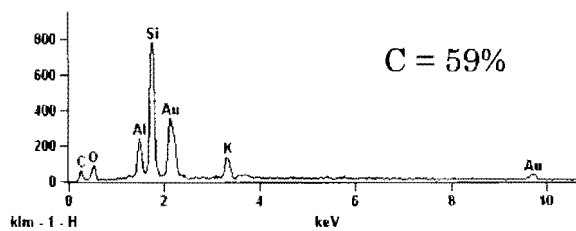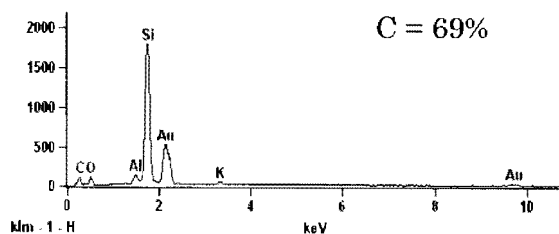
Point 1

C = 48%

Point 2

C = 64%

Point 3

C = 62%

Point 4

C = 59%
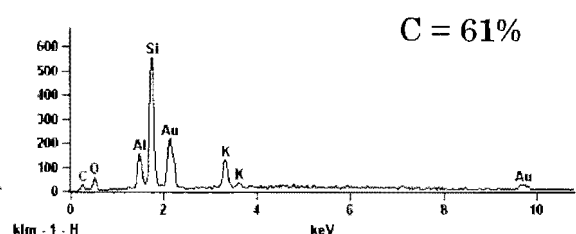
Point 5

C = 69%

Point 6

C = 61%
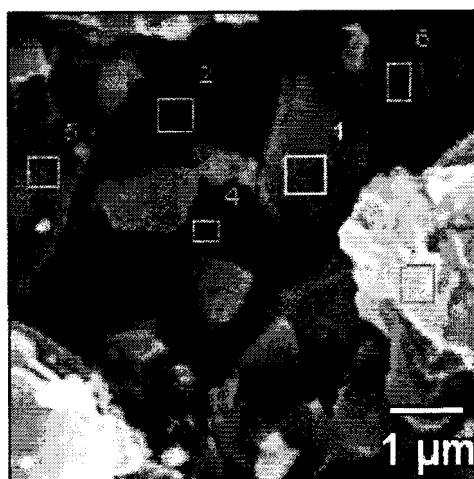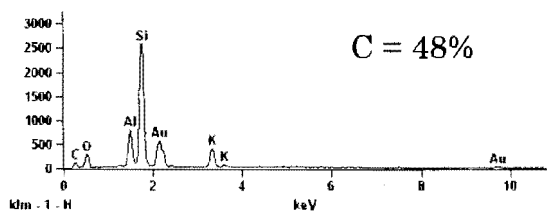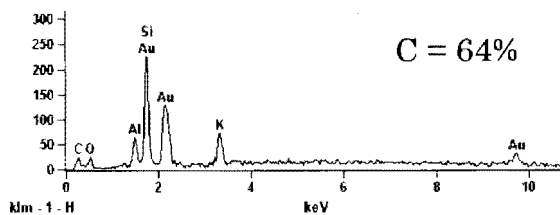
Figure 4.4. EDS data of light colored oil shale parallel to the bedding plane

68

Dark colored oil shale samples broken parallel to the bedding plane were also imaged with the SEM. Images show similar features to the platey structures seen in the light parallel samples. There are also rounded minerals and regions of a mineral matrix consisting of small crushed minerals held together with a binding material. Figure 4.5 shows SEM data of a dark colored oil shale broken parallel to the bedding plane. With many phases and features present, it was important for us to determine where the most kerogen was present and with what minerals it was associated with. An EDS analysis was performed on the dark colored oil shale and the results are shown in Figure 4.6. The elements that are present in all of the dark colored oil shale EDS spectra include calcium, silicon, magnesium, oxygen, some aluminum and sodium, iron and carbon. These elements confirm the presence of the mineral pyrite due to the presence of iron. There is also clay and analcite distinguished by the elements sodium, calcium, aluminum, silicon, and oxygen. A large amount of calcite and dolomite is in the dark colored oil shale due to large amounts of calcium, magnesium, oxygen, and carbon. The carbon bands are larger in dark colored samples, but does not mean that there is more carbon present since each element band has its own intensity. For instance, when a high amount of silicon is present, the carbon band appears smaller, but the actual amount of carbon present could be the same or even greater. The atom % from the EDS data
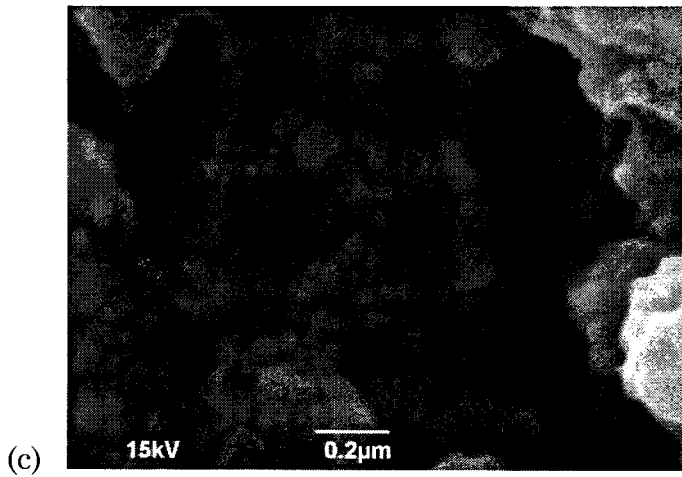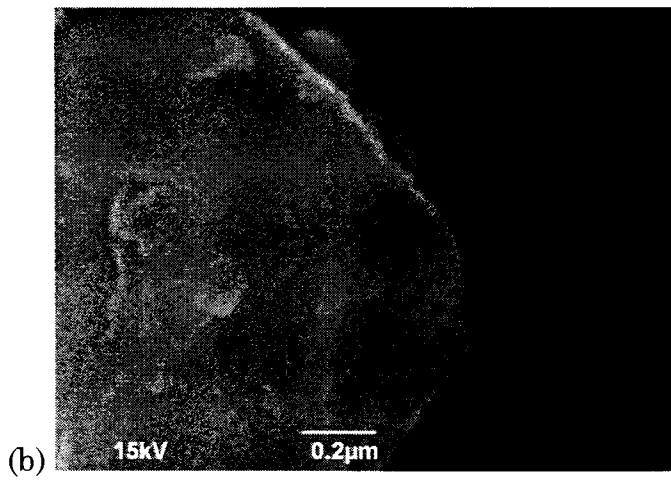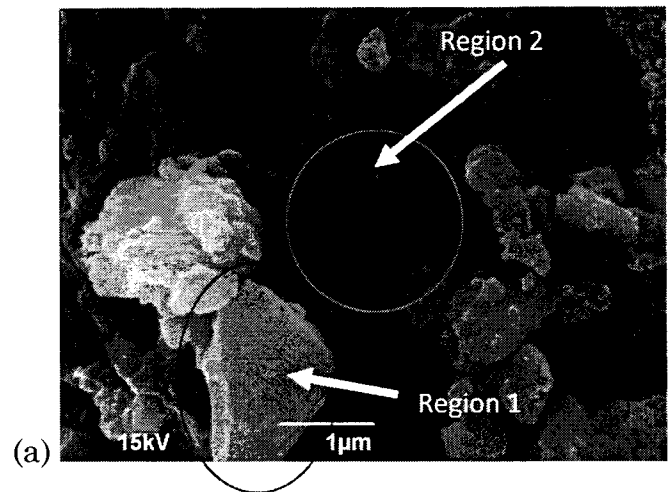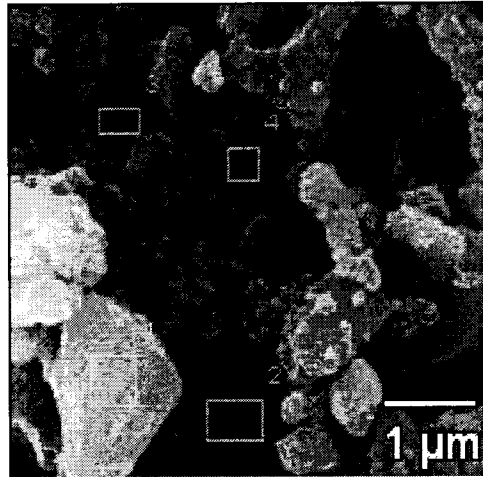
Figure 4.5. Dark colored oil shale samples broken and examined parallel to the bedding plane. The scale of (a) 1 μm , (b) enlargement of region 1, and (c) enlargement of region 2

is now important in determining how much kerogen is present in the dark colored oil shale. Calcite and dolomite both require a certain amount of carbon, more precisely two carbons to six oxygen to one magnesium and calcium atom. A conservative estimate of the left-over carbon was calculated and is displayed in Figure 4.6. Additional SEM images and EDS data can be found in Appendix E. After analysis, the most carbon appears to be located on the distinct mineral. Since no pockets or large areas of kerogen or carbon-rich regions were found or seen at a scale of 200 nm, this suggests that kerogen is on the mineral grain-boundaries in the scale of tens of nanometers.

Another SEM sample preparation was used by polishing the original oil shale samples with a cross-sectional polisher preparing them for examination in the SEM. Similar samples were cross-sectional polished and SEM images were taken. Figure 4.7.a shows an image of a light colored oil shale sample taken with the SEM looking parallel to the bedding plane. The minerals were all under 10 µm and varied in size. There are four shades of color contrast that can be identified representing difference densities of material. Figure 4.7.b shows an image of a light colored oil shale sample taken with the SEM looking perpendicular to the bedding plane. There were some larger size mineral grains as well as more small, fine minerals. The phase of tiny light and dark regions (sponge-like material) is also seen in these images. The perpendicular samples also had unique features of smooth surfaces with minerals embedded
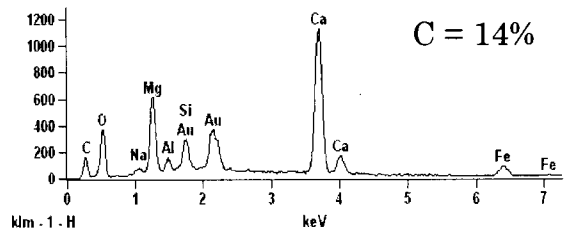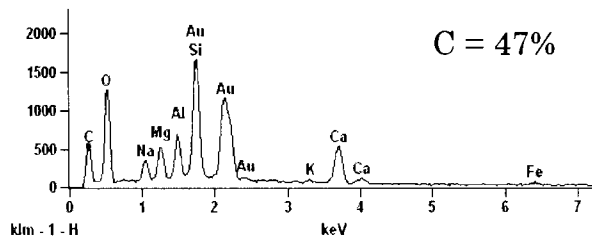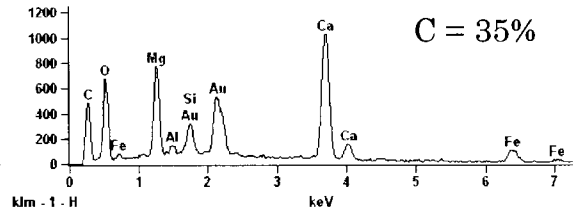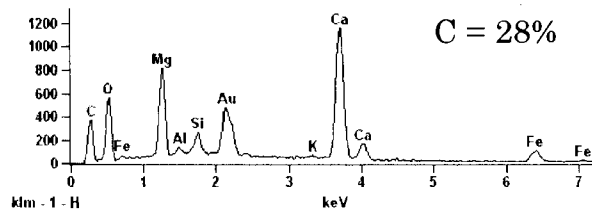
Figure 4.6. SEM image of a dark colored oil shale broken parallel to the bedding plane

within them and pores of 1 μm in size. Figure 4.7.c shows an SEM image of a

dark colored cross-sectional polished oil shale sample looking perpendicular to

the bedding plane. There seems to be some more frequent elongated minerals

and three phase contrasts of black, gray, and white. There are very small

minerals but not small enough to make the sponge-like appearance of the light
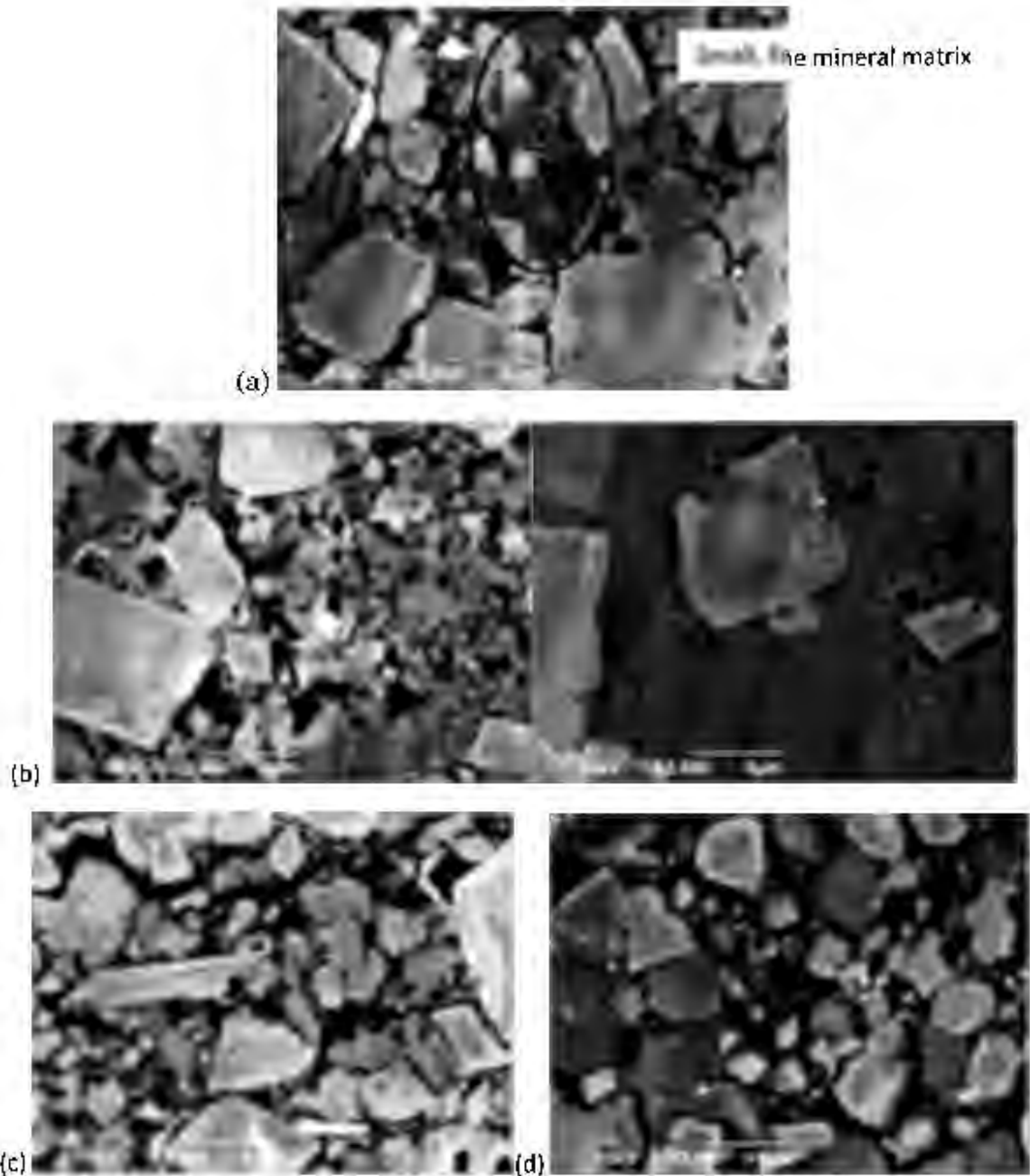
Figure 4.7. SEM images of cross-sectional polished oil shale. The images are of (a) light parallel (b) light perpendicular (c) dark perpendicular (d) dark parallel to the bedding plane

parallel samples. Figure 4.7.d shows an image of a dark colored oil shale sample taken with the SEM looking parallel to the bedding plane. This images shows rounded minerals with less crushed minerals and no sponge-like areas.

73

The most noticeable difference between the cross-sectional polished and broken samples was the very finely crushed or sponge-like texture seen in the cross-sectional polished samples. This feature was more noticeably present in the light colored samples examined parallel to the bedding plane. When a larger scan-size of the cross-sectional polished samples were examined, it was also clear that there seemed to be some orientational differences between the samples examined parallel and perpendicular to the bedding plane. SEM images of the cross-sectional polished dark and light colored samples are shown in Figure 4.8 looking parallel and perpendicular to the bedding plane.

The light-parallel image shows minerals of maximum size of 50 μm long down to regions of small, fine material. There are four noticeable phases of black, dark gray, light gray, and white. The SEM images were taken in backscatter mode so the darker regions are less dense representing organic material while lighter regions are more dense minerals such as pyrite. The light perpendicular images had several regions of varying color contrasts and textures on this surface. There are the medium gray and light gray minerals all less than a size of 40 μm surrounded by minerals and pores. Then there is the long strips of dark gray material that, upon closer examination, is very smooth with some pores on the surface and minerals are randomly embedded. There appears to be alternating layers of the dark gray material and the lighter minerals suggesting orientational pathways. The dark parallel sample is similar to the light parallel sample in minerals sizes and distribution with

similar color phases distinguishing different types of minerals. The only difference is dark spots that seem to be placed in or on top of light gray minerals in the dark parallel sample. The dark sample imaged perpendicular to the bedding plane shows similar mineral sizes and distinguishable mineral color phases. This image has some elongated cracks in the core sample that are parallel to the bedding plane. The dark perpendicular sample also appears to have layers of crushed and larger minerals creating pathways for migration. There appears to be a physical orientational difference seen in the oil shale. These differences are seen upon examination of the material and cracks lined parallel to the bedding plane supporting or evident from the fact that the oil shale had undergone heavy pressure and temperature changes over time.

An EDS spectrum was also taken of light colored oil shale perpendicular to the bedding plane that was polished with the cross-sectional polisher. Figure 4.9 shows areas of crushed minerals surrounded by a dark phase, light gray, medium gray, and dark gray areas. EDS analysis was performed on three different regions and the carbon content of each region is provided. The first spectrum is from point 1 showing elements of carbon, oxygen, sodium, aluminum, silicon, and traces of magnesium and calcium. Region 1 appears to be made up of one mineral, most likely clay. Region 2 has the elements of carbon, oxygen, sodium, magnesium, aluminum, silicon, calcium, and iron. There are strong amounts of calcium, magnesium, carbon, and oxygen so this is probably a dolomite mineral with some kerogen present. Region 3 is made of
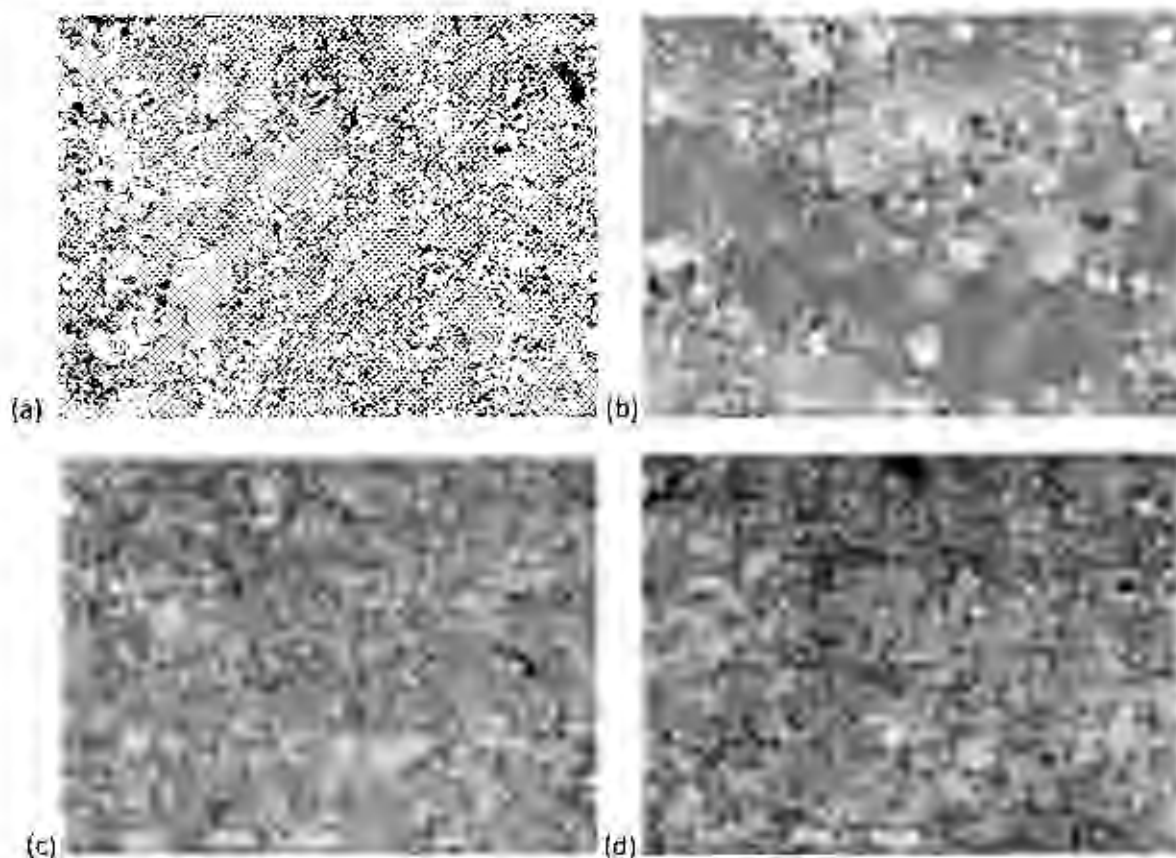
Figure 4.8. SEM images at a scale of 50 um showing orientation. Images are of (a) light parallel, (b) light perpendicular, (c) dark parallel, and (d) dark perpendicular to the bedding plane

a finely crushed mineral matrix. EDS data shows this region to contain the elements silicon, oxygen, and trace amounts of potassium, calcium, magnesium, sodium, and carbon. The carbon content for each EDS point is displayed in Figure 4.9 and shows that Region 3 had the most carbon at about 35% compared to 22% in Region 1 and 28% in Region 2. The EDS data confirms that more kerogen is present in the crushed mineral matrix and acts as a binding material. The size of the kerogen is assumed to be on the scale of tens of nanometers.
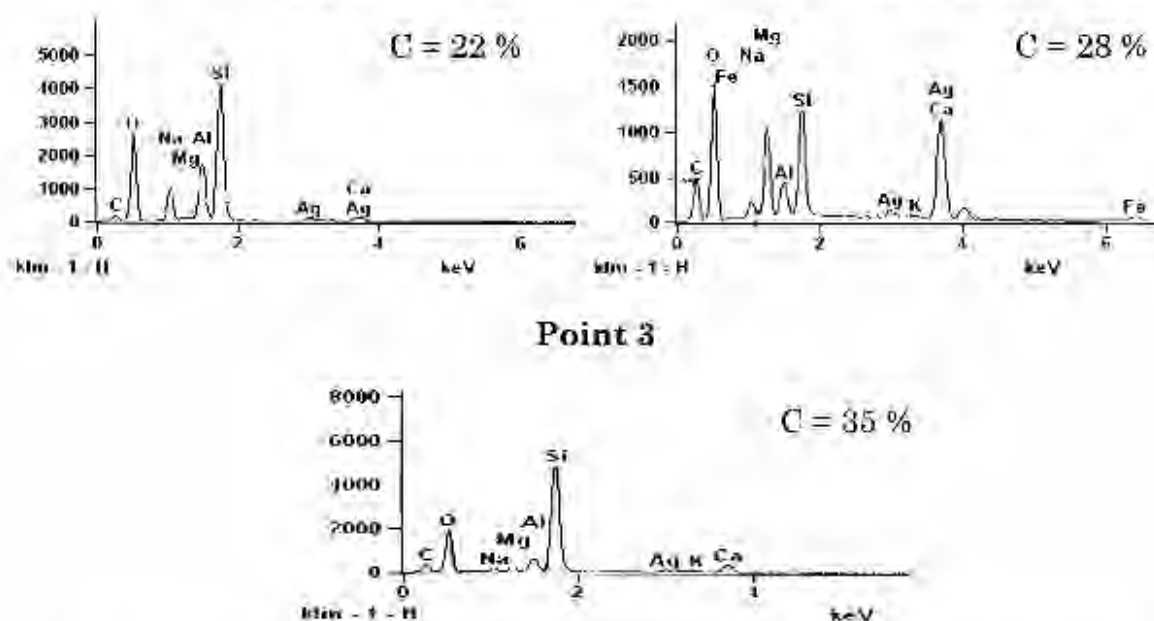
Figure 4.9. Light colored oil shale samples where EDS was performed perpendicular to the bedding plane. Data was collected at points 1, 2, and 3.

There were no pockets of noticeable regions of kerogen in any of our images but there is the assumption that the kerogen is adsorbed onto the mineral surface (Nix, 2003) (Vandenbroucke, 2007). SEM images and EDS

77

data of regions with very fine mineral grains surrounded by kerogen were confirmed by Figure 4.9. Another region of the oil shale that was high in kerogen content was the flakey sheets found in the light and dark colored samples broken parallel and perpendicular to the bedding plane. An SEM image of this region is shown in Figure 4.10. The EDS spectrum for this region shows strong amounts of silicon with trace amounts of carbon, oxygen, sodium, aluminum, and potassium. This region is most likely made up of quartz and clay minerals with a large amount of kerogen present. This type of discovery, of the significant amount of carbon in the crushed regions, leads us to conclude that the Green River kerogen is at the scale of tens of nanometers adsorbed onto mineral surfaces of quartz and clay, acting as a binder agent. The close proximity of the nano-size kerogen to the oil shale minerals will likely have some non-bonded interactions occurring between the minerals and organic

Figure 4.10. Light colored flakey sheet of oil shale broken parallel to the bedding plane

phase. Previous work by the Katti group has shown how bonded and non-bonded interactions between materials has an effect on their overall properties (Bhowmik, 2007) (Katti, 2006) (Khanna, 2009) (Ghosh, 2007) (Sikdar, 2006).
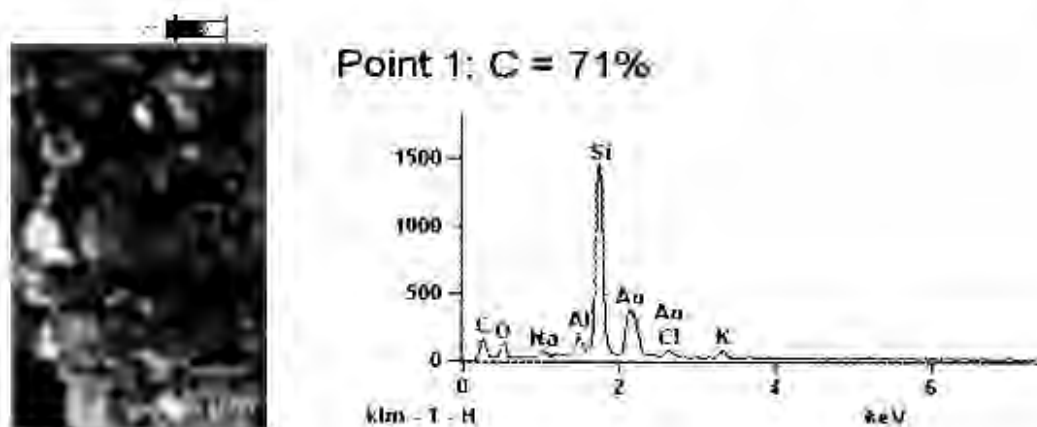
The elements found in our Green River oils shale confirm the Marlstone minerals and presence of kerogen. EDS spectra of dark oil shale samples show elements of carbon, oxygen, magnesium, silicon, sulfur, calcium, potassium, sodium and iron. These elements confirm the presence of the minerals of pyrite, analcite, quartz, clay, dolomite, calcite, and kerogen in dark colored oil shale samples. Elements found in the light colored samples consist of sodium, aluminum, strong amounts of silicon, oxygen, calcium, and carbon. Minerals assumed to make up the light colored regions include quartz, clay, K-feldspar and organic material of kerogen. The carbon content of all the EDS data taken of light and dark oil shale was analyzed to determine if there was a carbon content difference. It was found that there was more carbon content in the light colored samples with a total of ~52% carbon content compared to the dark colored samples having 42% carbon content. This would confirm our previous FTIR studies concluding that there is more kerogen present in the light colored regions than the dark colored regions with no significance to the orientation. These images have shown that all the samples of light and dark colored oil shale are made up of similar material. The minerals are in the size of 50 μm to very small, fine material imbedded between mineral components.

4.5. Conclusion

Light samples have a relative amount of more kerogen according to EDS data suggesting a 52% carbon content in light oil shale compared to ~42% in dark colored oil shale. The light colored samples have the minerals of quartz, k-feldspar, and clay. Dark colored sample minerals include pyrite, dolomite, calcite, analcite, clay. The higher kerogen content or more presence of carbon in light colored oil shale samples would suggest that kerogen is more closely associated more with the minerals quartz, K-feldspar, and clay. Perpendicular to the bedding plane samples appear to have orientation with alternating layers and more elongated cracks and mineral orientation. No large pockets or distinct regions of kerogen were seen at a scale of 300 nm suggesting kerogen is in spaces in the order of tens of nanometers. The small kerogen size would put the organic phase in very close proximity to that of the mineral phase. Due to the close proximity, it is very likely that the minerals may have a significant impact on the kerogen with non-bonded interactions that would have an effect on the organic phase.

CHAPTER 5. ELASTIC MODULUS AND LOAD DEFORMATION BEHAVIOR OF IN SITU GREEN RIVER KEROGEN

5.1. Introduction

Nanoindentation experiments measure the force and displacement of an indentation into a sample surface. The indentation load-displacement data can then be used to determine a sample's mechanical properties such as hardness and elastic modulus. These values are important in the study of Green River oil shale because the pressure environment experienced by kerogen and its orientation within the shale could play an important role in the oil extraction (Zeszotarski, 2004). The objective for performing nanoindentation on oil shale was to measure the mechanical properties (elastic modulus and hardness values) of kerogen and surrounding mineral components in order to determine if there is a distinguishable difference between light and dark colored oil shale as well as orientation properties parallel and perpendicular to the bedding plane. The intent of this study is to examine oil shale on a micro- and nano-scale in order to determine if the organic kerogen is affected by, or has an effect on, the properties of the mineral components.

In situ studies are important when trying to determine the elastic properties of kerogen as well as the interactions with the mineral matrix since oil shale is a multiphase composite. Ex situ or isolated samples lose their orientation along with any properties that it may have had while surrounded

by the oil shale minerals. In situ kerogen allows the examination of anisotropy due to lithostatic and hydrostatic pressure forces that has been experienced by the kerogen during burial, which can be seen in the mechanical properties of kerogen. This study can be used to provide information on how the elastic properties of kerogen effect the macroscopic properties of the oil shale. Oil shale samples were examined parallel and perpendicular to the bedding plane to obtain orientational data as well as determine the significance of varies nanoindentation depths.

5.2. Literature Review

In literature, there have been only two in situ studies of the elastic properties of kerogen using nanoindentation (Zeszotarski, 2004) (Ahmadov, 2009). Zeszotarski et al. found the kerogen to be isotropic or to have similar elastic properties irrelevant to the direction of indentation on the bedding plane. He concluded that the mechanical properties of kerogen show elasticity as well as plasticity behavior. Elasticity being the physical property of a material that returns to its original shape after the stress that caused deformation is removed. The relative amount of deformation is called the strain. Plasticity describes the deformation of a material undergoing non-reversible changes of shape in response to applied forces (Lubliner, 2008). Ahmadov performed nanoindentation experiments on Bazhenov Formation oil shale and found kerogen to have a Young's modulus value of 10 – 15 GPa and hardness of 0.57 GPa, coinciding with the values found by Zeszotarski

82

(Ahmadov, 2009). Mechanical analysis of shale alone has also been performed with results showing the particle stiffness to be anisotropic while the strength is isotropic (Bobko, 2008).

5.3. Materials and Methods

5.3.1. Sample Preparation

Light and dark colored oil shale samples were taken from various depths of the Green River oil shale core. The samples were cut with a diamond-wafering blade into 4 x 6 x 3 mm cubes perpendicular to the bedding plane and 5 x 5 x 3 mm cubes parallel to the bedding plane. They were then mounted onto 10 mm stainless steel discs. For nanoindentation tests a very smooth, level surface is required. Cut samples were first polished with 1000 and 4000 microcut silicon carbide grinding paper. They were then polished with diamond compound paste of grit size 1 μm, 0.5 μm and 0.1 μm. A finishing polish was performed with 0.02 μm non-crystallizing colloidal silica polishing suspension. Afterwards, samples were rinsed with de-ionized water and left to air dry. Refer to Appendix B.3 for a more detailed sample preparation procedure.

5.3.2. Methods and Technique

Nanoindenation tests were performed using the nondestructive contact mode. A Triboscope nanomechanical testing instrument [Hysitron Inc., Minneapolis, MN] capable of a load resolution of 1 nN and a displacement resolution of less than 1 nm was used for all experiments. Nanoindentation tests were performed with a trigonal pyramid Berkovich diamond tip having a

radius of 150 nm. Calibration for the nanoindentation testing used a fused quartz standard following the Oliver and Pharr procedure having an elastic modulus value of 69.6 GPa. The Oliver and Pharr method was used to obtain hardness and reduced modulus values of the kerogen and mineral matrix.

Two types of indentation control modes were used; displacement-controlled and load-controlled. Displacement-controlled nanoindentation allowed indents to be made at specified depths of 50, 100, and 150 nm. These depths were chosen in order to obtain the smaller indents required to determine the properties of a specific area such as harder minerals or softer kerogen regions. Deeper indents were assumed to display bulk properties of the oil shale showing combined values of the kerogen and mineral matrix (Katti, 2006) (Zhang, 2002) (Wei, 2004). The load-controlled nanoindentation tests consisted of loading at 250 μN/s for 4 seconds to a maximum load of 1000 μN which was held for 3 seconds then followed by an unloading of 250 μN/s for another 4 seconds. The indent depths for the load-controlled test ranged from 90 nm when indents were made on harder minerals, to depths of 200 - 300 nm when indents occured on softer regions. Refer to Appendix C for a detailed nanoindentation procedure.

The shape of the unloading curve and the total recovered displacement is related to the elastic modulus and the size of the contact impression (Oliver, 1992). The projected contact area (A) must be known at peak load

$$A = F \; x \; (h_c) \hspace{5cm} (1)$$

84

Where

$$h_c = h_{max} - h_s \qquad (2)$$

and h_{max} is the total displacement during loading, h_s is the displacement of the surface at the perimeter of contact, and h_c is the vertical distance along which contact is made called the contact depth. F is the force applied to the object. The reduced elastic modulus can be calculated from

$$\frac{1}{E_r} = \frac{(1-v^2)}{E} + \frac{(1-v_i^2)}{E_i} \qquad (3)$$

Where elastic modulus (E) and poisson's ratio (v) are for the experiment specimen. The i represents the diamond tip indenter parameters having an elastic modulus value of $E_i = 1141$ GPa and $v_i = 0.07$.

Stiffness of a sample can be determined using Bulychev and co-worker's (Bulychev, 1975), mechanical properties of materials studied from kinetic diagrams of load versus depth of impression during microimpression, having an equation of

$$E_r = \frac{1}{\beta} \frac{\sqrt{\Pi}}{2} \frac{S}{\sqrt{A_p(h_c)}} \qquad (4)$$

where S is the stiffness of the material, ß is a geometrical constant on the order of unity, and $A_p(h_c)$ is the projected area of the indentation at the contact depth h_c, often approximated by a fitting polynomial as shown below for a Berkovich tip:

$$A_p(h_c) = 24.5h_c^2 + C_1 h_c^1 + C_2 h_c^{1/2} + C_3 h_c^{1/4} + ... + C_8 h_c^{1/128} \qquad (5)$$

To find the hardness (H) of a material the maximum load (P_{max}) is divided by the indentation area (A_r):

$$Hardness(H) = \frac{P_{max}}{A_r} \qquad (6)$$

All modulus values shown are the elastic modulus values found using the equation:

$$E = \frac{(1 - v^2)(E_r)}{(1 - .0008729(E_r))} \qquad (7)$$

A poisson's ratio of 0.25 was used for our samples when determining the elastic modulus from the reduced modulus value, a good representation of the harder shale and softer kerogen (Ahmadov, 2009).

5.4. Results and Discussion

The first step in determining the mechanical properties of kerogen was to confirm the presence of organic matter on the surface of the oil shale samples that had been prepared for nanoindentation experiments. The reflection method of Fourier Transform Infrared (FTIR) was performed on all oil shale samples that were used in the nanoindentation study. Spectra of light and dark colored oil shale surfaces analyzed parallel and perpendicular to the bedding plane confirm the presence of kerogen on the sample surfaces. The kerogen bands have been identified as those from Green River oil shale using accepted bands characteristic of kerogen found in literature and from our previous photoacoustic FTIR studies of oil shale samples which are similar to

86

those used for nanoindentation tests. The infrared bands that are characteristic of kerogen include the O-H stretching band at 3600 cm^{-1}, the C-H stretching band at 2900 cm^{-1}, the C=O stretching band at 1700 cm^{-1}, CH$_3$ bending and CH$_2$ scissor vibration at 1455 cm^{-1}, and the long chains alkane bands around 686 cm^{-1} (Robinson, 1969b). The kerogen bands found to be on the surface of the oil shale samples confirms the presence of organic matter with the opportunity to indent on kerogen or a kerogen-rich region.

An important feature of the reflection FTIR spectra shown in Figure 5.1 of the light and dark colored samples surfaces scanned parallel and perpendicular to the bedding plane, is the presence of two types of C-H stretching bands. The presence of CH$_3$ and CH$_2$ asymetric and symmetric stretching bands are found in all the oil shale spectra. These bands are the most important signature kerogen bands confirming kerogen presence on our sample surface. The dark parallel and light perpendicular samples have similar bands with dominate CH$_3$ or aromatic bands while the dark perpendicular and light parallel samples have similar bands with more aliphatic or CH$_2$ stretching bands present. The similarities between the different colored oil shales parallel and perpendicular to the bedding plane suggest that there are no orientation differences in our samples.

For this study, it was important to know the nano-mechanical properties of all the minerals assumed to be present in the Green River oil shale samples. The hardness and elastic modulus values were found for pyrite, calcite, dolomite,

quartz, k-feldspar, and clay with the results shown in Table 5.1. The lowest

elastic modulus value for all the minerals in the oil shale was for clay and

calcite having values of 60 – 80 GPa. These values are significant in that they

indicate an indent with a value of 60 GPa or higher would signify the

properties of a mineral or group of minerals. It is safe to assume that an indent

with a modulus value lower than 30 GPa would indicate an indent on a softer

material thus an indent on kerogen or a kerogen-mineral matrix (Ahmadov,

2009).
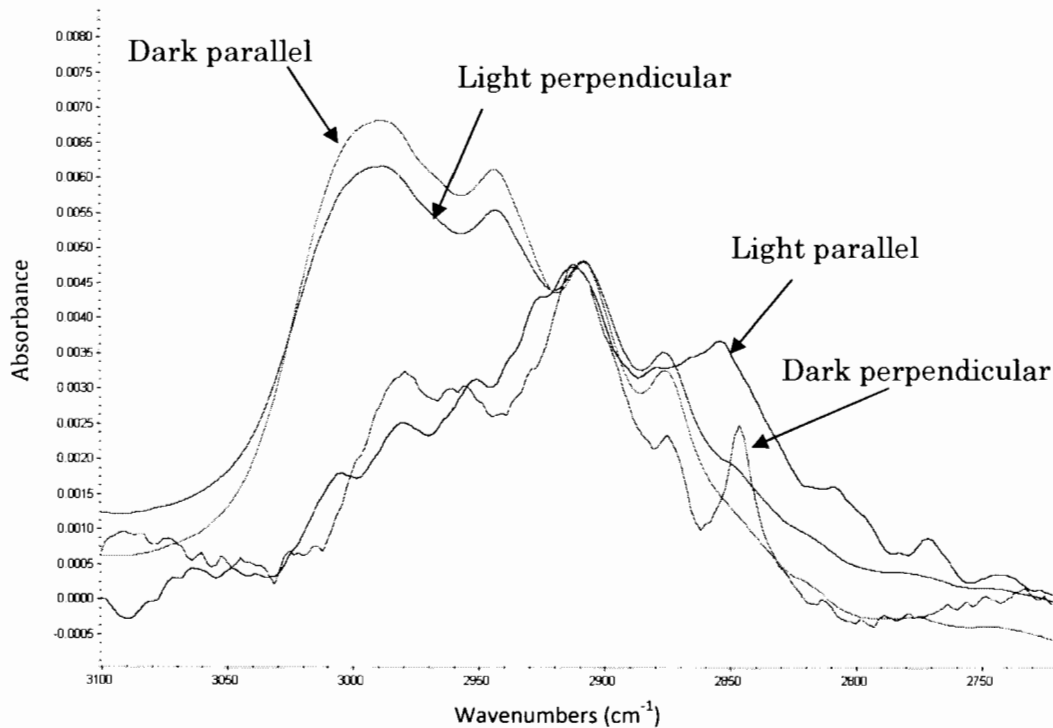
Wavenumber	Assignment
$2975 - 2950$ cm^{-1}:	*CH$_3$ asymmetric stretch*
2930 cm^{-1}:	*CH$_2$ asymmetric stretch*
2885-2865 cm^{-1}:	*CH$_3$ symmetric stretch*
2870-2840 cm^{-1}:	*CH$_2$ symmetric stretch*

Figure 5.1. Reflectance FTIR spectra of the oil shale sample surfaces. The C-H
bands confirm the presence of kerogen on the sample surface.

Table 5.1. Young's modulus and hardness values of minerals present in Green River oil shale

Mineral	Hardness (Gpa)	Modulus (Gpa)	Reference
Pyrite		135	(Aguilar-Santillan, 2008)
Calcite	2	78	(Broz, 2006)
Quartz	15	117	(Broz, 2006)
Dolomite	6.5	120	(Agersborg, 2009)
K-feldspar	9	80-90	(Zhu, 2007)
Mg/Fe Muscovite	3.3	60	(Zhu, 2007)

The displacement-controlled indentation method was used to determine the elastic modulus values of dark and light colored oil shale tested parallel and perpendicular to the bedding plane at indents of 50, 100, and 150 nm. Different indentation depths were used to obtain the mechanical properties of individual minerals assumed to be found with indents of 50 nm and bulk values of the oil shale assumed to be from indentation depths of 150 nm. Figure 5.2 shows a phase image of a nanoindentation indent of kerogen on light and dark colored oil shale perpendicular to the bedding plane.

An average of 130 indents were taken at each depth of 50, 100, and 150 nm on dark colored oil shale parallel and perpendicular to the bedding plane and on light colored oil shale parallel and perpendicular to the bedding plane. Tests were performed on oil shale samples from different depths of the core which provided similar results to those that are shown. Figure 5.3 displays a bar graph consisting of the data collected from a light colored oil shale sample

that was indented parallel to the bedding plane at a depth of 150 nm. The bar

graph shows data from 122 indents that were made on this sample, with the

number of indents plotted on the x-axis. The y-axis indicates the elastic

modulus value of each indent with the highest, median, and lowest elastic

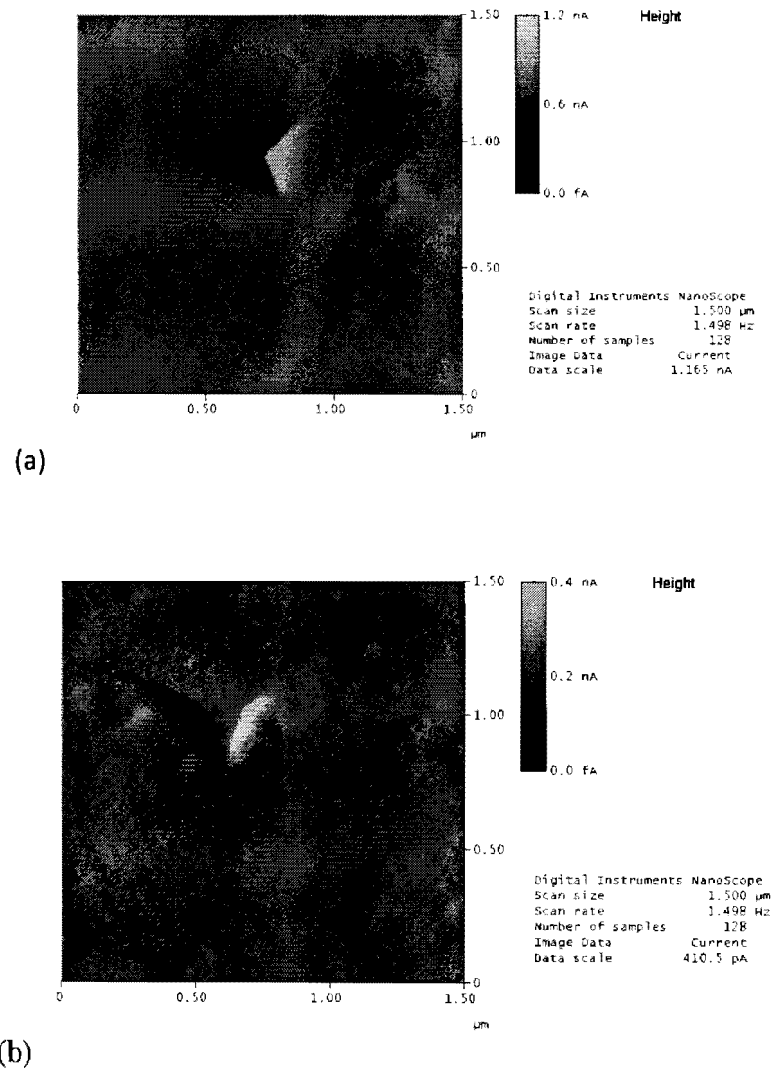modulus value is displayed. The bar graph in Figure 5.3 has a highest

(a)

(b)

Figure 5.2. AFM phase images of a 150 nm indent perpendicular to the
bedding plane. The indents have an elastic modulus value of 11 GPa for (a)
light colored oil shale and (b) dark colored oil shale

modulus value of 148 GPa, median value of 55 GPa, and lowest value of 4.5

GPa. The highest value is assumed to represent an indent that occurred on an

individual mineral. The lowest modulus value provides the mechanical

properties of a soft region of the oil shale most likely representing indents on

soft kerogen-rich areas. The median value is displayed to represent the overall

data and when plotted in a distribution graph, such as that of Figure 5.4,

shows the spread of harder and softer indent values. For example, a sample

that had more indents on harder oil shale or minerals would have a median

value closer to that of the highest modulus value, compared to a sample with

more indents on softer material having a median value closer to that of the

lowest elastic modulus. A good distribution of high and low elastic modulus

indents would provide a median value close to the average elastic modulus

value. Additional bar and distribution graphs of indents on light and dark oil

shale samples tested parallel and perpendicular to the bedding plane can be

seen in Appendix F.

The data for each sample of light and dark, parallel and perpendicular

to the bedding plane at indents of 50, 100, and 150 nm was then combined into

a distribution graph to show the highest, median, and lowest elastic modulus

values of that sample. The results for all samples at varying indentation

depths are shown in Figures 5.4a-d with the highest, median, and lowest

elastic modulus values plotted on the y-axis and the indentation depths plotted

on the x-axis. The Figure 5.4a distribution graph shows a light-colored oil shale

sample indented parallel to the bedding plane. This sample has a high elastic

modulus outlier at the 50 nm indent indicting an indent on a single mineral

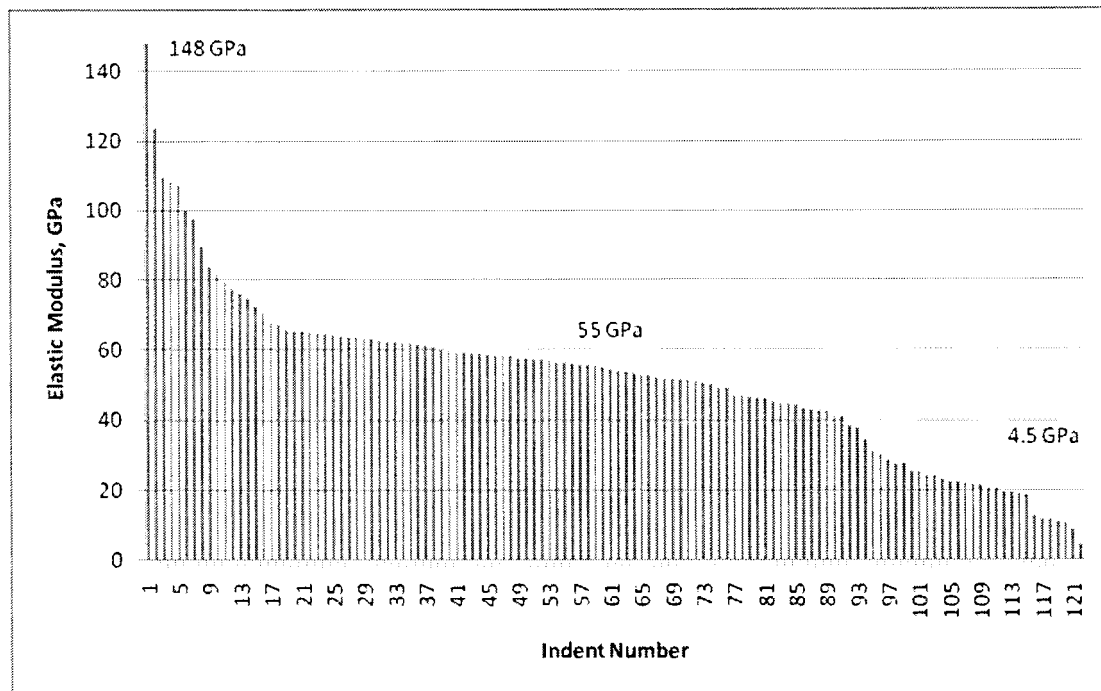having an elastic modulus value of 150 GPa. The median elastic modulus

Figure 5.3. Bar graph of indentation data at a displacement depth of 150 nm.
The samples were taken on the surface of light colored oil shale samples
indented parallel to the bedding plane.

values at indentation depths of 50, 100, and 150 nm are all relatively similar

with a value of 55 GPa. The light-colored oil shale sample scanned parallel to

the bedding plane also had the lowest elastic modulus value of all the samples

indented at an indent depth of 150 nm with a modulus value of 9 GPa. The low

modulus values for this sample show a trend of decreasing elastic modulus

with increasing indentation depth. At 50 nm the lowest elastic modulus value

is 20 GPa, at 100 nm indent the elastic modulus is 12 GPa, and is 9 GPa at an indent of 150 nm.

The Figure 5.4b distribution graph shows a light-colored oil shale sample indented perpendicular to the bedding plane. This sample also has the highest elastic modulus value at the 50 nm indent indicting an elastic modulus value of a single mineral. The highest elastic modulus values at indents of 50, 100, and 150 nm show a similar pattern to the light colored oil shale indented parallel to the bedding plane. The median values have an identical pattern to the highest elastic modulus values with a high value at 50 nm, low value at 100 nm, and medium value at 150 nm. The average of these median values being about 80 GPa. Again we see a similar pattern to the light parallel sample with the lowest elastic modulus values which is a decreasing pattern from 38 GPa to 20 GPa with increasing indentation depth from 50 to 150 nm. The differences between light parallel and perpendicular samples is the lower elastic modulus values for the light oil shale sample parallel to the bedding plane and there does not seem to be any particular trend in median elastic modulus values for the light perpendicular sample.
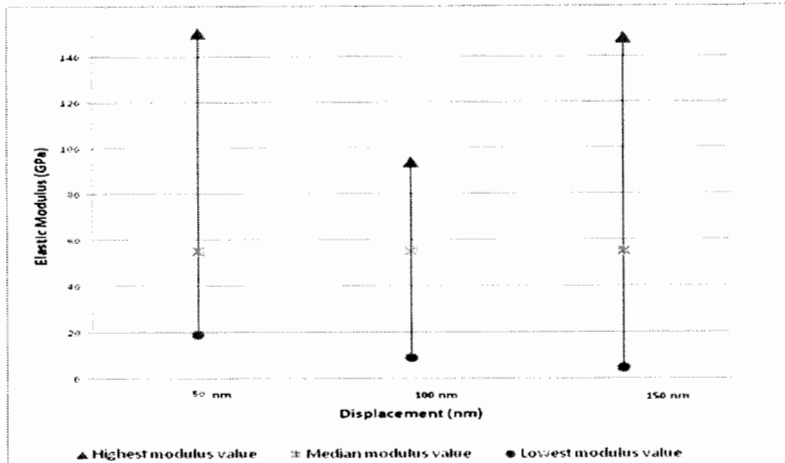
The Figure 5.4c distribution graph shows a dark-colored oil shale sample indented parallel to the bedding plane with the highest elastic modulus outlier at the 50 nm indent indicting an elastic modulus value of a single mineral similar to the light colored oil shale indents. The median elastic modulus values at indentation depths of 50, 100, and 150 nm are all very close to the

average elastic modulus values suggesting an even distribution of values. There is also a consistent deviation of about 50 GPa from the median value to the highest and lowest modulus values at each indentation depth. There is a distinct pattern for the highest, median, and lowest values that show a decrease of elastic modulus value with an increase in indentation depth from 50 to 150 nm. The lowest elastic modulus values decrease from 38 GPa to 20 GPa.
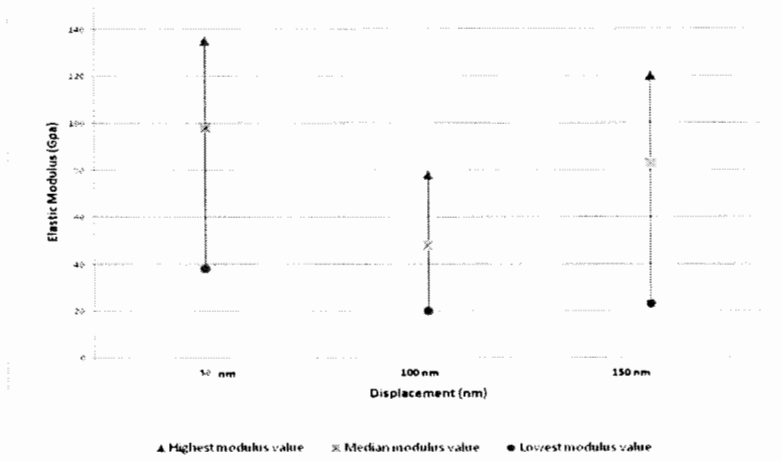
The Figure 5.4d distribution graph shows a dark-colored oil shale sample indented perpendicular to the bedding plane having a very similar pattern and elastic modulus values at indentation depths of 50, 100, and 150 nm. The highest elastic modulus values are all around 115 GPa, the median elastic modulus values are around 80 GPa, and the lowest values decrease from 30 GPa to 19 GPa with an increase in indentation depth from 50, to 150 nm. Of the dark samples tested, the lowest elastic modulus values were found in the samples indented perpendicular to bedding plane.

The distribution graphs show that the light parallel, light perpendicular, and dark parallel samples all have a high elastic modulus outlier at the 50 nm indent indicting an indent on a single mineral. The highest elastic modulus values for the light parallel and perpendicular samples were similar in that the 50 nm indent had a value of ~ 140 GPa, the 100 nm indent a value of 85 GPa, and the 150 nm indent had a value of 120 GPa. The dark colored samples had a decreasing high elastic modulus value with increasing depth. The average
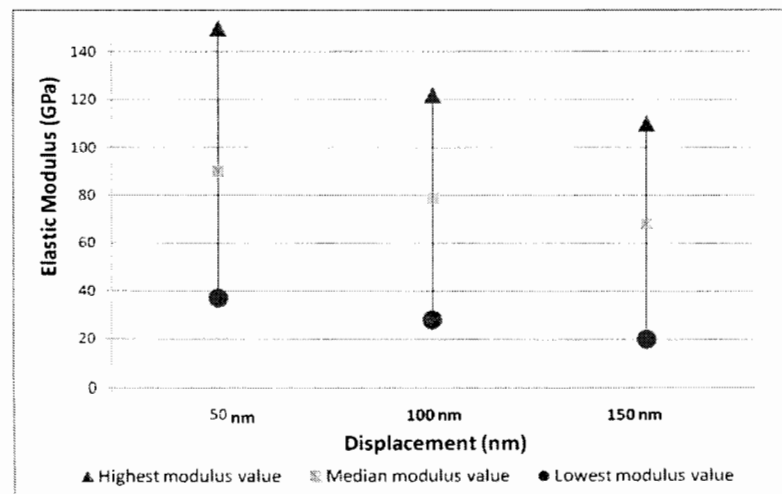
94

a)

Figure 5.4. (Continued)

b)

Figure 5.4. (Continued)

c)

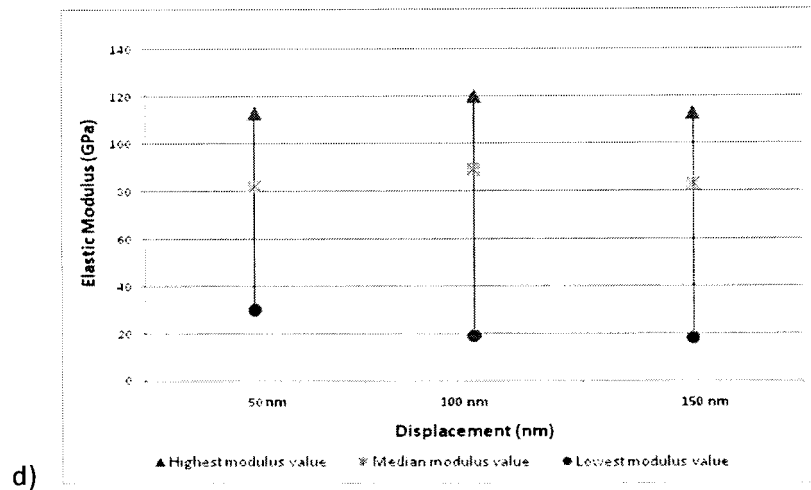Figure 5.4. (Continued)

95

d)

Figure 5.4. Distribution graph showing the highest, lowest, and median values of indents on oil shale. The displacement depths are 50, 100, and 150 nm on (a) light parallel, (b) light perpendicular, (c) dark parallel, and (d) dark perpendicular to the bedding plane

elastic modulus value for the dark samples parallel and perpendicular to the bedding plane is 120 GPa.

The median elastic modulus values at indentation depth of 50, 100, and 150 nm are about the same for the light parallel sample with a value of 55 GPa. The average median value of the light perpendicular sample is 65 GPa. The average median value of the dark parallel sample is 78 GPa. The average median value of the dark perpendicular sample is 85 GPa. The median elastic modulus value suggest that the light oil shale has lower elastic modulus values than the dark oil shale samples. A median value for any oil shale could be assumed to be in the range 55 – 85 GPa, most likely an indent on a mineral of dolomite.

The low modulus values all show a trend of decreasing elastic modulus with increasing indentation depth. For example, the light parallel sample indented at 50 nm had a value of 20 GPa, at 100 nm the elastic modulus is 12 GPa, and is 9 GPa at an indent of 150 nm. All of the samples show the same pattern with a decreasing elastic modulus value from 30 GPa at a 50 nm indent to a value of 20 GPa for a 150 nm indent. The lowest elastic modulus values was 9 GPa at an indent of 150 nm on a light parallel sample.

Results indicate that there does seem to be some mechanical property differences between the dark and light colored samples. The light samples appear to be softer with lower elastic modulus values parallel and perpendicular to the bedding plane compared to dark colored samples. There does not seem to be any orientation property differences when examined parallel and perpendicular to the bedding plane. The lowest elastic modulus values were found in the light-parallel and dark-perpendicular to bedding plane. These two samples also have similar FTIR spectra with more aliphatic C-H bands. There is significant importance in the indentation depth since lower indents at 50 nm had higher elastic modulus values while the deeper indents at 150 nm resulted in the lowest elastic modulus values. An explaination assumes that the larger indents were able to reach softer layers or material underneath the initial surface or were able to find areas of a soft matrix containing portions of soft and hard minerals and organic matter. This suggests that larger indentations would obtain more of a response from softer

regions and underlaying material. Shallower indents were on individual minerals and in soft regions where there was still influence from minerals. There could also be a layer of kerogen smeared on the minerals from polishing the sample's surface. We conclude that kerogen is spread on the mineral grain boundaries and in areas of soft material.

Load-controlled tests were performed on the same Green River oil shale samples. An average of thirty indents were performed on each sample with a maximum load of 1 mN. The indents were around an indent depth of 200 nm for kerogen-rich regions and about 90 nm for hard shale indents. The elastic modulus values collected were sorted from the highest to lowest values then plotted in a bar chart as shown in Figure 5.5. The highest elastic modulus value at 154 GPa and the lowest modulus value being 5 GPa with the median value at 66 GPa. Similar bar charts were made for dark colored samples tested parallel to the bedding plane as well as light and dark colored samples tested perpendicular to the bedding plane.

The results of the highest, median and lowest elastic modulus values for all light and dark samples indented parallel and perpendicular to the bedding plane is shown in distribution graph in Figure 5.6 with the elastic modulus values plotted on the y-axis and the type of sample plotted on the x-axis.

Results indicate from the lowest elastic modulus values that the light colored oil shale has areas of softer material compared to dark colored oil shale. This does not necessarily mean there is more soft regions since the median

value will be skewed towards a location of more indents. The light-parallel

sample had the lowest elastic modulus value of 5.2 GPa and the light-

perpendicular sample had a modulus value of 7.7 GPa. The median elastic

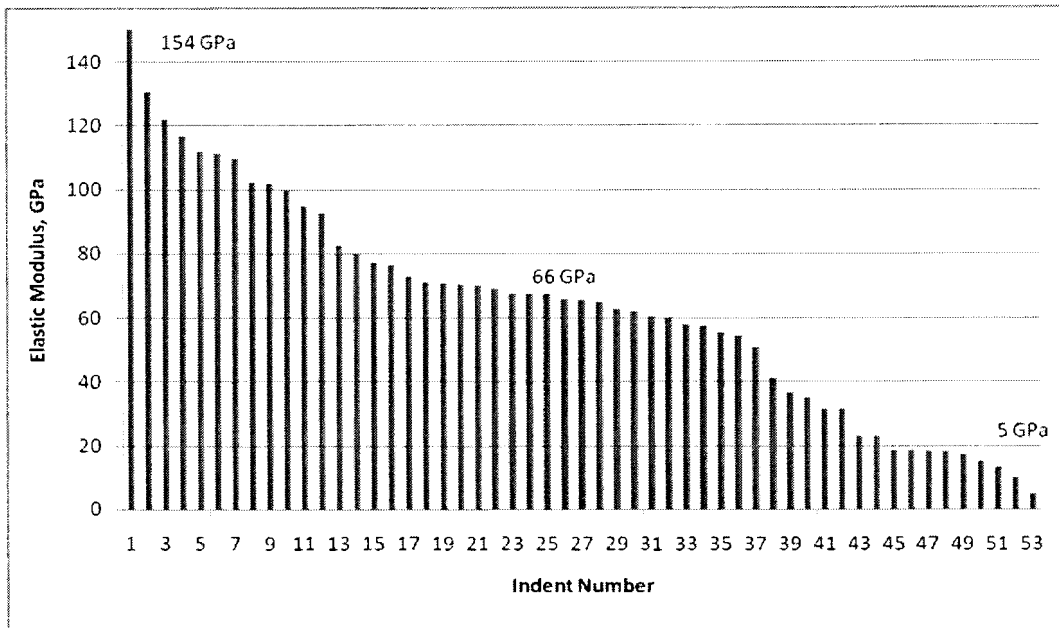modulus values were found to be the same (~75 GPa) for all the samples except

Figure 5.5. Bar graph of load-controlled indents on light colored oil shale
sample indented parallel to the bedding plane.

the light perpendicular which had a median modulus value of 95 GPa. The

highest values for all four samples are all very similar with an elastic modulus

of 130 GPa. The dark colored indentation data parallel and perpendicular to

the bedding plane is very similar to each other. The only distinguishable

difference is the lower elastic modulus value for the dark perpendicular

samples which is consistent with the displacement controlled data. The data

would suggest that the dark and light colored regions and different core

locations of the oil shale is made up of similar materials with a softer material

(kerogen) located more abundantly, or in larger regions of softer material, in

the lighter colored oil shale.
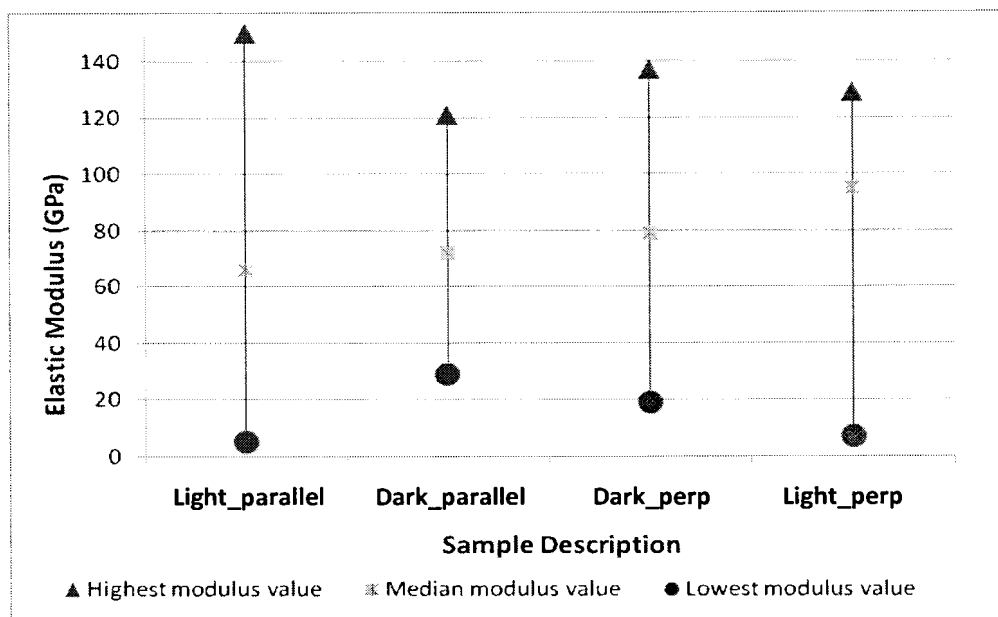
Figure 5.6. Distribution graph showing the highest, lowest, and median values
for load-controlled indents. Data consists of dark and light-colored oil shale
samples indented perpendicular and parallel to the bedding plane.

The nanoindentation curves will be able to provide information of how

the kerogen is sitting in the surrounding minerals and if there are any

property differences between light and dark colored oil shale. We first

examined the dark colored oil shale sample curves and saw similar results on

indents made parallel and perpendicular to the bedding plane and at depths

from 50 to 150 nm. The light colored oil shale indented perpendicular to the

bedding plane also shows similar results to the dark colored samples. What we

100

saw in the curves was the harder mineral curves were wider while soft material curves were narrower resulting in less unrecoverable distance. This could be contributed to the fact that less force is used for softer material and shallower indents. Harder material curves also show a more linear unloading curve indicated in Figure 5.7 showing curves from a dark colored sample indented at a depth of 150 nm perpendicular to the bedding plane. The harder mineral indent has an elastic modulus value of 85 GPa, force of 1909 µN, and unrecoverable displacement distance of 64 nm. The softer material has an elastic modulus value of 24 GPa, force of 805 µN, and unrecoverable displacement distance of 24 nm.

The light colored oil shale samples indented parallel to the bedding plane saw slightly different curves than the other samples at depths from 50 to 150 nm. These curves are very narrow for hard indents. The softer regions had curves with less unrecoverable distance similar to the other samples. An example of the light parallel curves can be seen in Figure 5.8 indented at a depth of 150 nm parallel to the bedding plane. The harder mineral has an elastic value of 106 GPa, force of 4012 µN, and unrecoverable displacement of 39 nm. The softer material has an elastic modulus value of 9.4 GPa, force of 428 µN, and unrecoverable displacement of 30 nm.
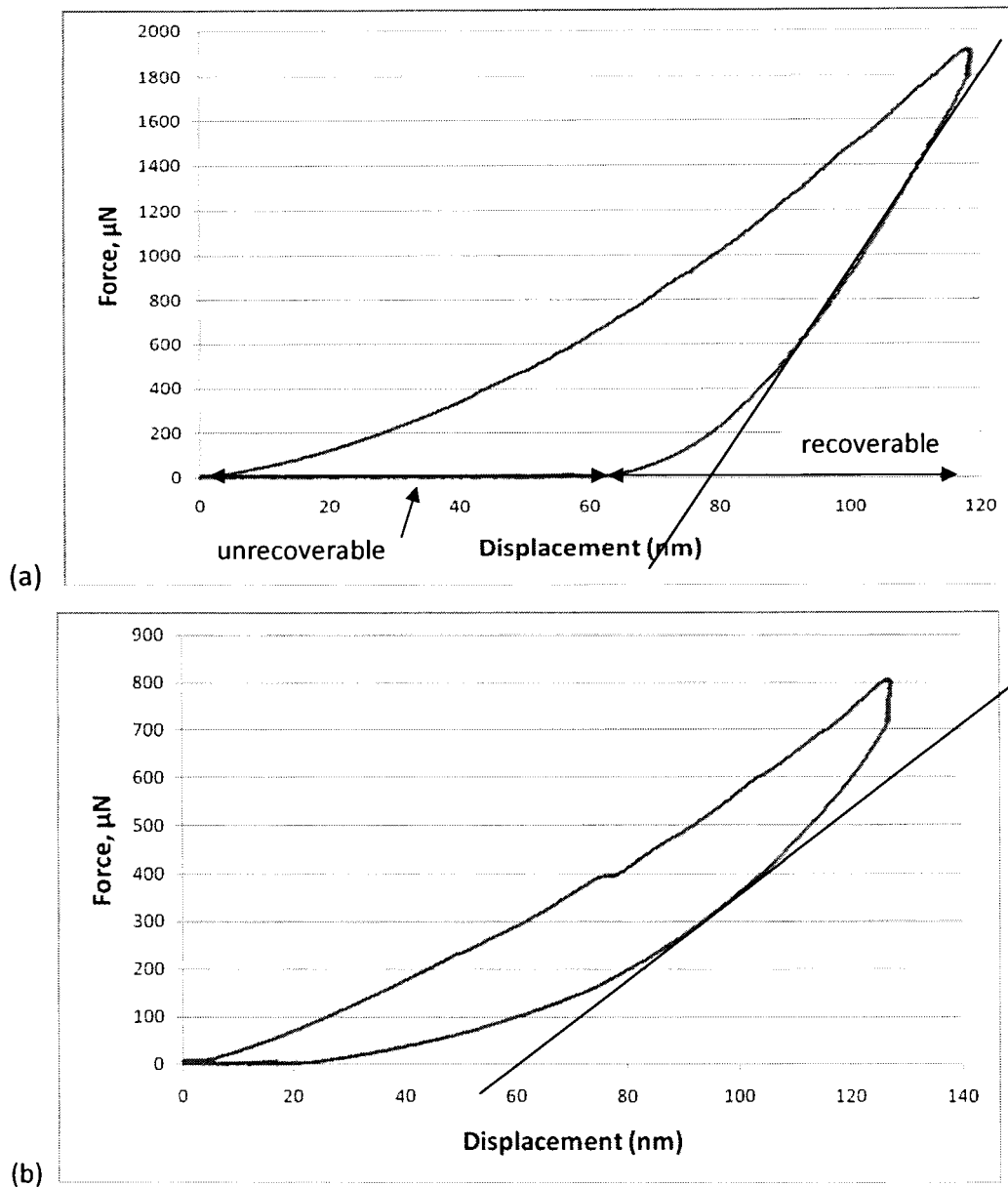
Figure 5.7. Dark colored oil shale samples indented at 150 nm perpendicular to the bedding plane. The graphs have (a) an elastic modulus of 85 GPa, force of 1909 µN, and unrecoverable displacement of 64 nm and (b) an elastic modulus of 24 GPa, force of 805 µN, and unrecoverable displacement of 24 nm.
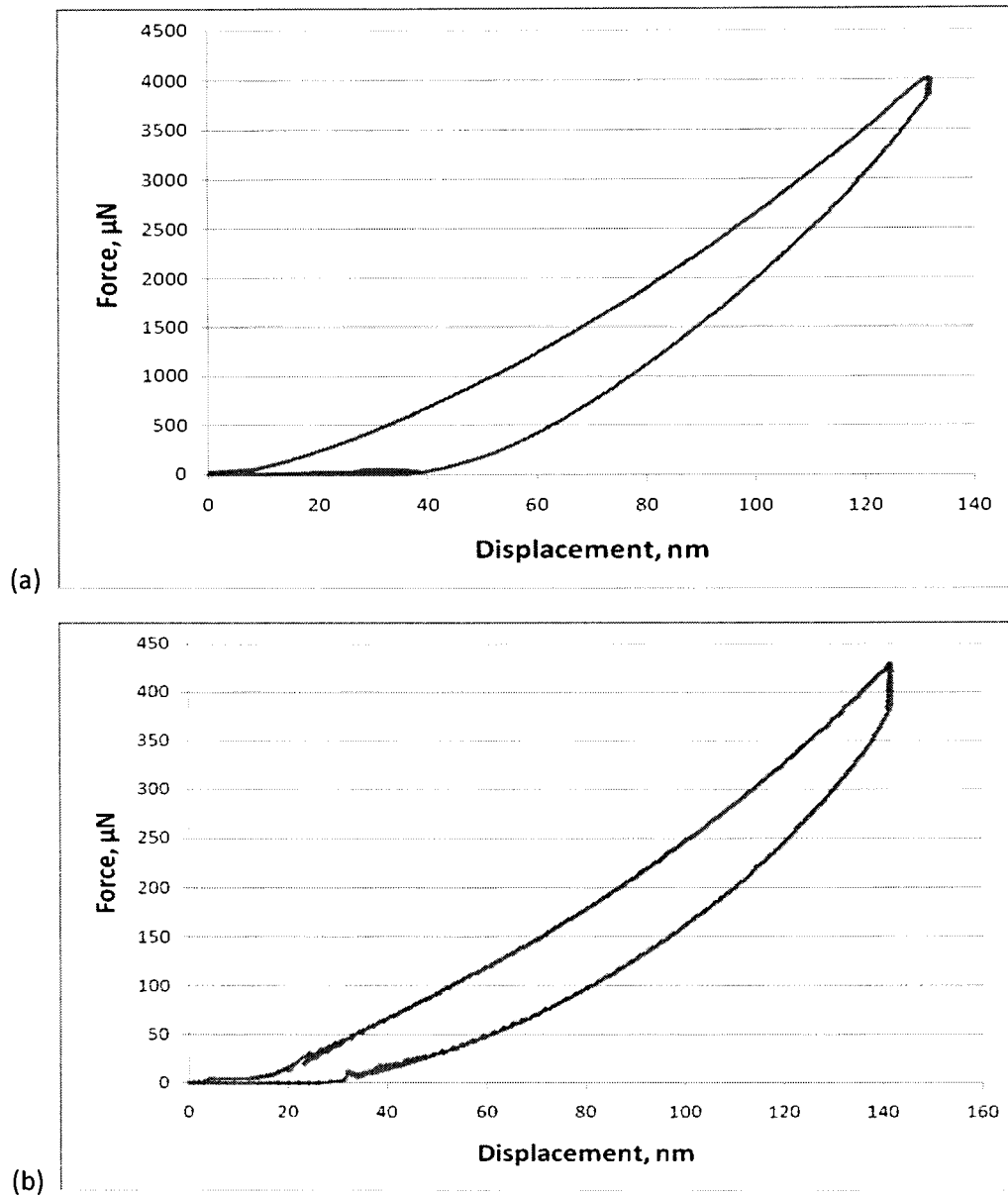
(a)

(b)

Figure 5.8. Light colored oil shale samples indented at 150 nm parallel to the bedding plane. The graphs have an (a) elastic modulus of 106 GPa, force of 4012 µN, and unrecoverable displacement of 39 nm and (b) elastic modulus of 9.4 GPa, force of 428 µN, and unrecoverable displacement of 30 nm.

The load-controlled curves also showed a noticeable difference between hard and soft material indents. Each indent had a force of 1000 µN but the

indent depth was much deeper in soft material, around 250 nm, compared to a harder material having an indent depth of about 90 nm. Figure 5.9 shows load-controlled indentation curves of hard shale, soft shale, and kerogen. There is also noticeable phase changes that can be seen on the kerogen loading curve as indicated by line 1 and line 2 in Figure 5.9. The figure shows a light colored oil shale that was indented perpendicular to the bedding plane. All dark and light colored sample curves indented parallel and perpendicular to the bedding plane had similar results.
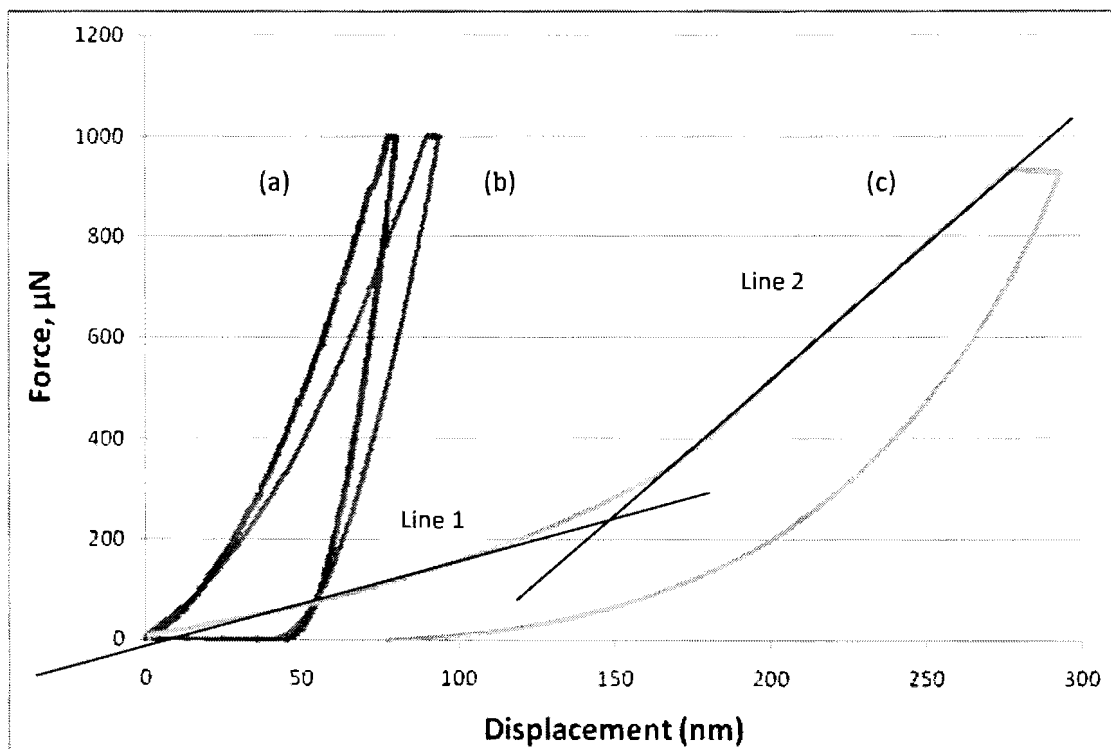
Figure 5.9. Load-controlled curves of light colored oil shale indented perpendicular to the bedding plane. The graph shows (a) hard shale with a value of 113 GPa, (b) softer shale with an elastic modulus of 65.4 GPa and (c) kerogen with an elastic modulus value of 7.7 GPa

104

After examination of the displacement-controlled and load-controlled curves, several conclusions were made. The hard shale indents for the displacement and load controlled curves had less recoverable. They also had a more linear unloading curve. For indents on soft kerogen regions, the displacement-controlled curve required less force for the same depth of indent. The load-controlled curve saw a deeper indent on soft kerogen with several phases seen on the loading curve.

All displacement-controlled indentation curves were collected and examined for light and dark samples, parallel and perpenedicular to the bedding plane. A feature that was noticed on several of the loading curves was a step-like region. An example of these steps is shown in Figure 5.10 of a light colored oil shale samples indented at a depth of 150 nm having an elastic modulus of 65 GPa. The curves were examined further and the percent of steps for each sample and indent depth were recorded in Table 5.2.

Table 5.2. The amount, in percent, of steps found on indentation loading curves. Results are shown for light and dark colored oil shale indented parallel and perpendicular to the bedding plane at indents of 50, 100, and 150 nm.

	50 nm	100 nm	150 nm	Total %
Light_parallel	0%	10%	25%	35%
Light_perp	52%	24%	43%	119%
Dark_parallel	42%	26%	58%	126%
Dark_perp	18%	18%	12%	48%
Total %	112%	78%	138%	

These steps are a consistent 3 nm in length with no distinguishable pattern to their occurrence or depth displacement wihin the sample. The indentation depth did not seem to have a significant impact on the amount of steps for that sample. The oil shale with the most steps were the dark parallel and light perpendicular samples with about three times the amount of steps
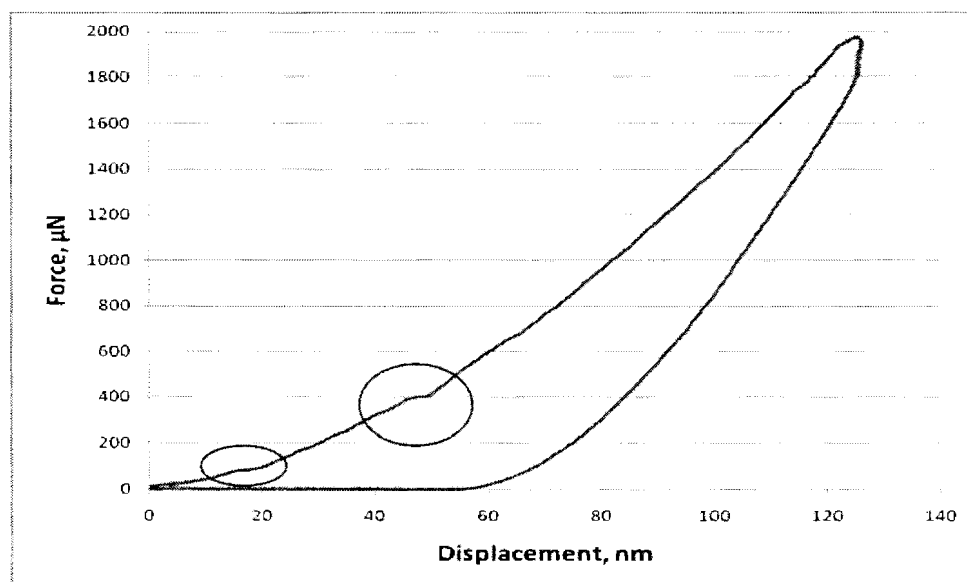

Figure 5.10. Indentation curve showing two steps on the loading curve. The graph is of a light colored oil shale sample indented parallel to the bedding plane at 150 nm.

compared to the light parallel and dark perpendicular samples. The two samples with the least amount of steps also had the lowest elastic modulus values as well as similar FTIR spectra with dominant aliphatic C-H. Some steps are very flat while others have a slight negative or positive slope. The steps could be an indication of pores found in the oil shale consistant with harder shale having more steps. The steps could also signify small pockets of

kerogen which would mean the Green River kerogen is at the scale of nanometers. Literature has reported oil shale to have a 30 % porosity with the size of pores to be in the range of 2 – 85 nm (Eseme, 2007).

The displacement-controlled data of Green River oil shale samples at indents of 50nm, 100nm, and 150 nm were also analyzed according to their hardness values. The highest, median, and lowest value for each sample at an indent of 50, 100, and 150 nm were determined and plotted in a distribution graph which can be seen in Figure 5.11a-d. The hardness values were plotted on the y-axis and the indentation depths plotted on the x-axis. The distribution graphs show that softer values are more frequent since the median values are closer to the lower hardness values with some high hardness value outliers in the light samples. There appears to be a more noticeable difference between the light parallel and light perpenicular samples. Their pattern and values vary from each other as well as the light perpendicular hardness pattern is

(a)
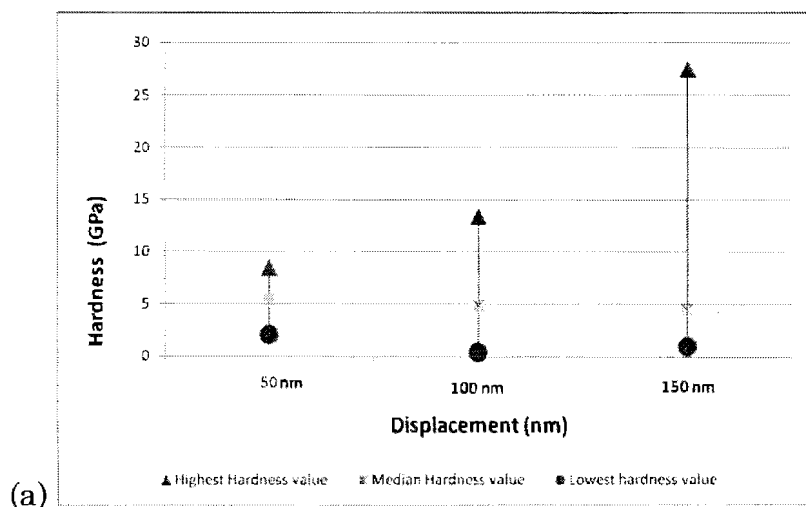
Figure 5.11. (Continued)
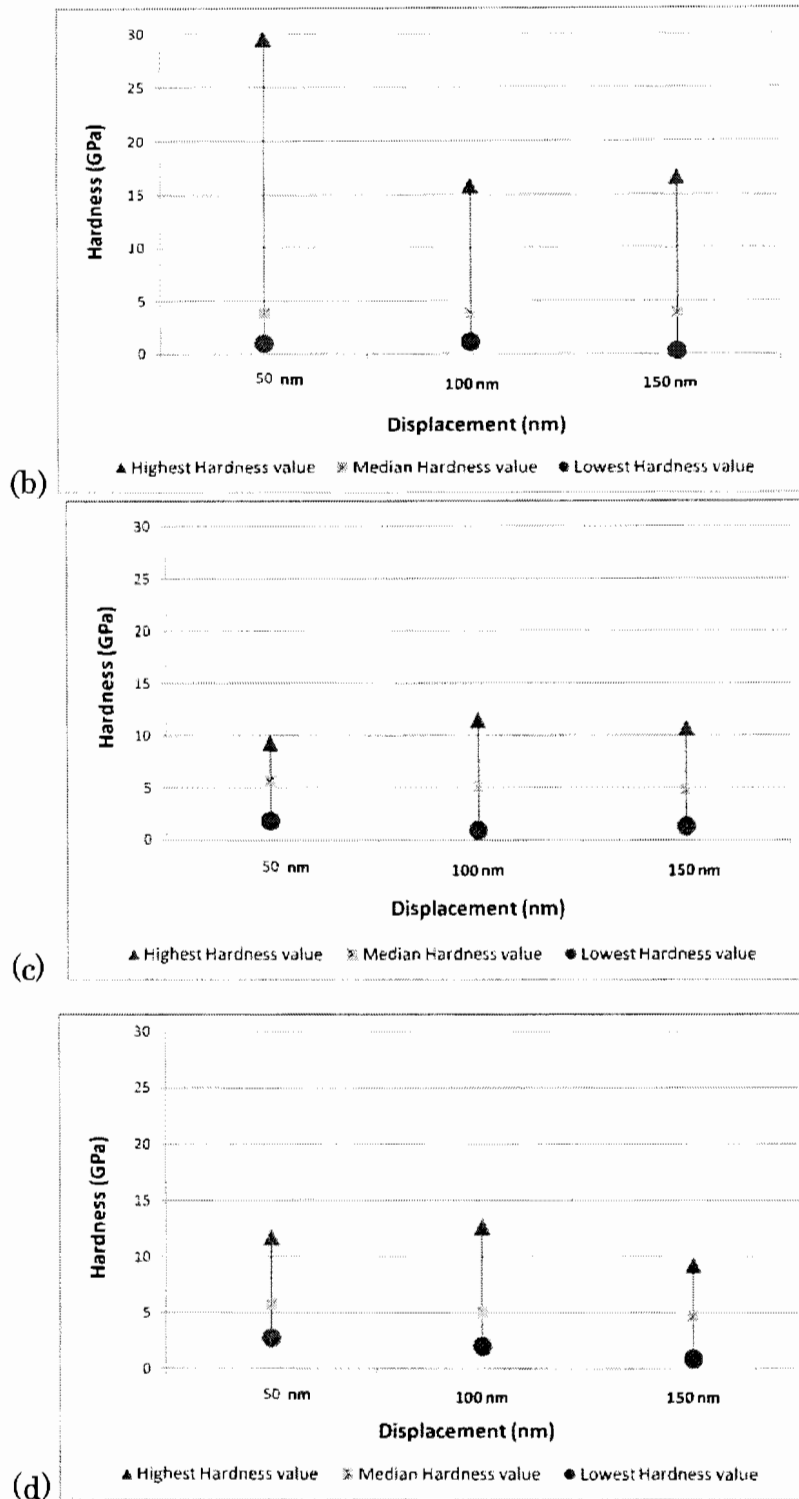
Figure 5.11. Hardness values of oil shale indented at 50, 100, and 150 nm. The data is of (a) light perpendicular, (b) light parallel, (c) dark perpendicular and (d) dark parallel

very different from its elastic modulus graph. The lowest hardness values of all the oil shale samples range from 0.3 to 2.76 with a good representative hardness value of kerogen to be around 1 GPa.

The dark colored oil shale samples all have a very similar hardness pattern at different indentation depths with a small range of values from the highest to lowest hardness and the median values skewed towards the lower hardness values. The average highest hardness value is around 10 GPa, the average median hardness value around 5 GPa, and the lowest hardness value at 1.5 GPa. The light colored oil shale had similar hardness value for the median and lowest hardness, but no pattern is seen in the highest hardness values with an average value of 15 GPa. The median values are all skewed very close to the lowest hardness values all having a similar average value of 4.5 GPa. The light colored oil shale lowest hardness values are all softer than the dark oil shale with an average lowest value of around 1 GPa. These results lead to the conclusion that there are more median valued indents and that the light colored oil shale is softer.

5.5. Conclusion

In situ kerogen has an elastic modulus value in the range of 5 - 11 GPa and hardness value of 0.9 – 1.3 GPa. A range of values is given since the mechanical properties can be impacted by the composition of kerogen which can vary in location due to the size of soft regions and mineral proximity. Steps found on loading curves were less than 5 nm in size and were observed in light

and dark colored oil shale indented parallel and perpendicular to the bedding plane. These steps could signify pores in the oil shale or small regions of kerogen suggesting that Green River kerogen may be in the size of no more than tens of nanometers. Light colored oil shale samples appear to be composed of softer material according to the hardness and elastic modulus values. Light parallel samples and dark perpendicular samples are very similar in the amount of steps present on their indentation curves, their elastic modulus values, and aliphatic FTIR spectra indicating no major orientation differences in the Green River oil shale. Indentation depth plays an importance role in elastic modulus values since lower indents at 50 nm had higher elastic modulus values while the deeper indents at 150 nm resulted in the lowest elastic modulus values.

CHAPTER 6. ADDITIONAL TESTS PERFORMED

6.1. Two Dimensional Imaging

X-ray imaging was attempted on one of our dark colored oil shale

samples examined perpendicular to the bedding plane. Images of the results

are shown in Figure 6.1. This test was performed in order to provide us with an

idea of the pore sizes in our Green River oil shale samples. From literature, the

pore sizes in oil shale tend to be in the range of 0 – 85 nm (Eseme, 2007). The

3D x-ray inspection equipment available to us through North Dakota State

University research buildings was the XiDAT 2.0 X-ray Inspection System
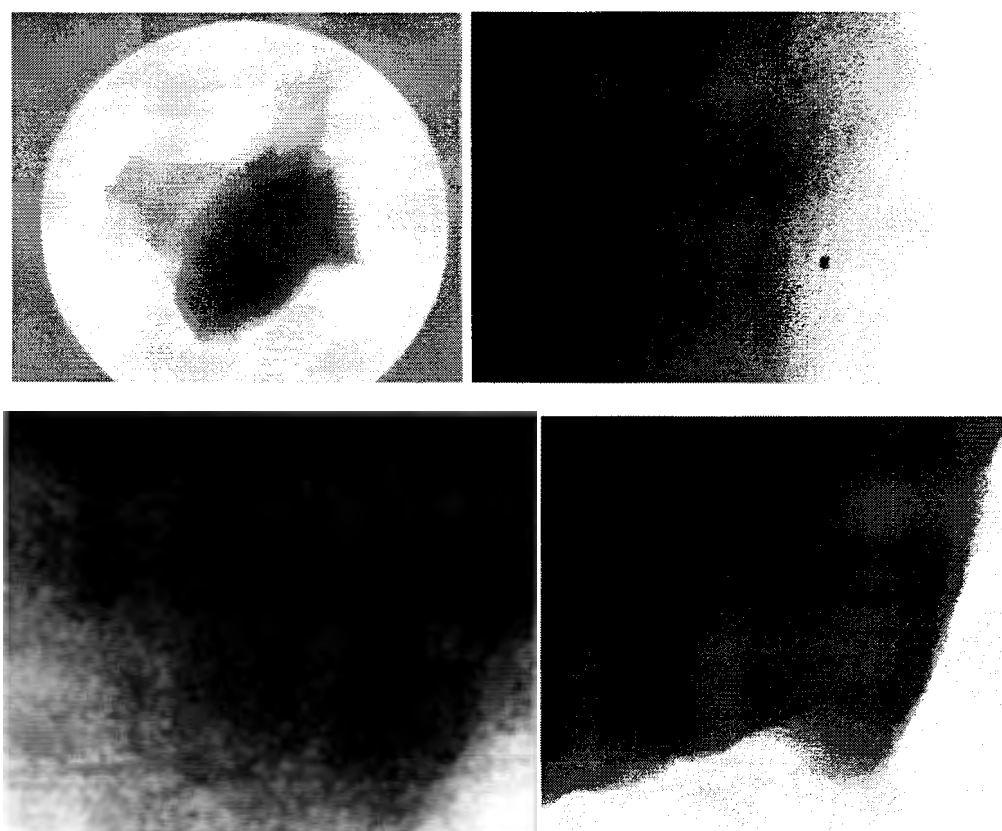
Figure 6.1. X-ray images of dark colored oil shale examined perpendicular to the bedding plane.

111

capable of a 250 nm feature recognition, 2 Mpixels @ 30 fps, stabilization system, and a 70° Isocentric angular view. Due to the equipment, we were limited to viewing features greater than 250 nm. No pores of pockets of kerogen were seen at the scale of 250 nm confirming the SEM and nanoindentation conclusions that Green River kerogen is on the scale of tens of nanometers or smaller.

6.2. AFM Imaging

The atomic force microscope (AFM) is a technique that enables a tip to be scanned / dragged / vibrated across a surface while the inter-atomic force between the tip, mounted on a flexible cantilever, and surface is measured. The interaction force can depend on the type of probe tip, distance between the probe and sample surface and the nature of the sample. A capable imaging force is in the range of $1 - 50$ nN and can detect deflections less than 0.1 nm. The first AFM was invented in 1986 by Finnig, Qaute and Gerber. The AFM and nanoindentation experiments were performed using a Veeco Multimode AFM [Veeco Metrology Group, Santa Barbara, CA] equipped with a Nanoscope-IIIa controller and J-type piezo scanner. The z-axis resolution is around 0.5 Å.

Oil shale samples were collected from various depths of the oil shale core. They were cut with a diamond-wafering blade into 5 x 5 x 3 mm samples orientated parallel and perpendicular to the bedding plane and then mounted on 10 mm stainless steel discs. To obtain a smooth imaging surface, samples

were polished with 1000 and 4000 microcut silicon carbide grinding paper, and then polished with diamond compound paste of 1 μm, 0.5 μm, and 0.25 μm. Samples were rinsed with de-ionized water and left to air dry. Refer to Appendix B.4 for a more detailed description on sample preparation.

A review of literature shows AFM images and mechanical properties of Woodford shale (Zeszotarski, 2004). The samples were cut about 1mm thick, mounted on stainless steel discs and wet polished by hand with 0.3um alumin and 0.05 um silica suspensions. They were rinsed and sonicated briefly in deionized water and air dried. A Hysitron Triboscope 20D AFM equipped with 100_mX100_m scanner and a diamond indenter tip, three-sided pyramid with 150 nm radius. AFM images show polished kerogen displaying a rippled surface randomly oriented (Figure 6.2). The physical properties of Woodford
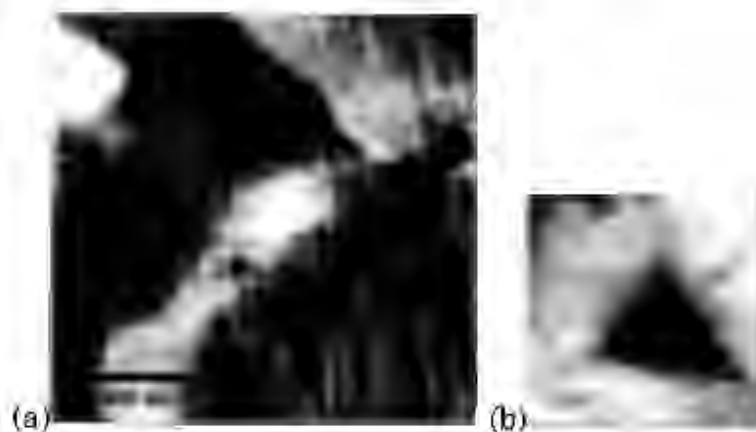
Figure 6.2. AFM image of kerogen on oil shale from literature. The image is of (a) polished kerogen as a rippled surface next to smooth features of minerals and (b) indent on kerogen (Zeszotarski, 2004)

shale kerogen are isotropic and the samples were found to have a softer material over harder substrate.

The purpose of performing AFM was to obtain a surface profile image of the oil shale and kerogen locations. Atomic Force Microscope images give a true 3-D suface profile with no treatment or damage to the sample. Images were taken of light and dark colored samples scanned parallel and perpendicular to the bedding plane. The AFM figures shown have two images. The left image will be the height image showing the z-range data. The scale shows higher areas as lighter than the shallower, dark areas. The right image is a phase image indicating differences between soft (darker colored) and hard (lighter colored) regions. The image scan size is located along the bottom of the
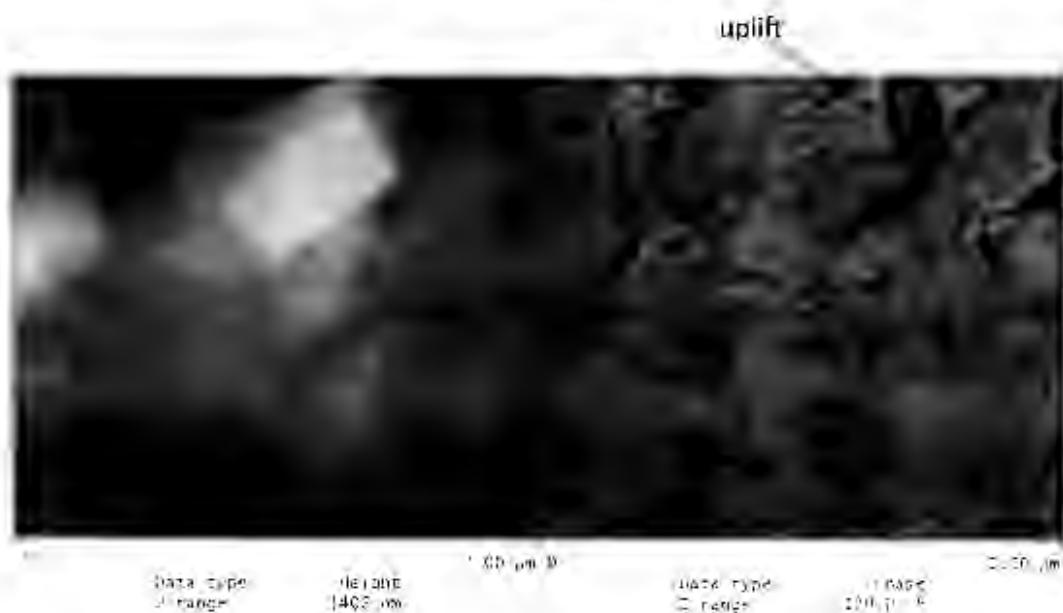
Figure 6.3. AFM image of dark colored oil shale diamond cut and imaged parallel to the bedding plane showing uplift.

114

image. Several images were taken of oil shale samples that were either broken, saw cut, or polished. The first AFM tests were performed on a dark samples diamond cut parallel to the bedding from a core depth of 571 ft @ 15 cm. Nice images were obtained but some regions were affected by the diamond cutter since there were uplifted areas as can be seen in Figure 6.3 of a dark parallel oil shale sample.

We then decided to image a surface that was broken off of a dark oil shale sample perpendicular to the bedding plane at a depth of 571 ft @ 15 cm. The images obtained, like that of Figure 6.4, were very rough and were not useful in collecting data of the kerogen location in oil shale. Dark colored oil shale samples were then polished parallel to the bedding plane with a P4000 microcut silicon carbide grinding paper. The resulting images were much smoother but we could see two types of phases. One of the phases was smooth
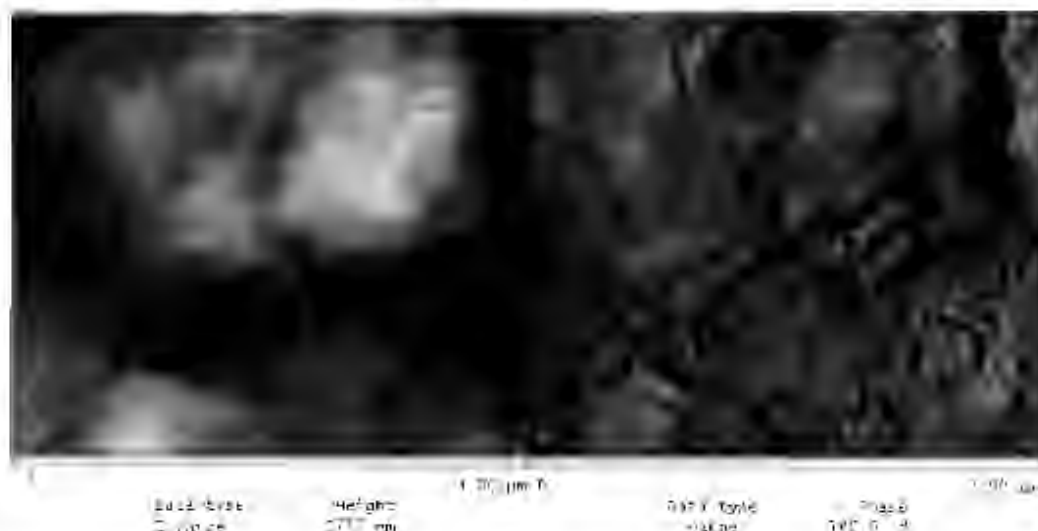
Figure 6.4. Dark colored oil shale broken from the core surface perpendicular to the bedding plane.

and polished while the other phase is an unaffected area underneath, as shown

in Figure 6.5. For this reason we have chosen to polish with diamond paste

down to a scale size of 0.25 μm. These results were satisfactory, with a

smoothness that provided good quality AFM images.
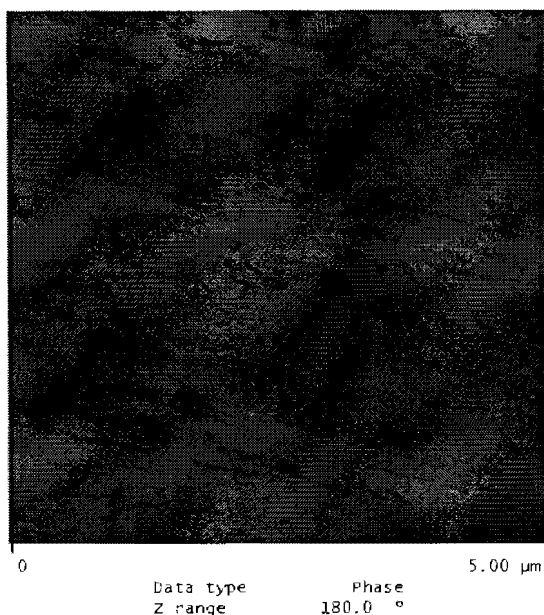
Figure 6.5. Phase image of a dark colored oil shale diamond cut and polished
parallel to the bedding plane

The surface features of oil shale on light and dark colored samples

imaged parallel and perpendicular to the bedding plane are shown in Figures

6.6 – 6.8. Figure 6.6 shows a light colored oil shale scanned parallel to the

bedding plane. The surface is verysmooth with cavities of minerals. Figure 6.7

shows a dark colored oil shale scanned parallel to the bedding plane. The

surface is slightly rough and uneven with round embedded minerals the size of

100 nm. Figure 6.8 shows a dark colored oil shale sample scanned
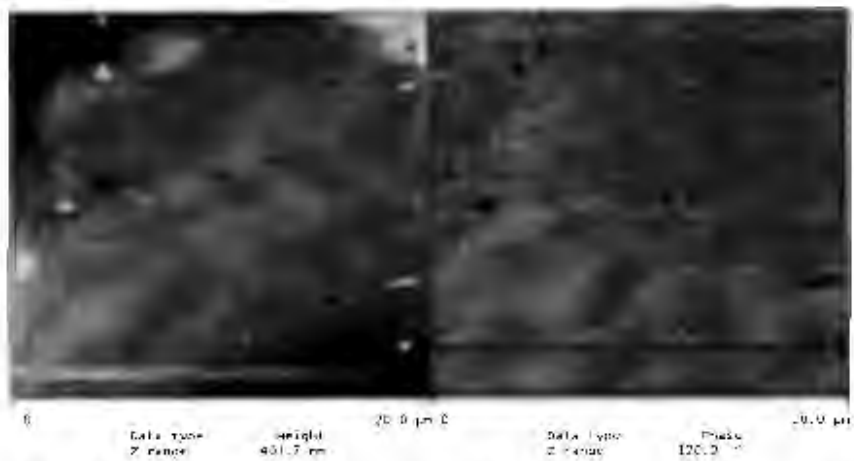
Figure 6.6. AFM image of light colored oil shale scanned parallel to the bedding plane
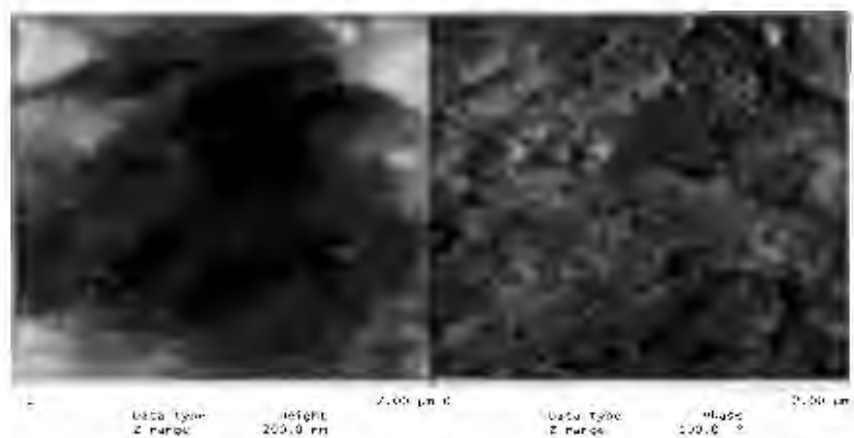
Figure 6.7. AFM image of dark colored oil shale scanned parallel to the bedding plane
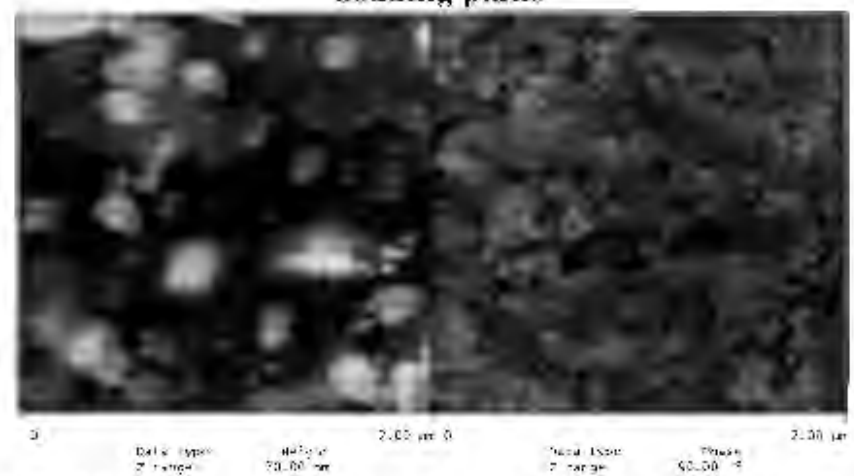
Figure 6.8. AFM image of dark colored oil shale scanned perpendicular to the bedding plane

117
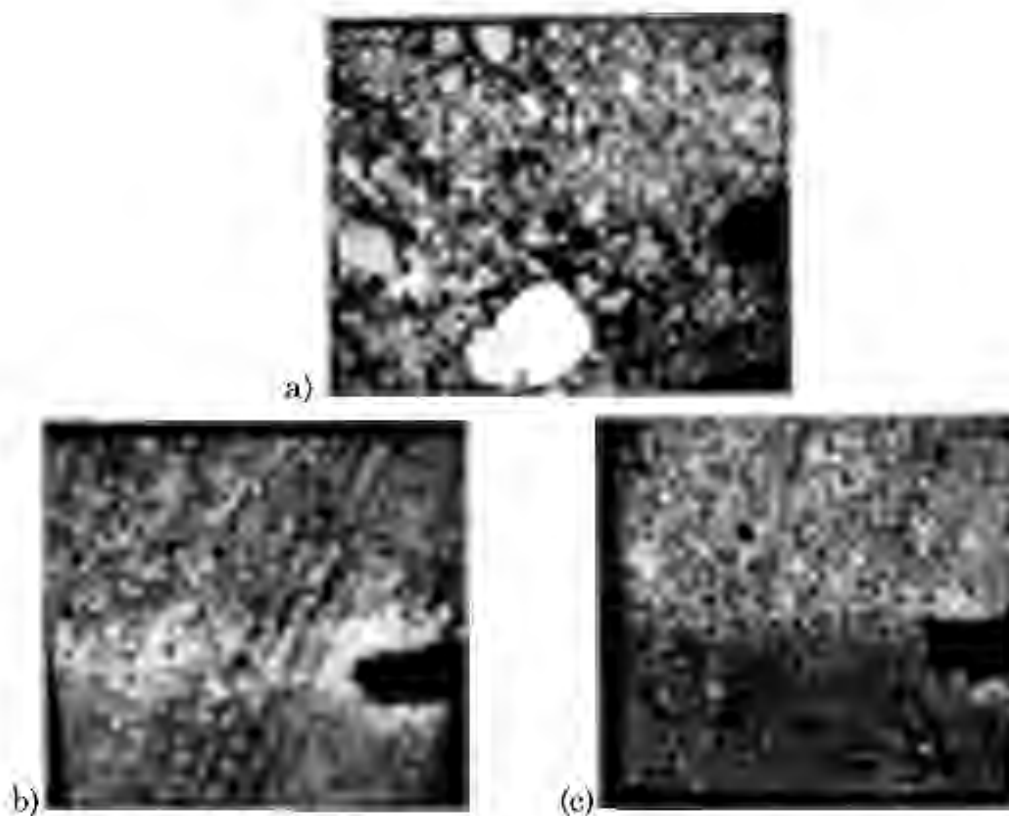
Figure 6.9. Microscope images of oil shale. The images are of (a) dark colored oil shale scanned parallel to the bedding plane, (b) dark colored oil shale scanned perpendicular to the bedding plane, and (c) light colored oil shale scanned perpendicular to the bedding plane.

perpendicular to the bedding plane. The surface is also uneven but full of smooth and rounded minerals ranging in the size of 350 nm to less than 50 nm. These images show varying surface differences of oil shale in light and dark regions as well as differences parallel and perpencidular to the bedding plane. The mineral grain sizes seen were all less than 1 μm. The surface features could also be seen by a microscope on a television screen and are shown in Figure 6.9. AFM images with a length scale of 750 nm were also taken showing smooth surfaces with mineral grain boundaries. No regions of kerogen were

seen at this length scale providing further evidence that Green River kerogen

is on the scale of tens of nanometers or smaller. Figure 6.10 displays phase

images of dark colored oil shale scanned parallel to the bedding plane on a

scale of 1.5 μm to 750 nm.
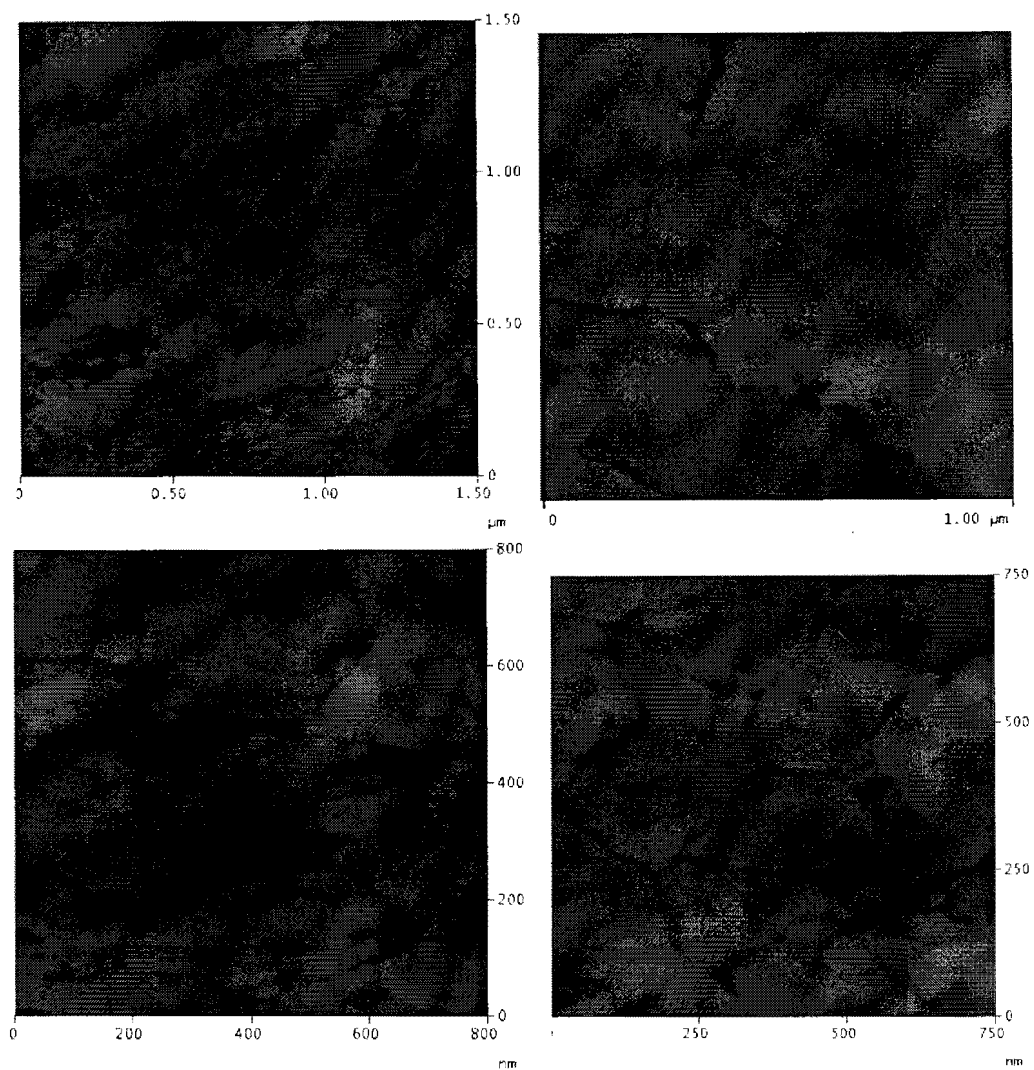
Figure 6.10. Small scale AFM images of dark colored oil shale parallel to the
bedding plane.

6.3. Modulus Mapping

The modulus mapping technique plots a sample's stiffness and, from knowing that and the geometry of the tip, the modulus can be calculated as a function of its position. The indenter probe scans a sample surface in a raster mode. The lock-in amplifier sends a dynamic signal to the drive plate of the transducer which causes the tip to oscillate. The electrostatic force of the force-displacement transducer sinusoidally modulates at 200 Hz when in contact mode. An image is generated while the phase and amplitude signals are analyzed to find the storage and loss modulus. Modulus mapping tests were performed in order to obtain the mechanical properties of oil shale on the surface of the sample with indents of about 3 nm. Several tests were taken in at least three different areas on the surface of a sample. The samples used for modulus mapping were the same samples used for nanoindentation experiments. A detailed sample preparation description is given in Appendix B.3 and the modulus mapping procedure followed can be found in Appendix D.

Modulus Mapping results are shown in Figures 6.11 – 6.14. The oil shale surface was scanned at a size of 2 μm and the darker regions represent lower areas on the surface of the oil shale core (which at times contributes to a smaller elastic modulus value). The resulting values show that the average surface elastic modulus for a dark colored sample indented parallel to the bedding plane is about 97 GPa. The average surface elastic modulus for a dark
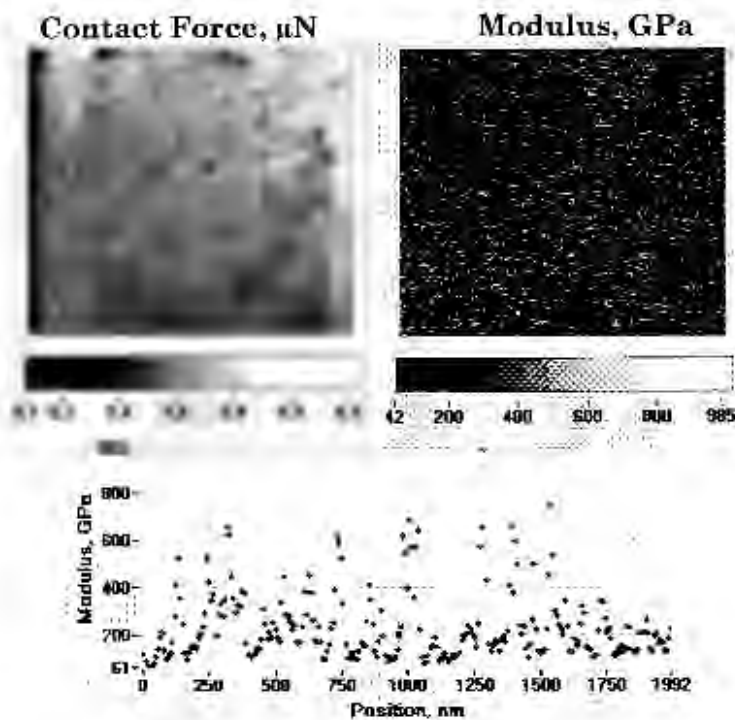
Contact Force, μN　　　**Modulus, GPa**

Figure 6.11. (Continued)

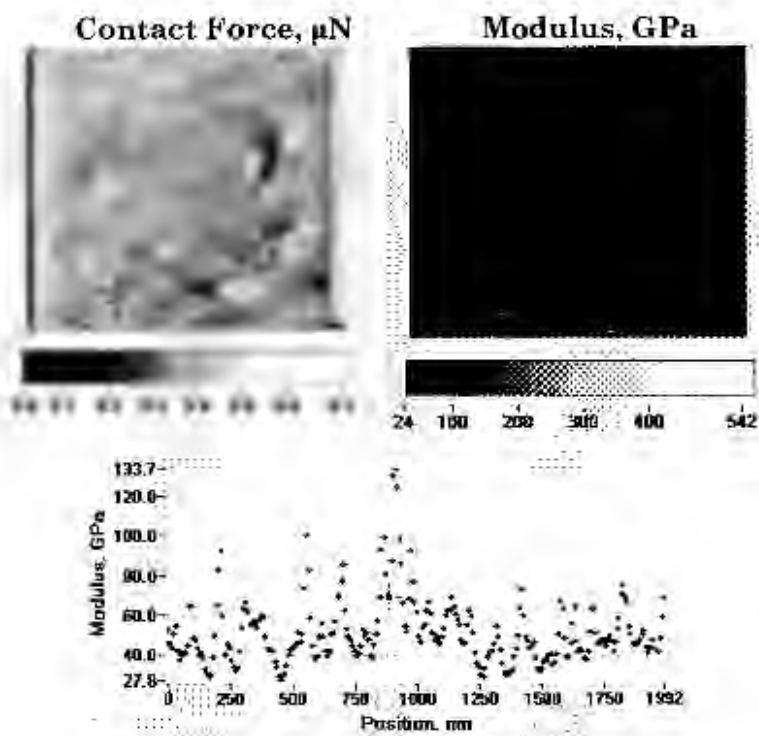**Contact Force, μN**　　　**Modulus, GPa**

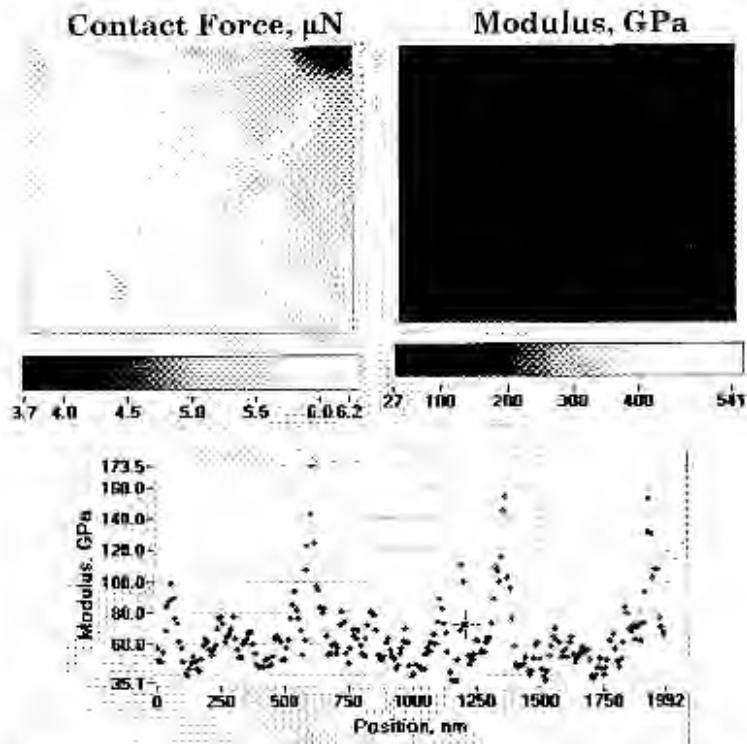
Figure 6.11. (Continued)

121

Figure 6.11. Modulus mapping data of a dark colored oil shale parallel to the bedding plane.
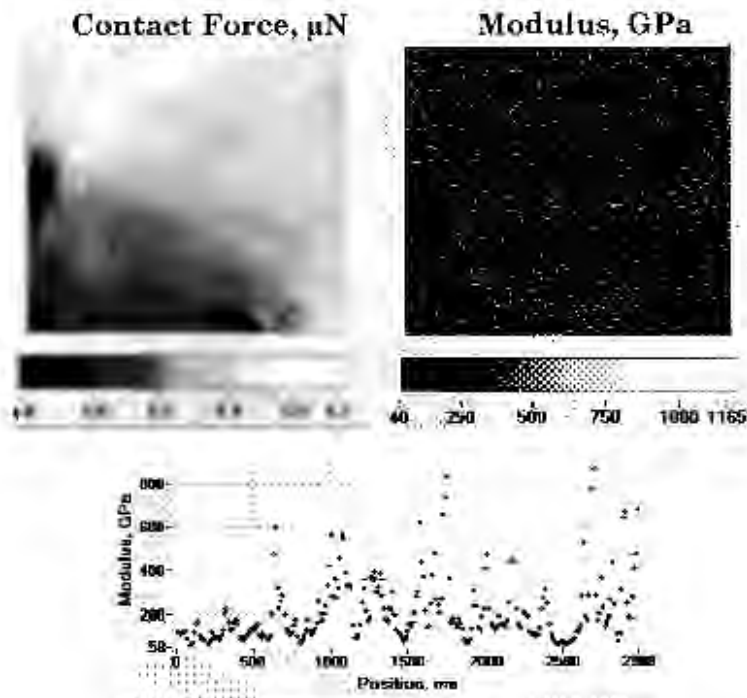

Figure 6.12. (Continued)
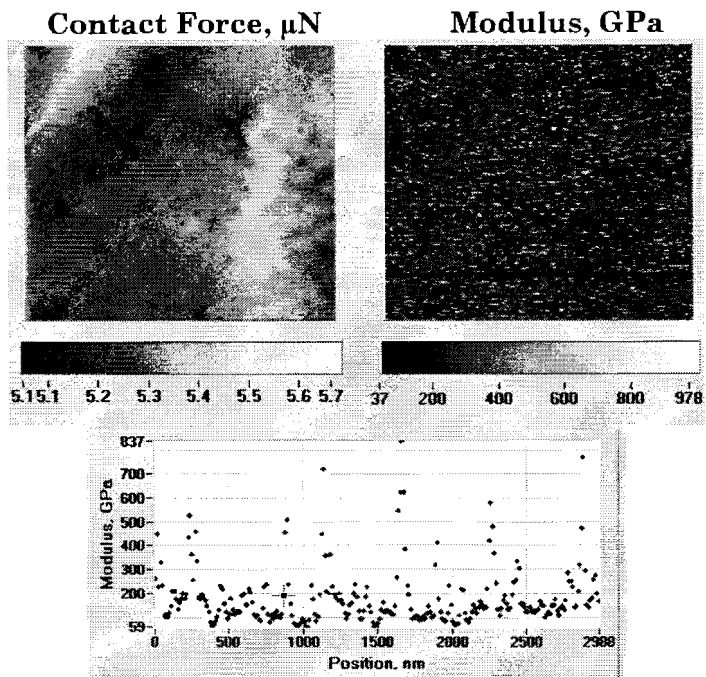
122

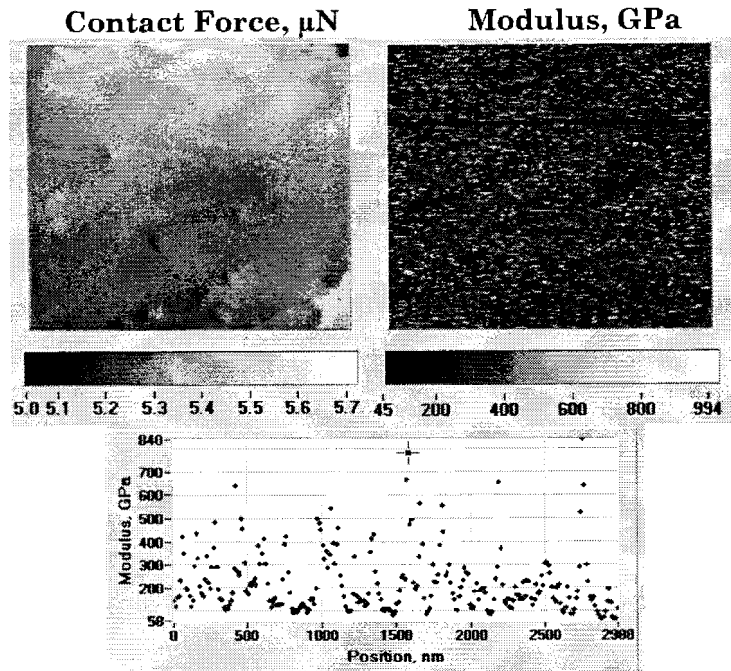Figure 6.12. Modulus mapping data of a dark colored oil shale perpendicular to the bedding plane.

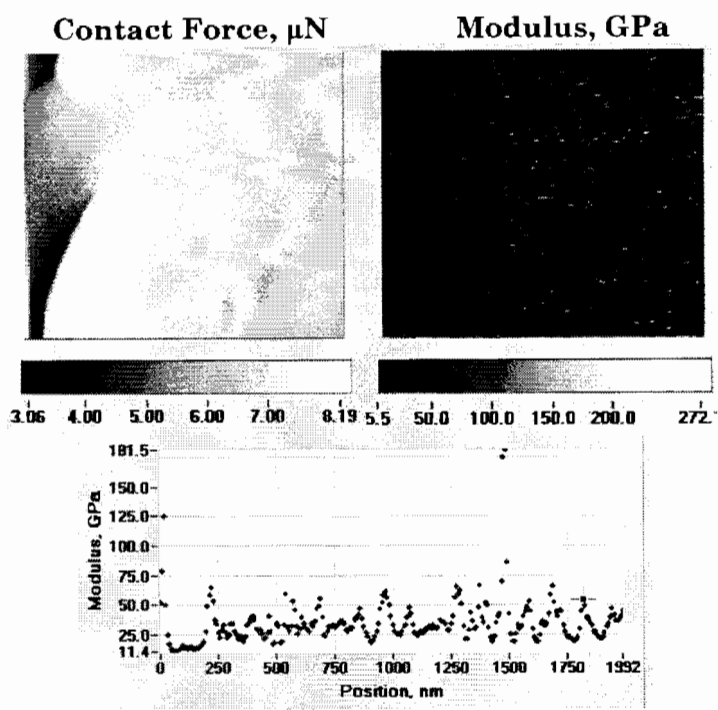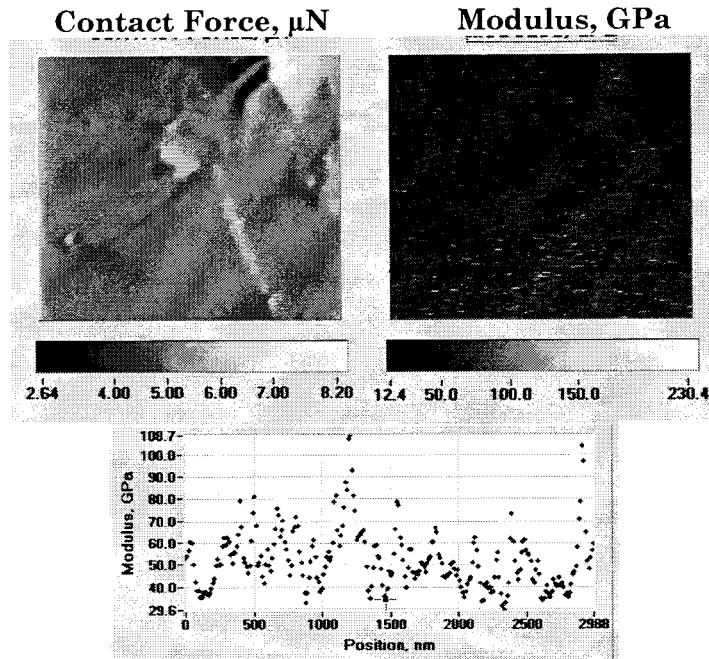Contact Force, μN   Modulus, GPa

3.06 4.00 5.00 6.00 7.00 8.19   5.5 50.0 100.0 150.0 200.0 272.

Figure 6.13. (Continued)

Contact Force, μN   Modulus, GPa

3.4 4.0 4.5 5.0 5.5 6.0 6.5 7.0   7.8 50.0 100.0 167.1

Figure 6.13. (Continued)

124
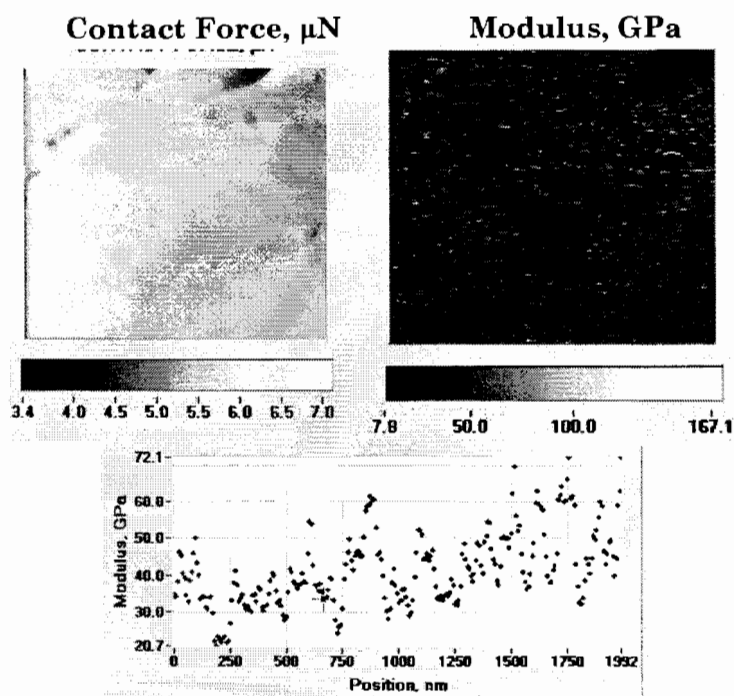
Figure 6.13. Modulus mapping data of a light colored oil shale parallel to the bedding plane.

sample indented perpendicular to the bedding plane is about 157 GPa. The average surface elastic modulus for a light sample indented parallel to the bedding plane is about 40 GPa. The average surface elastic modulus for a light sample indented perpendicular to the bedding plane is about 26 GPa. These values tell us that the surface of light colored oil shale is much softer than dark colored oil shale which is consistent with nanoindentation results. The low elastic modulus values could possibly be contributed to a shallow layer of kerogen that could have been smeared on the surface during polishing.
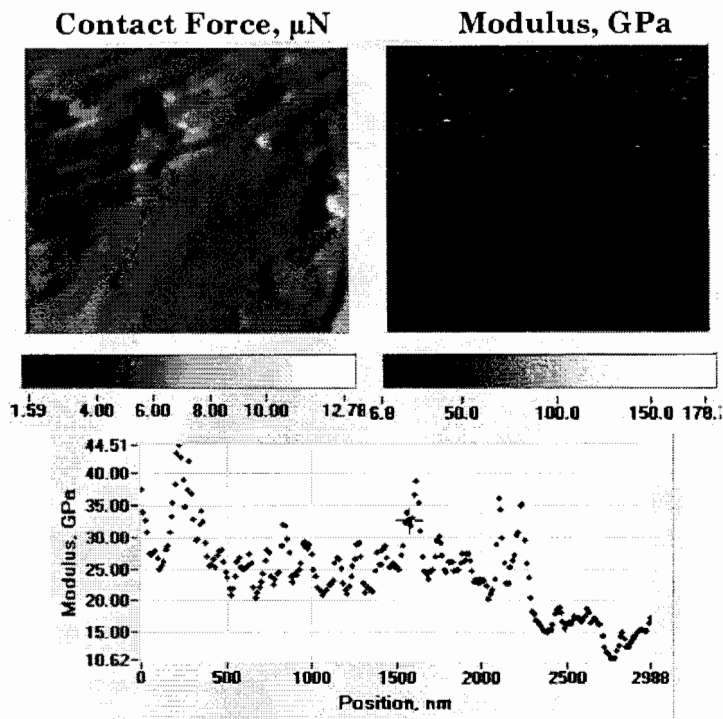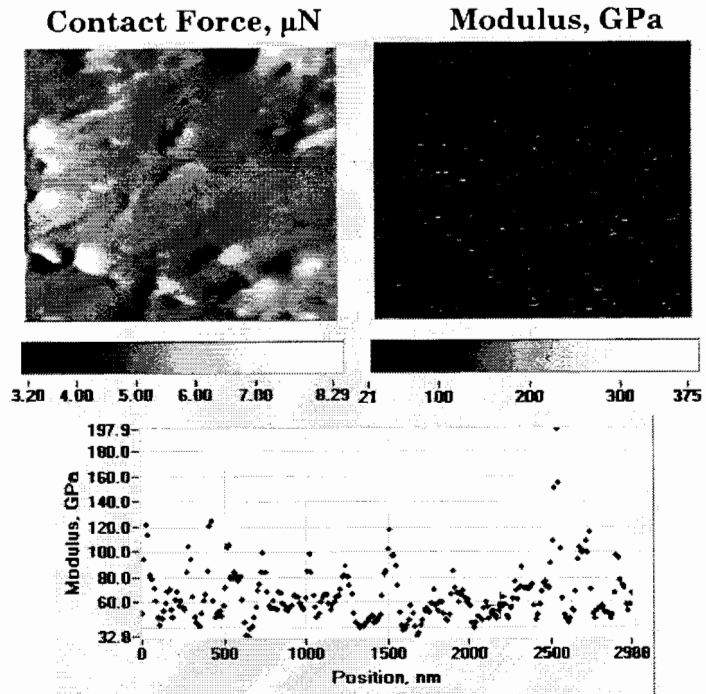
125

Figure 6.14. Modulus mapping data of a light colored oil shale perpendicular to the bedding plane.

6.4. TEM Sample Preparation

Oil shale samples were taken from three different locations on the oil shale core at; 571 ft @ 8cm, 571 ft @ 15 cm, and 567 ft @ 2 cm. Dark and light colored oil shale sections were cut into 1.5 mm thick slices parallel and perpendicular to the bedding plane. These samples are then brought to the Electron Microscopy lab where they could be cut into 3 mm diameter circles, the size and shape required for mounting in the ion mill. The samples were then grinded, following the correct procedure provided, to a thickness of 40 – 60 μm thick. The correct grinding procedures are important to follow since the grit causes depth damage up to three times the grit size. Water is used during this process to reduce heat. After this the samples will be dimple grinded to a thickness of 20 – 25 μm thick and polished with diamond paste to a thickness of 5 μm. They can then be inserted into the ion mill where they will remain with a very low beam angle until the oil shale sample is 400 – 1000 Å thick.

CHAPTER 7. SUMMARY AND CONCLUSIONS

A nanoscale approach was used in evaluation of Green River oil shale, minerals, and kerogen. An in situ study of the kerogen was performed in order to obtain a better understanding of any interactions that occur between the organic matter and the mineral phase surrounding it. Samples that were experimented on include light and dark colored regions of the oil shale core examined parallel and perpendicular to the bedding plane. Several different types of tests were performed to provide information on the Green River oil shale's chemical composition as well as physical and mechanical properties. The intent of this study was to obtain data that would lead to a more economical, better understood, and accepted method of shale oil extraction.

The first objective of our research was to obtain information on how kerogen is "locked" in the Green River mineral matrix by performing SEM, nanoindenation, and AFM experiments. SEM images provided information on the location of kerogen in Green River oil shale by showing us a complex mineral matrix of individual minerals and compacted kerogen-rich regions. The EDS data confirmed that kerogen was present in our sample by its signiture carbon band in the EDS spectra. After several trials, the best images obtained of oil shale were cross-sectional polished samples. There were some differences between the dark and light samples with a sponge-like looking region of small, fine minerals and binder that are more dominant in the light colored samples. No pockets or large regions of kerogen were observed

suggesting that Green River kerogen is on the scale of nanometers and is a binding material between the minerals located on grain boundaries. Nanoindentation experiments provided the mechanical properties of the shale oil including indents on minerals and kerogen-rich regions. Several AFM images were also taken of light and dark colored oil shale samples parallel and perpendicular to the bedding plane showing no evidence of kerogen deposits, indicating kerogen is on a scale of less than 200 nm. AFM images of indents suggest that kerogen in not in large pockets, but that oil shale consists of a mixture of kerogen and minerals creating softer regions on the surface of the oil shale. The indents taken on these areas show an elastic modulus value of 9 GPa and hardness value of 1 GPa. It is assumed that kerogen alone, without any minerals present, would have a smaller elastic modulus and hardness when there is no mineral phase to influence the property values. These results suggest that kerogen in interlocked with the minerals and is dispersed randomly in the oil shale core which would have an effect on the mechanical properties of in situ kerogen.

The second objective was to better understand with what minerals the kerogen has bonded and non-bonded interactions by performing photoacoustic FTIR and SEM images. EDS data on SEM images of dark and light colored oil shale samples scanned parallel and perpendicular to the bedding plane provided the elements that constitute the Green River oil shale. The minerals in the dark colored oil shale consist of dolomite, calcite, clay, pyrite, analcite,

and kerogen. The majority of minerals in the light colored samples consist of quartz, clay, K-feldspar, and kerogen. After examining the carbon content of each sample and the atom %, it was deduced that there is more carbon present in the light colored samples which confirms the results from FTIR experiments. Photoacoustic FTIR results of light colored oil shale showed more distinct and noticeable kerogen signature bands compared to spectra of dark colored oil shale samples.

The third and most complicated of the three objectives was to show how and why kerogen-mineral interactions occur using FTIR experiments and Molecular Dynamics (MD) simulations. We have shown that kerogen exists in the shale on the very small scale of nanometers and is in very close proximity to the surrounding minerals. The FTIR data saw chemical band shifts in the spectra that were taken of photoacoustic step-scan data. This procedure had never been performed on oil shale before and allowed the chemical properties of oil shale to be seen of kerogen and the minerals together. We assumed that any band shifts would indicate interactions between the minerals and kerogen. There were two very noticeable band shifts on the band signature of C=O carbonyl stretch from kerogen and the CH_3 asymmetric deformation and CH_2 scissor vibration. These shifts of about 50 cm^{-1} indicate interactions on the molecular scale occurring between the kerogen and mineral components.

In summary, the results of the work on Green River oil shale have shown that there are some strong interactions occurring between kerogen and

the surrounding mineral matrix. The Green River kerogen has dimensions on the scale of nanometers and is closely associated with or in a close proximity to the minerals. Our FTIR results confirmed previous work that kerogen is interacting with minerals through oxygen bridges.

CHAPTER 8. FUTURE WORK

The Green River Formation will be a huge natural resource for the United States. Future progress showing the carbon bands in TEM spectra would indicate the type of carbon present and interactions in oil shale. To further support the FTIR experiments already performed, kerogen from our samples can be isolated and continued FTIR experiments analyzed. A molecular model would be the most important representation of kerogen since it would allow us to view a structure of kerogen and see the bonds, interaction energies, and atom changes that occur when kerogen in near minerals. Future work will continue to provide valuable data on Green River oil shale. The most important concentration is on the non-bonded and/or bonded interactions between kerogen and the mineral matrix.

REFERENCES

Agersborg, R., Johansen, T. A., & Jakobsen, M. (2009). Velocity variations in carbonate rocks due to dual porosity and wave-induced fluid flow. *Geophysical Prospecting*, 57, 81-98.

Aguilar-Santillan, J. (2008). Elastic and hardness anisotropy and the indentation size effect of pyrite (FeS_2) single crystal. *Acta Materialia*, 56, 2476-2487.

Ahmadov, R., Vanorio, T., & Mavko, G. (2009). Confocal laser scanning and atomic-force microscopy in estimation of elastic properties of the organic-rich Bazhenov Formation. *The Leading Edge*, 18-23.

Bajc, S., Cvetkovic, W., Ambles, A., & Vitorovic, D. (2008). Characterization of type III kerogen from Tyrolean shale based on its oxidation products. *Journal of the Serbian Chemical Society* , 73, 463-478.

Balmain, J., Hannoyer, B., & Lopez, E. (1999). Fourier Transform Infrared Spectroscopy (FTIR) and X-Ray Diffraction Analyses of Mineral and Organic Matrix During Heating of Mother of Pearl (nacre) from the Shell of the Mollusc Pinctada maxima. *Material Research*, 48, 749-754.

Baxter, C. D., Bradshaw, A. S., Green, R. A., & Wang, J.-H. (2008). Correlation between Cyclic Resistance and Shear-Wave Velocity for Providence Silts. *Geotechnical and Geoenvironmental Engineering, ASCE* , 134, 37-46.

Behar, F., & Vandenbroucke, M. (1987). Chemical modelling of kerogens. *Organic Geochemistry*, 38, 15-24.

Behar, F., Vandenbroucke, M., & Faulon, J. L. (1997). Molecular Modelling of Kerogens and Related Compounds as a Tool for Prediction of Fossil Fuels Genesis . *Organic Geochemistry*, 26, 412-419.

Beskoski, V. P., Mili, J., Mandic, B., Takic, M., & Vrvic, M. M. (2008). Removal of organically bound sulfur from oil shale by iron(III)-ion generated-regenerated from pyrite by the action of Acidithiobacillus ferrooxidans - Research on a model system. *Hydrometallurgy*, 94, 8-13.

Beutelspacher, H., & Van der Marel, H. W. (1976). *Atlas of Infrared Spectroscopy of Clay Minerals and their Admixtures.* Elsevier Scientific Publishing Company.

Bhowmik, R., Katti, K. S., & Katti, D. R. (2007). Mechanics of molecular collagen is influenced by hydroxyapatite. *Journal of Material Science, 42,* 8795 - 8803.

Bobko, C., & Ulm, F.-J. (2008). The nano-mechnical morphology of shale. *Mechanics of Materials, 40,* 318-337.

Bradley, W. H. (1929). *The Varves and Climate of the Green River Epoch.* U.S. Geological Survey Professional Paper - 158-E, 87-110.

Brownfield, M. E., Johnson, R. C., Self, J. G., & Mercier, T. J. (2009). *Nahcolite resources in the Green River Formation, Piceance Basin, northwestern Colorado.* U.S. Geological Survey Fact Sheet 2009-3011.

Broz, M. E., Cook, R. F., & Whitney, D. L. (2006). Microhardness, toughness, and modulus of Mohs scale minerals. *American Mineralogist, 91,* 135-142.

Buchheim, P. H., & Biaggi, R. (1988). *Laminae Counts Within a Synchronous Oil Shale Unit:A Challenge to the Varve Concept.* GSA ABSTRACTS & PROGRAMS.

Bulychev, S. I., Alekhin, V. P., Shorshorov, M., & Ternovskii, A. P. (1975). Determination of Young's modulus according to an indentation diagram. *Ind. Laboratory, 41,* 1409-1412.

Bulychev, S. I., Alekhin, V. P., Shorshorov, M., & Ternovskii, A. P. (1976). Mechanical properties of materials studied from kinetic diagrams of load versus depth of impression during microimpression. *Strength Materials, 8,* 1084-1089.

Burlingame, A. L., & Simoneit, B. R. (1968). Isoprenoid Fatty Acids Isolated from the Kerogen Matrix of the Green River Formation. *Science, 160,* 531-533.

Carr, N., & Norman, D. (2009). Encyclopedia Britannica. *Britannica .*

Chalmers, J. M., & Griffiths, P. R. (2002). *Handbook of Vibrational Spectroscopy.* John Wiley & Sons, Ltd.

Coshell, L., McIver, R. G., & Chang, R. (1994). X-ray computed tomography of Australian oil shales: non-destructive visualization and density determination. *Fuel*, 73, 1317-1320.

Cummins, J. J., & Robinson, W. E. (1929). *Thermal Degradation of Green River Kerogen at 150 to 350 °C*. Laramie, Wyoming: United States Department of the Interior: Bureau of Mines.

De Alba, P., Baldwin, K., Janoo, V., Roe, G., & Celikkol, B. (1997). Elastic-wave velocities and liquefaction potential. *Geotechnical Testing Journal*, 34, 510-519.

Decora, A. W., & Kerr, R. D. (1979). Processing Use, and Characterization of Shale Oil Products. *Environmental Health Perspectives*, 30, 217-223.

Donnell, J., Cashion, W. B., & Brown, J. H. (1953). Geology of the Cathedral Bluffs oil-shale area, Rio Blanco and Garfield counties, Colorado. *Map* .

Duncan, D. C., & Belser, C. (1950). Geology of oil shale resources of eastern Piceance Creek by Rio Blanco and Garfield counties.

Durand, B. (1985). Diagenetic modification of kerogens. *Phil. Trans. Soc. Lond.*, 315, 77-89.

Dyni, J. R. (2003). Geology and Resources of Some World Oil-Shale Deposits. *Oil Shale*, 20, 193-252.

Eseme, E., Urai, J. L., Krooss, B. M., & Littke, R. (2007). Review of mechanical properties of oil shales: Implications for exploitation and basin modelling. *Oil Shale*, 24, 159-174.

Farmer, V. (1974). *The Infrared Spectra of Minerals*. Mineralogical Society. Monograph 4.

Ghosh, P., Katti, D. R., & Katti, K. S. (2007). Mineral Proximity Influences Mechanical Response of Proteins in Biological Mineral-Protein Hybrid Systems. *Biomacromolecules*, 8, 851-856.

Goklen, K., Stoecker, T., & Baddour, R. (1984). A Method for the Isolation of Kerogen from Green River Oil Shale. *Ind. Eng. Chem. Prod. Res. Dev.*, 23, 308-311.

Hascakir, B. B. (2008). Experimental and Numerical Simulation of Oil Recovery from Oil Shales by Electrical Heating. *Energy & Fuels*, 22, 3976-3985.

Holmes, J. L., Blair, N. E., & Leithold, E. L. (2001). The Fate of Kerogen in a River-Dominated Active Margin.

Huang, Y.-T., Huang, A.-B., Kuo, Y.-C., & Tsai, M.-D. (2004). A laboratory study on the undrained strength of a silty sand from central Taiwan. *Soil Dynamics Earthquake Engineering*, 24, 733-743.

Huntsman, J. M., & Fletcher, E. (2007). *Development of America's Strategic Unconventional Fuels Resources*. Task Force on Strategic Unconventional Fuels, volume 2.

Ikan, R. (2003). Formation of Young Kerogen: Protein-based melanoidin hypothesis and heating experiments under mild conditions. In R. Ikan, *Natural and Laboratory - Simulated Thermal Geochemical processes*. Jerusalem, Israel: Kluwer Academic Publishers.

Katti, K. S., & Urban, M. W. (2003). Conductivity model and photoacoustic FT-IR surface depth profiling of heterogeneous polymers. *Polymer*, 44, 3319-3325.

Katti, K. S., Mohanty, B., & Katti, D. R. (2006). Nanomechanical properties of nacre. *Journal of Materials Research*, 21, 1237-1242.

Katti, K. S., Sikdar, D., Katti, D. R., Ghosh, P., & Verma, D. (2006b). Molecular interactions in intercalated organically modified clay and clay-polycaprolactam nanocomposites: Experiments and modeling. *Polymer*, 47, 403-414.

Kelemen, S. R., Afeworki, M., Gorbaty, M. L., Sansone, M., Kwiatek, P. J., & Walters, C. C. (2007). Direct Characterization of Kerogen by X-ray and Solid-State C-13 NMR Methods. *Energy & Fuels*, 21, 1548-1561.

Khanna, R., Katti, K. S., & Katti, D. R. (2009). Nanomechanics of Surface Modified Nanohydroxyapatite Particulates Used in Biomaterials. *Journal of Engineering Mechanics*, 135, 468-478.

Killops, S., & Killops, V. (2005). *Introduction to Organic Geochemistry*. Malden: Blackwell Publishing.

Lee, W., Speight, J. G., & Loyalka, S. (2007). *Handbook of Alternative Fuel Technology*. Baca Raton, FL: CRC Press.

Lille, U. (2003). Current knowledge on the origin and structure of Estonian kukersite kerogen. *Oil Shale, 20,* 253-263.

Lubliner, J. (2008). *Plasticity Theory*. Dover Publications.

Mahajan, K. K., & Shastri, S. (1997). Has the ionospheric F2 region changed permanently during the last thirty years? *MIDDLE ATMOSPHERE: CHANGES AND ELECTRODYNAMICS*, vol. 20, series 11.

McClelland, J. F., Jones, R. W., & Bajic, S. J. (2002). *FT-IR Photoacoustic Spectroscopy*. Ames, IA: MTEC Photoacoustics, Inc.

Mirabella, F. M. (1998). *Modern techniques in applied molecular spectroscopy*. John Wiley & Sons, Ltd.

Mongenot, T., Derenne, S., Largeau, C., Tribovillard, N. P., Lallier-Verges, E., Dessort, D., et al. (1999). Spectroscopic, kinetic and pyrolytic studies of kerogen from the dark parallel laminae facies of the sulphur-rich Orbagnoux deposit (Upper Kimmeridgian, Jura). *Organic Geochemistry, 30,* 39-56.

Moreau, J. W., & Sharp, T. G. (2004). A Transmission Electron Microscopy Study of Silica and Kerogen Biosignatures in ~ 1.9 Ga Gunflint Microfossils. *Astrobiology, 4,* 196-210.

Natural Resources Conservation Services - United States Department of Agriculture. (2010, August 8). *NRCS* . Retrieved January 24, 2009, from NRCS - Colorado: http://www.co.nrcs.usda.gov/

Nix, T., & Feist-Burkhardt, S. (2003). New methods applied to the microstructure analysis of Messel oil shale: confocal laser scanning microscopy and environmental scanning electron microscopy. *Geol. Mag., 140,* 469-478.

O'Brien, N. R., Slatt, R. M., & Senftle, J. (1994). The significance of oil shale fabric in primary hydrocarbon migration. *Fuel, 73,* 1518 - 1522.

Oliver, W. C., & Pharr, G. M. (1992). An improved technique for determining hardness and elastic modulus using load and displacement sensing indentation experiments. *Journal of Materials Research, 7,* 1564-1583.

137

Pan, C., Geng, A., Zhong, N., Liu, J., & Yu, L. (2009). Kerogen pyrolysis in the presence and absence of water and minerals: Amounts and compositions of bitumen and liquid hydrocarbons. *Fuel*, 88, 909-919.

Petersen, H. I., Rosenberg, P., & Hytoft, H. P. (2008). Oxygen groups in coals and alginite-rich kerogen revisited. *International Journal of Coal Geology*, 74, 93-113.

Prats, M., & O'Brien, S. M. (1975). The thermal conductivity and diffusivity of Green River oil shales. *Journal of Petroleum Technology*, 27, 97-106.

Premovic, P. I., Nikolic, G. S., Premovic, M. P., & Tonsa, I. R. (2000). Fourier transform infrared and electron spin resonance examinations of kerogen from the Gunflint stromatolitic cherts (Middle Precambrian, Ontario, Canada) and related materials. *Journal of the Serbian Chemical Society*, 65, 229-244.

Radlinski, A. P., Mastalerz, M., Hinde, A. L., Hainbuchner, A., Rauch, H., Baron, M., et al. (2004). Application of SAXS and SANS in evaluation of porosity, pore size distribution and surface area of coal. *International Journal of Coal Geology*, 59, 245-271.

Rajeshwar, K., Nottenburg, R., & Dubow, J. (1979). Thermophysical properties of oil shales. *Journal of Materials Science*, 14, 2025-2052.

Razvigorova, M., Budinova, T., Tsyntsarski, B., Petrova, B., Ekinci, E., & Atakul, H. (2008). The composition of acids in bitumen and in products from saponification of kerogen: Investigation of their role as connecting kerogen and mineral matrix. *International Journal of Coal Geology*, 76, 243-249.

Riddle, H. I. (2009, January 28). *Organic Geochemistry and Petrology*. Retrieved June 28, 2009, from Asbury Carbons: http://www.asbury.com/ Organic-Geochemistry-and-Petrology.html

Robinson, W. E. (1969). Isolation Procedures for Kerogens and associated soluble organic materials. In G. Elginton, & M. Murphy, *Organic Geochemistry: Methods and Results* (pp. 181-193). New York: Springer-Verlag.

Robinson, W. E. (1969). Kerogen of the Green River Formation. In G. Eglinton, & M. Murphy, *Organic Geochemistry: Methods and Results* (pp. 619-635). New York: Springer-Verlag.

Robinson, W. E., & Cook, G. L. (1971). *Compositional Variations of the Organic Material of Green River Oil Shale - Colorado No. 1 Core.* United States Department of Interior: Bureau of Mines, R.I. #7492

Rosencwaig, A., & Gersho, A. (1976). Theory of photoacoustic effect with solids. *Journal of Applied Physics, 47,* 64-69.

Shastri, S. (1998). An estimate for the size of cycle 23 using multivariate relationships. *Solar Physics, 180,* 499-504.

Sikdar, D., Katti, D. R., Katti, K. S., & Bhowmik, R. (2006). Insight into molecular interactions between constituents in ploymer clay nanocomposites. *Polymer, 47,* 5196-5205.

Siskin, M., & Katritzky, A. (1991). Reactivity of Organic Compounds in Hot Water: Geochemical and Technological Implications . *Abstracts of Papers of the American Chemical Society, 254,* 231-237.

Smith, P. J. (2008-2009). *Clean and Secure Energy from Coal, Oil Shale & Oil Sands.* University of Utah: Quarterly Progress Reports.

Snape, C. (1995). *Composition, geochemistry, and conversion of oil shales.* Kluwer Academic Publishers; Boston, MA.

Socrates, G. (2001). *Infrared and Raman Characteristic Group Frequencies.* John Wiley & Sons, Ltd.

Thompson, S. (2010). *Oil Shale and Tar Sands Programmatic EIS.* Retrieved March 15, 2009, from Bureau of Land Management: http://ostseis.anl.gov /index.cfm

Tissot, B. P., & Welte, D. H. (1984). *Petroleum Formation and Occurrence.* Springer-Verlag.

Tokimatsu, K., & Uchida, A. (1990). Correlation between liquefaction resistance and shear wave velocity. *Soils Foundation, 30,* 33-42.

Vandenbroucke, M. (2003). Kerogen: from Types to Models of Chemical Structure. *Oil & Gas Science and Technology, 58,* 243-270.

Vandenbroucke, M., & Largeau, C. (2007). Kerogen origin, evolution and structure. *Organic Geochemistry, 38,* 719-833.

Waples, D. W., & Waples, J. S. (2004). A Review and Evaluation of Specific Heat Capacities of Rocks, Minerals, and Subsurface Fluids. *Natural Resources Research*, 13, 97-122.

Wei, Y., Wang, X., & Zhao, M. (2004). Size effect mearsurement and characterization in nanoindentation test. *Journal of Materials Research*, 19, 208-217.

Xiangxin, H. (2008). Change of Pore Structure of Oil Shale Particles during Combustion. 2. Pore Structure of Oil-Shale Ash. *Energy & Fuels*, 22, 972-975.

Yen, T. F., & Chilingarian, G. V. (1976). *Oil Shale: Development in Petroleum Science*. New York: Elsevier Scientific Publishing Company.

Yen, T. (1975). *New Structural Model of Oil Shale Kerogen*. Los Angeles, CA: University of Southern California; Departments of Medicine.

Zeszotarski, J. C., Chromik, R. R., Vinci, R. P., Messmer, M. C., Michels, R., & Larsen, J. W. (2004). Imaging and mechanical property measurements of kerogen via nanoindentation. *Geochimica et Cosmochimica Acta*, 68, 4113 - 4119.

Zhang, T. Y., & Xu, W. H. (2002). Surface effects on nanoindentation. *Journal of Materials Research*, 17, 1715-1720.

Zhou, Y.-G., Chen, Y.-M., & Ke, H. (2005). Correlation of liquefaction resistance with shear wave velocity based on laboratory study using bender element. *Science*, 97, 805-812.

Zhu, W., Hughes, J. J., Bicanic, N., & Pearce, C. J. (2007). Nanoindentation mapping of mechanical properties of cement paste and natural rocks. *Materials Characterization*, 58, 1189-1198.

APPENDIX A. BAND ASSIGNMENTS FOR KEROGEN AND MINERALS OF DARK AND LIGHT COLORED GREEN RIVER OIL SHALE

Intensity	Wavenumber, cm⁻¹ Dark	Light	Kerogen Band Assignments	Mineral Band Assignments
m	3649 and 3613			O-H stretch of structural hydroxyl from MMT (Katti, 2006b)
m-s	3613	3600		Al-O-H stretch from Colorado shale (Beutelspacher, 1976)
m-w	3450		C=O stretch overtone; free NH asymmetric stretch; primary amides (Socrates, 2001)	H-OH hydrogen bonded water from MMT (Katti, 2006b)
m	3360 - 3022	3294	OH stretch intermolecular bonding; NH₂ asymmetric and symmetric stretch (Socrates, 2001)	H-OH hydrogen bonded water due to MMT and Dawsonite (Farmer, 1974)
m	3062 and 3022	3050	Aromatic C-H stretch (Socrates, 2001) (Premovic, 2000) (Radlinski, 2004)	
m	2956	2945	Aliphatic asymmetric CH₃ stretch (Beskoski, 2008)	
m	2926	2922	Aliphatic asymmetric CH₂ stretch (Durand, 1985) (Mongenot, 1999)	
m	2896	2890	Aliphatic symmetric CH₃ stretch (Razvigorova, 2008) (Snape, 1995)	

m	2851	2813	Aliphatic symmetric CH_2 stretch (Vandenbroucke 2007)	
w	2624	2626	N-H and S-H stretching (Socrates, 2001)	OH stretch from Nahcolite (Beutelspacher, 1976)
m	2514	2526	OH stretch due to HCO_3 (Balmain, 1999)	OH stretch due to $CaCO_3$ (Balmain, 1999)
w	2362 and 2333	2361 and 2334	C-O stretch from CO_2 (Socrates, 2001)	
m	1818 and 1808	1795		C-O stretch characteristic of aragonite (Balmain, 1999)
m	1747		Unsaturated ester (C=O) Doublet so two esters close together (Socrates, 2001)	
m	1699		Carbonyl C=O stretch of aliphatic carboxylic acids (ketone) (Socrates, 2001) (Cummins, 1929)	
m	1671		Aromatic C=C, Quinone (Socrates, 2001) (Petersen, 2008)	C=O stretch due to Nahcolite (Farmer, 1974)
m / s	1644	1637	Carbonyl C=O stretch highly conjugated(Socrates, 2001) (Petersen, 2008)	OH deformation from MMT (Katti, 2006b); Analcite; quartz

m	1606		Naphthalene; aromatic C=C stretch; Phenanthene (Socrates, 2001) (Petersen, 2008) (Holmes, 2001)	C=O stretch due to Dolomite and Nahcolite (Farmer, 1974)
	1550		Phenanthene; C=C stretch (Petersen, 2008) (Socrates, 2001)	CO_3^{-2} from Dawsonite (Farmer, 1974)
m-s	1538		Primary amines of NH_3 deformation; phenolic hydroxyl (OH) (Petersen, 2008)(Socrates, 2001)	
m-s	1505		Naphthalene; aromatic C=C stretch; phenanthene; C=C in-plane thiophene (Socrates, 2001)	
m-s	1454	1454	CH_3 asymmetric deformation overlapped by CH_2 scissor vibration (Razvigorova, 2008) (Vandenbroucke, 2003)	C-O and C=O stretch from Nahcolite (Farmer, 1974).
m-s	1436		CCO stretch; CH_2 and C-O scissoring; OH bending; aliphatic CH_3 (Socrates, 2001)	CO_3^{-2} from dolomite and calcite (Farmer, 1974)
m-s	1395		CH_2 symmetric deformation; NH_4 naphthalene; CH_3 aliphatic deformation (Robinson, 1969b)	hydrated FeOH from Pyrite; C-O and C=O stretch from Nahcolite (Farmer, 1974)

m-s	1368		CH$_2$ symmetric deformation; NH$_4$ naphthalene; CH$_3$ aliphatic deformation (Robinson, 1912)	
m-s	1350		CH$_3$ aliphatic deformation (Socrates, 2001)	
m-s	1325		CCO stretch (Socrates, 2001)	
m-s	1302		CH$_2$ wagging vibration (Socrates, 2001)	OHO in-plane bend from Nahcolite (Farmer, 1974)
s	1270		Phenolic OH (Holmes, 2001)	
s	1245		Asymmetric C-O-C stretch; methyl esters of long chain aliphatic acids (Socrates, 2001)	
s	1230	1210		Si-O orientation dependent band from MMT (Katti, 2006b)
s	1184	1180	Aliphatic ether (OCH$_3$) rocking vibration (Socrates, 2001)	Quartz, pyrite (Beutelspacher, 1976)
s	1154	1150	C-O stretch; aliphatic ether (Socrates, 2001) (Petersen, 2008)	Si-O inplane stretch from MMT (Katti, 2006b), Quartz; pyrite

s	1115		Aromatic C-H deformation; COC asymmetric stretch; single chain alkane (Socrates, 2001)	Si-O inplane stretch from MMT (Katti, 2006b); analcite; feldspar
s	1092 - 1063		CCO symmetric stretch; single chain alkane	Si-O out of phlane stretch from MMT (Katti, 2006b), Quartz; pyrite; CO_3^{-2} from dawsonite and calcite; feldspar; C-O and C=O stretch from Nahcolite (Farmer, 1974)
s	1034		CCO stretch; long paraffin chains (Razvigorova, 2008)	Si-O in plane stretch from MMT (Katti, 2006b); analcite; C-O and C=O stretch from Nahcolite (Farmer, 1974)
s	1000		CCO stretch; C=C stretch (Socrates, 2001)	Si-O inplane stretch from MMT (Katti, 2006b); pyrite; OHO stretch out-of-plane from Nahcolite (Farmer, 1974); feldspar
s	973 - 942	974	Aliphatic C-C stretch; COOH out-of-plane deformation. (Socrates, 2001)	
m-s	919		Symmetric COC stretch; C=O broad-out-of plane bending (Socrates, 2001)	Al-O/Al-OH stretch from MMT (Katti, 2006b)

145

m-s	868	878	CCO stretch; out-of-plane deformation vibration of aromatic CH groups with 3-4 rings (Socrates, 2001) (Radlinski, 2004)	Al-FeOH deformation from MMT (Katti, 2006b); CO_3^{-2} from dawsonite dolomite, calcite; quartz (Farmer, 1974)
m-s	837 - 800		out-of-plane deformation vibration of aromatic CH groups with two or more adjacent hydrogen atoms (Socrates, 2001) (Razvigorova, 2008)	CO_3^{-2} dawsonite; CO_3 out-of-plane from Nahcolite; Quartz (Farmer, 1974)
m	785		CH out-of-plane deformation from three adjacent hydrogen atoms on a ring (Socrates, 2001)	Si-O stretch of quartz and silica from MMT (Katti, 2006b), Quartz; pyrite; analcite; feldspar (Farmer, 1974)
m	756		out-of-plane deformation vibration of 3-4 ring aromatic CH groups with two or more adjacent hydrogen atoms (Socrates, 2001)	analcite; fledspar (Beutelspacher, 1976)
m-w	725		Skeletal vibration of straight chains with more than four CH_2 groups (Razvigorova, 2008) (Robinson, 1912)	Si-O deformation perpendicular to optical axis from MMT (Katti, 2006b), bending CO_3^{-2} From dolomite, calcite and dawsonite (Farmer, 1974); feldspar

146

m-w	694			Si-O deformation parallel to optical axis (Katti, 2006b); pyrite; quartz (Farmer, 1974); calcite; C=O, OCO, CO, OH stretch due to Nahcolite (Farmer, 1974)
m-w	670		Aromatic CH (Durand, 1985) (Vandenbroucke, 2007)	pyrite; dolomite; feldspar (Farmer, 1974)
w	637 and 615			coupled Al-O, Si-O out of plane vibration from MMT (Katti, 2006b); pyrite; analcite (Beutelspacher, 1976)
w	583			Al-O Si deformation from MMT (Katti, 2006b); feldspar
w	548			Feldspar (Beutelspacher, 1976)
w	509		Alkanes with 3 or more branches (Socrates, 2001)	Quartz;pyrite (Beutelspacher, 1976)
w	484		Out-of-plane naphthalene ring vibration (Socrates, 2001)	Si-O (Beutelspacher, 1976)
w	462		C-C straight chain alkanes (Socrates, 2001)	quartz, Si-O-Fe vibration from MMT (Katti, 2006b); pyrite; analcite; feldspar (Beutelspacher, 1976)

w = weak, m = medium, s = strong

APPENDIX B. PREPARATION OF SAMPLES

- It is important that the samples remain in closed containers kept in a moderate environment.
- At no time should the samples be touched with bare hands. Use plastic gloves!
- When using the tile cutter it is important to wear safety goggles, a mask, and gloves. It is also important to have other people around in case an accident would occur!

B.1. FTIR Sample Preparation

1. The two inch diameter core was cut with a tile cutter into cylinders of about 1 inch tall.

2. The now 1 inch thick piece is cut once again with the tile cutter in half

3. These two sections can now be cut into desired samples parallel and perpendicular to the bedding plane with the diamond cutter at a speed of 2 Hp. One half will remain in a labeled container while the other is cut in half again so you have two smaller pieces to work with.

4. Now using the diamond-wafering blade you can start cutting out your samples. I would usually cut the parallel to the bedding plane samples into 5 x 5 x 3 mm and 6 x 4 x 3 mm pieces for perpendicular to the bedding plane samples. This way you will still be able to know the sample orientation if there was ever confusion. Start by cutting the thickness of your pieces, so about 3 mm thick.

This picture shows the diamond saw cutting samples that will be used for experiment perpendicular to the bedding plane.

These samples were cut along the layers of the oil shale so will be used for experiments parallel to the bedding plane.

5. Once you have pieces that are your desired thickness (3 mm) you can start cutting out the height of your samples; 5 mm thick for parallel samples and 4 mm for perpendicular samples.

Parallel to the bedding plane

3 mm

5 mm

5 mm

Perpendicular to the bedding plane

4 mm

3 mm

6 mm
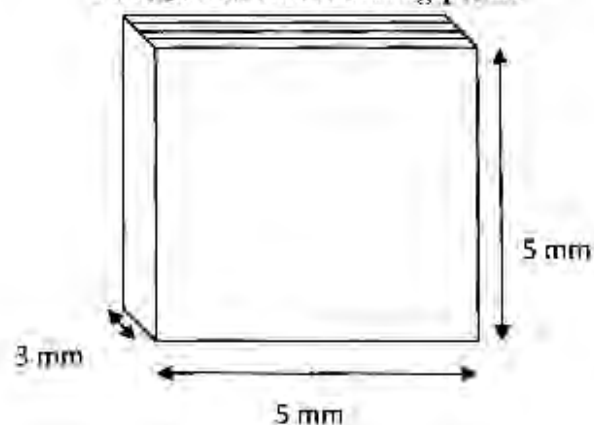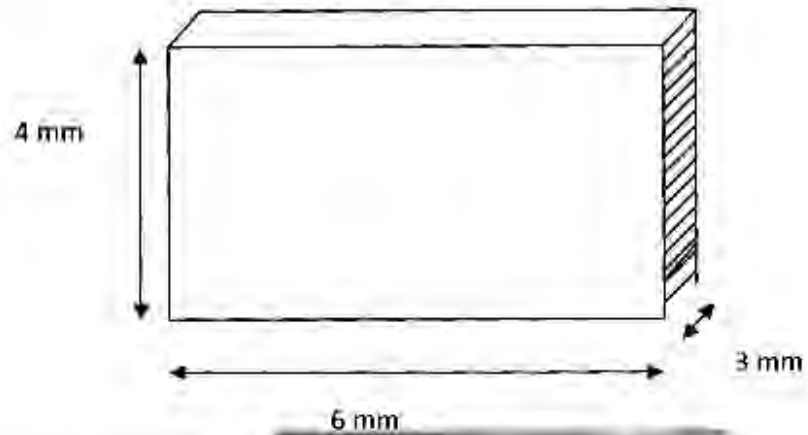
6. It is now easy to cut as many samples as you are able to from the length you have. For parallel samples cut them into 5 mm long pieces and perpendicular samples will be 6 mm long.
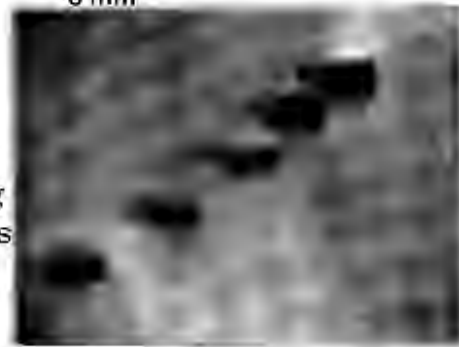
7. Place all your samples in a marked location either together or separately.

8. The sample should easily fit into the FTIR photoacoustic sample chamber

B.2. SEM Sample Preparation

Light and dark colored oil shale samples are prepared for SEM analysis from several locations in the seven feet of core with known orientation parallel and perpendicular to the bedding.

1. Broken oil shale samples used for SEM imaging were 3 mm thick with sampling area of 6 x 6 mm. Samples were broken off of the oil shale core with a hammer or were knocked against a hard surface.

2. At the Electron Microscopy lab, samples are mounted and then coated with a conductive gold coating (about 20 nm thick) to provide an electrical ground from the sample to the plug.
3. Cross-sectional polished samples were cut with a diamond-wafering blade into 1 x 10 x 11 mm using the exact same procedures as shown in the B.1. FTIR sample preparation. The 1 mm side was the surface that was cross-sectional polished for SEM examination.

B.3. Nanoindentation/Modulus Mapping Sample Preparation

1. Light and dark colored oil shale samples were prepared into 4 x 6 x 3 mm cubes perpendicular to the bedding plane and 5 x 5 x 3 mm cubes parallel to the bedding plane using the same procedures as shown in B.1. FTIR sample preparation.

2. The samples are then mounted onto 10 mm stainless steel discs using superglue.
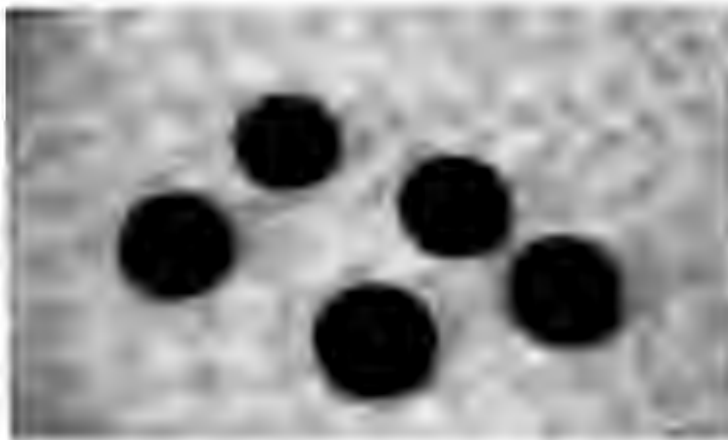
3. For nanoindentation tests, a very smooth level surface is required so samples were polished with 1000 and 4000 Microcut silicon carbide grinding paper. It is best to use the Model 900 grinder/polisher at a low speed. The surface of the sample is placed onto the grinding paper (upside down) and your finger is gently placed on the steel disc to hold it in place. It is most important to have a level surface! The grinder allows for a very smooth and, if done properly, level sample surface. I would polish for 1 hour first using the 1000 grid paper and then for another 1 hour using the 4000 grid paper.

4. Since the objective of polishing is to get a very smooth surface, we then polish with a diamond compound paste. These pastes work as a gradual grinding-away of the sample surface using decreasing grit size. We have available to us a diamond compound set containing 6, 3, 1, 0.5, 0.25, and 0.1 μm diamond polish. I would start polishing with the 3 μm for half an hour, then work my way down using the 1 μm, 0.5μm and 0.1 μm. A flat surface is needed so a mirror or glass can be used. A small dot of paste is placed on the flat surface and the sample surface is moved back and forth, and up and down across the paste. After each paste size, it is very important to have a clean sample and polishing surface by rinsing with de-ionized water. It is important to remove the previous paste used because the grit can damage up to three times its size so any remains will defeat any further polishing.

5. A finishing polish is then performed with 0.02 μm non-crystallizing colloidal silica polishing suspension. The polish is poured onto a black circle pad and the sample surface is rubbed in the same manner as used previously. Afterwards, samples were rinsed with de-ionized water and left to air dry in a sealed container. These black pads can be used to dry sample surfaces any time after washing with de-ionized water.

B.4. AFM Sample Preparation

1. Cutting samples is the same procedure described in FTIR sample preparation
2. Polishing samples is the same procedure as described in Nanoindentation / Modulus mapping sample preparation. The only difference is that you can polish the surface to the desired smoothness since a very flat, level surface is not required.

B.5. TEM Sample Preparation

Oil shale samples are taken from different locations in the oil shale core.

1. Dark and light colored oil shale sections were cut into 1 mm thick large slices parallel and perpendicular to the bedding plane using the diamond-wafering blade.

2. These samples are then brought to the Microscopy lab where they can be cut into 3 mm diameter circles which is the size and shape required for mounting into the ion mill.
3. The samples are then grinded following the correct procedure to a thickness of 40 – 60 μm thick. The correct grinding procedures are important since the grit causes depth damage up to three times the size of the grit. Water is used during this process to reduce heat.
4. After this the samples will be dimple grinded to a thickness of 20 – 25 μm thick and polished with diamond paste to a thickness of 5 μm.
5. They can then be inserted into the ion mill where they will remain till the oil shale sample is 400 – 1000 Å thick.

# APPENDIX C. NANOINDENTATION PROCEDURE

1. Turn on the power strips located back of the computers
2. Turn on the computers (middle-no password, left-rose)
3. Turn on the control unit
4. Make sure the Blue Box is turned to QSM for indentation

   ### If the transducer system was on the AFM stage
   a. Make the tip up sufficiently by pushing the switch to **up** position
   b. Bring the transducer assembly system down from the AFM stage and place it on the black indentation stage
   c. Detach the AFM head (make sure to apply enough pressure on both sides of the head when removing the springs)
   d. Carefully remove the AFM feedback cable (black) by lifting the two flips with fingers
   e. Connect two feedback cables together
   f. Connect that to the transducer assembly base

5. After making sure that there is going to be enough space between the sample and the tip, place the sample on the magnetic stage.
6. Place the indentation head. Attach the springs
7. Lower the tip until you are confident that tip is not touching the sample
8. Turn on the light and bring the microscope closer to the system
9. Turn the Display gain to 1
10. Load on the panel should be very close to -201
11. Lower the tip by looking through the microscope. If the sample is smooth you can see the reflection of the tip on the sample. Tip should not touch this reflection. If the sample is not smooth lower the tip one short stroke at a time until the number on the panel appears slightly positive compared to -201 (ex. -199). This means the tip has touched the surface to move the tip up 2-3 taps.
12. Open the Triboscope software
13. Turn the Displacement gain to 100
14. Make the front panel to zero by doing auto and fine tuning

   ### To do the air calibration
   a. In the Triboscope menu go to **set up** and then **indent**
   b. A new window will be opened
   c. Go to **file** and open **load function**. Select **air-calibration** and load this option.
   d. In the menu go to **set up** and then **advance Z axis calibration** and then click on the **Calibrate transducer**

e. Compare the values in the dialog box with the values in the paper (on the computer).
f. Make the displacement in the properties screen, Displacement and Gain to 100.
g. If the values match click on **Done** and close calibrate transducer window.

15. Open the load function that you choose (clicking on the icon)
16. Make any changes you wish to make (eg. Peak Force from 500 um to 5000 um)

To engage the Tip

17. Open the **Nanoscope software** in the other computer
18. Click on the microscope icon
19. In the menu go to **Microscope** and then **Profile** and then choose **Hysitron** to **Load** the parameters
20. In the menu go to **Microscope Offset**
21. In the dialog box the head offest should be 10 times the value in the front panel
    a. Make sure the microscope feedback is at 1000
22. In the feedback control make
    a. Current Set Point 5.00 nA
    b. Integral Gain 1.5
    c. Proportional Gain 2.5
23. In the Scan
    a. Make the Scan Size 0
24. Before engaging tip, re-zero the front display panel
25. Engage the tip by clicking on the tip engage icon
26. After tip has engaged change
    a. Current Set Point to 1.5 nA
    b. Scan Size to desired size (5 um maximum)
27. Select the area to be indented

To do the indentation
    a. Change scan size to 0.00
    b. Change Integral Gain to 0
    c. Change Proportional Gain to 0
28. On the Triboscope software window (on the other computer) click on **Make Indent**
29. Immediately after the indentation change
    a. Change Proportional Gain to 2.5
    b. Change Integral Gain to 1.5
    c. Change scan location and the size to desired values

157

30. If the displacement gain of the indent (on the graph) is less than 500, change the output 1 gain displacement to 1000
    a. Also have to change this value on the computer under the transducer constants
    b. If the displacement gain is greater than 500, leave the output 1 gain displacement at 100
31. To get the elastic modulus and hardness from the graph
    a. Change the unloading segment to 3
    b. Specify your upper and lower fit percentages
    c. Click **Execute Fit**
32. Save the data

33. **If tip gets retracted**
    a. Withdraw the tip twice
    b. Make the front panel zero
    c. Engage the tip as done before without changing the x and y offset
    d. Change the scan location
34. Continue from step 21

To export data to Excel
    a. Save data in raw data file (C drive)
    b. Open **Triboscope**
        i. Click yes when it asks you if the tip is far enough away from the sample
        ii. There is no need to zero the front panel
    c. Go to file and click open
        i. Open the raw data you saved from before
    d. Click **Execute Fit**
    e. Now open a new **Excel** file
    f. On the new Excel file, click paste
        i. The raw data will show up in a row
        ii. For some bazaar reason, you do not need to copy the data, when you click paste it transfers to excel automatically

APPENDIX D. MODULUS MAPPING PROCEDURE

1. Turn on the power strips located back of the computers
2. Turn on the computers (middle-no password, left-rose)
3. Turn on the control unit
4. Make sure the Blue Box is turned to QSM for indentation

   ### If the transducer system was on the AFM stage
   a. Make the tip up sufficiently by pushing the switch to **up** position
   b. bring the transducer assembly system down from the AFM stage and place it on the black indentation stage
   c. Detach the AFM head (make sure to apply enough pressure on both sides of the head when removing the springs)
   d. Carefully remove the AFM feedback cable (black) by lifting the two flips with fingers
   e. Connect two feedback cables together
   f. Connect that to the transducer assembly base

5. After making sure that there is going to be enough space between the sample and the tip, place the sample on the magnetic stage.
6. Place the indentation head. Attach the springs
7. Lower the tip until you are confident that tip is not touching the sample
8. Turn on the light and bring the microscope closer to the system
9. Turn the Display gain to 1
10. Load on the panel should be very close to -201
11. Lower the tip by looking through the microscope. If the sample is smooth you can see the reflection of the tip on the sample. Tip should not touch this reflection. If the sample is not smooth lower the tip one short stroke at a time until the number on the panel appears slightly positive compared to -201 (ex. -199). This means the tip has touched the surface to move the tip up 2-3 taps.

Load of 260 μN

On the Computer
12. Choose DSI 3.0
13. Turn the Displacement gain and Feedback gain to 100
14. Make the front panel to zero by doing auto and fine tuning
15. Calibration -> ESF -> blue box to QSM
16. Transducer constant displacement gain, Output 1 and 2 Gain = 100 -> OK
17. Click air Indent. Should look like graph on the right

Displacement of 1800 nm
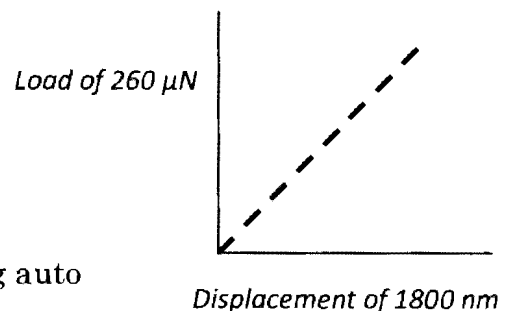
18. Click calibrate and compare Transducer constants to Calibration results
19. Close window and change blue box to DSM, Displacement Gain 1 = 100, Feedback Gain 2 = 1000
20. Calibration -> dynamics -> Turn on amplifier -> wait for stabilization -> OK
21. Transducer constants displacement gain and output 1 = 1000
22. OK -> zero panel -> Test (takes about 15 – 20 minutes)
23. Save in MM_calibration_date
24. Bring 2 blue lines to both ends of the graph and click
    a. On Calibrate giving k, m, and C values (if blue line moves,
    b. Move it back to the left and right side of screen and
    c. Recalibrate
25. Click Export and close window
26. Setup -> Lock-in -> OK
27. Zero Panel

<u>Air calibrate</u>
28. 200 Hz frequency -> click Initialize and wait for phase to show
29. Change dynamic force to 0.5 -> click Set
30. AC displacement should read close to ~1.0

<u>To engage the Tip</u>
31. Open the **Nanoscope software** in the other computer
32. Click on the microscope icon
33. In the menu go to **Microscope** and then **Profile** and then choose **Hysitron** to **Load** the parameters
34. In the menu go to **Microscope Offset**
35. In the dialog box the head offest should be 10 times the value in the front panel
    a. Make sure the microscope feedback is at 1000
36. In the feedback control make
    a. Current Set Point 5.00 nA
    b. Integral Gain 1.5
    c. Proportional Gain 2.5
37. In the Scan
    a. Make the Scan Size 0
    b. Scan rate 0.3 Hz
38. Engage the tip by clicking on the tip engage icon
39. After tip has engaged change
    a. Current Set Point to 1.5 nA
    b. Scan Size to a maximum size of 20 μm to find a smooth area
40. Select a 2 μm area to be indented

160

<u>To perform mapping</u>
41. Change Channel Data
    a. Channel 1:
        i. Offline planefit: none
        ii. Data Type: Current
    b. Channel 2:
        i. Offline planefit: none
        ii. Data Type: Aux 2
    c. Channel 3:
        i. Offline planefit: none
        ii. Data Type: Aux 3
    d. Change scan size to 3.00 μm
    e. Change Setpoint to 3.0 nA
    f. Change Integral Gain to 0.3
    g. Change Proportional Gain to 0
42. Change Dynamic Force to $0.5 - 2$ nA on MM computer (this gives a total force of 4.0 μN) and click Set
43. In Nanoscope, make sure an image is captured and is on during modulus mapping.
44. Click Export when image capture is complete
45. Disengage tip

APPENDIX E. SEM AND EDS DATA

E.1. Light Colored Oil Shale Broken Parallel to the Bedding Plane
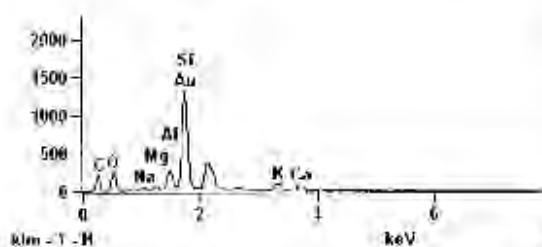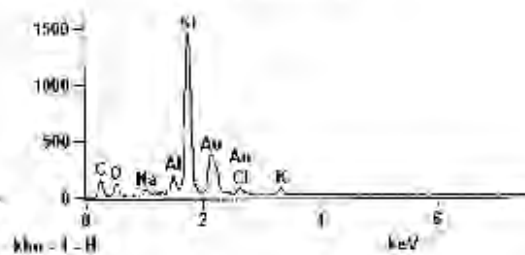
Point 1
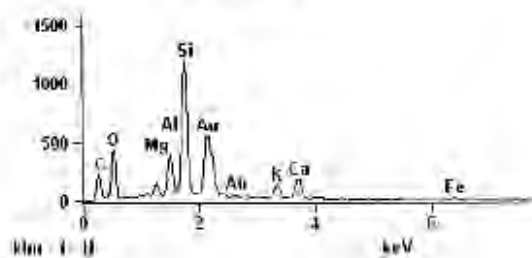
Point 2
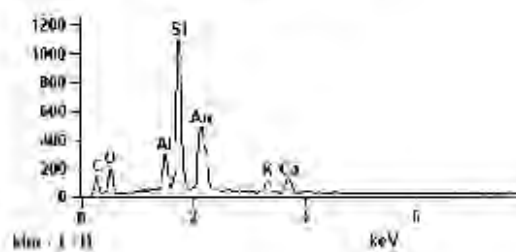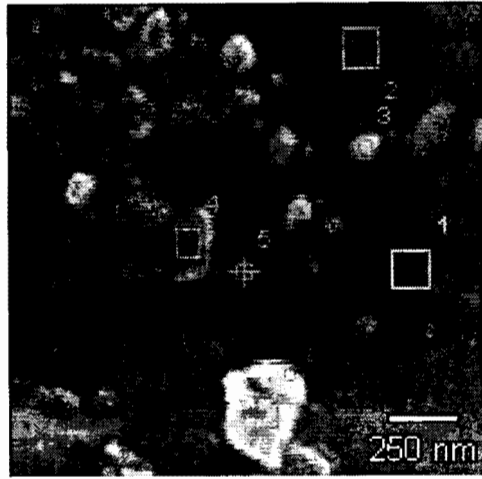
Point 3

Point 4

Point 1

Point 2
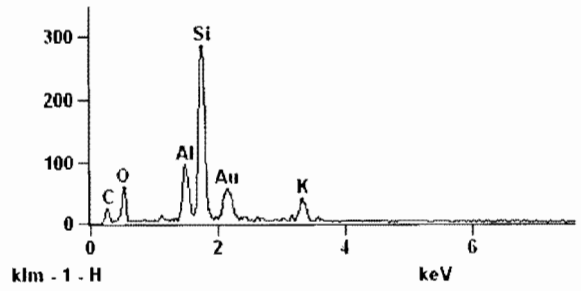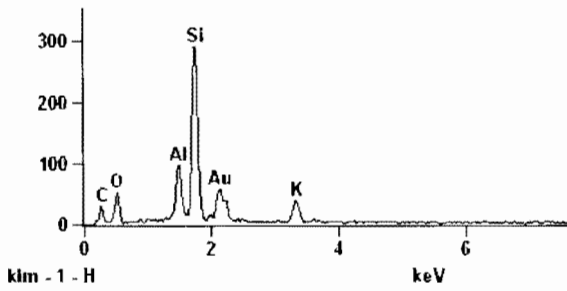
Point 3
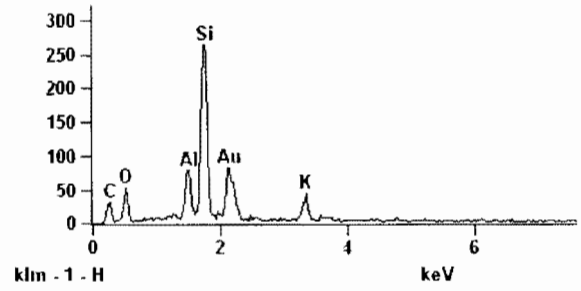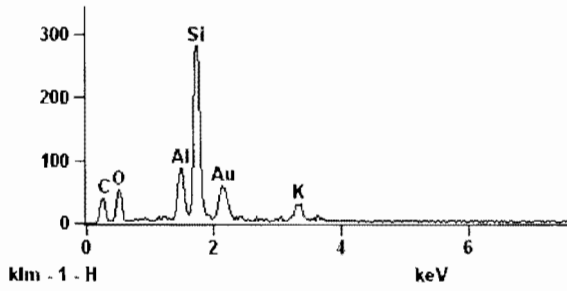
Point 4

Point 5

Point 6
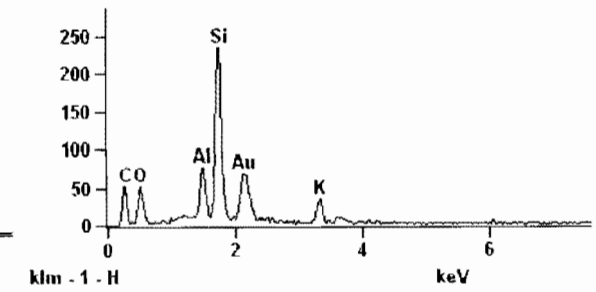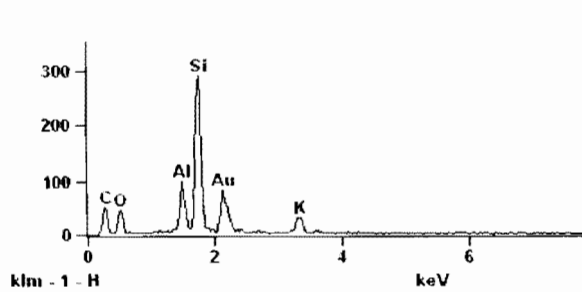
E.2. Dark Colored Oil Shale Broken Parallel to the Bedding Plane
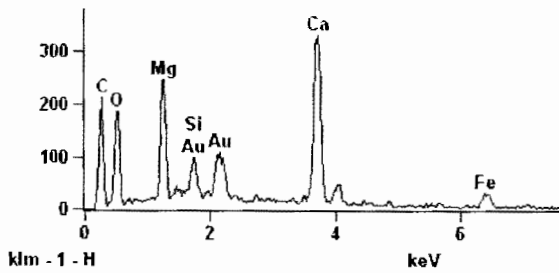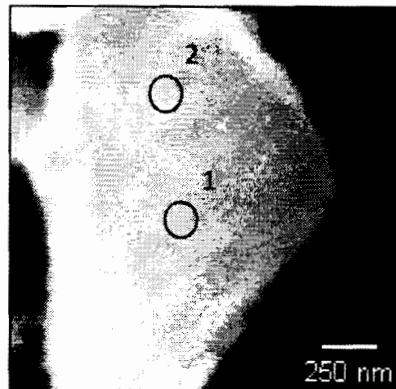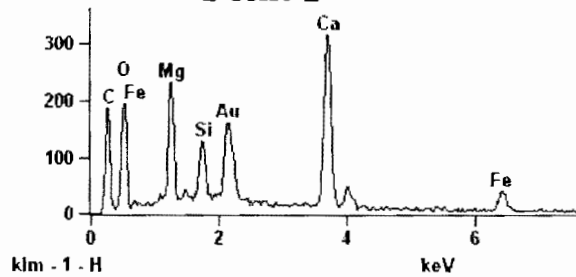
Point 1

Point 2

Point 1
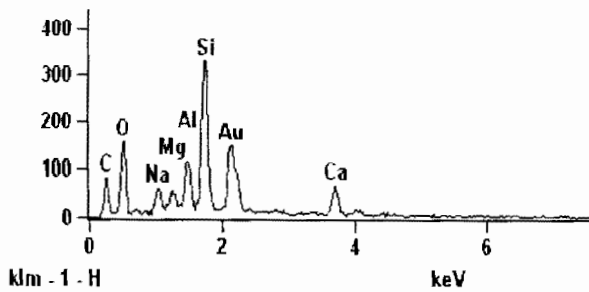
Point 2
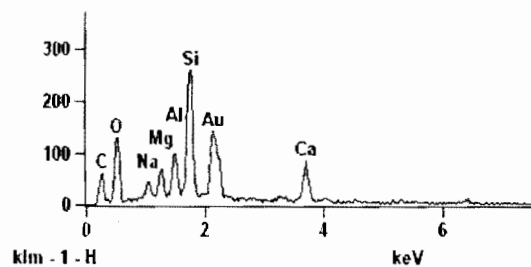
E.3. SEM Images and EDS Data of Dark Colored Oil Shale Broken Perpendicular to the Bedding Plane
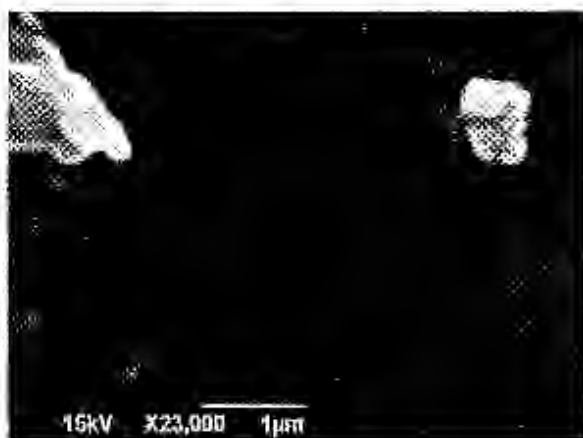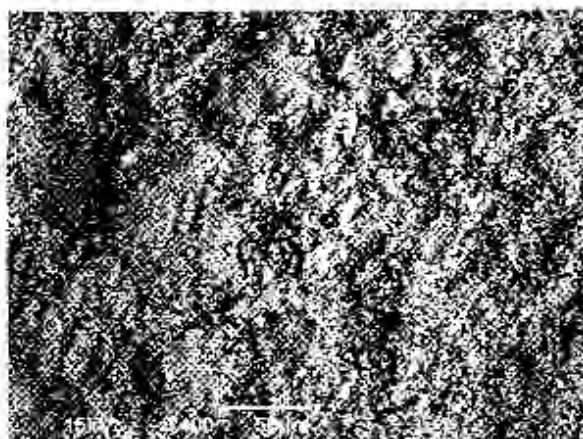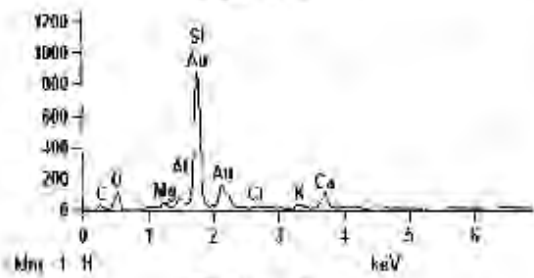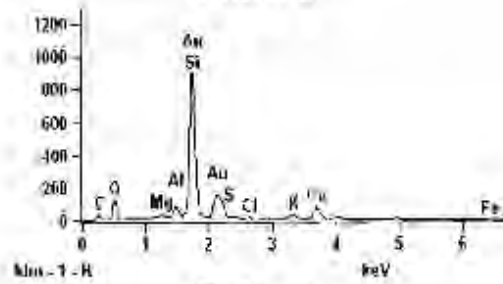
Point 1
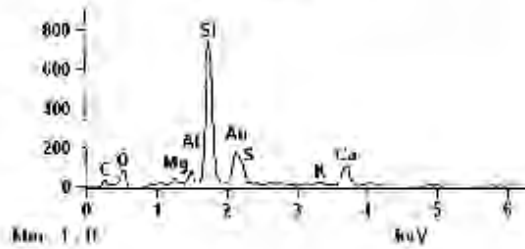
Point 2
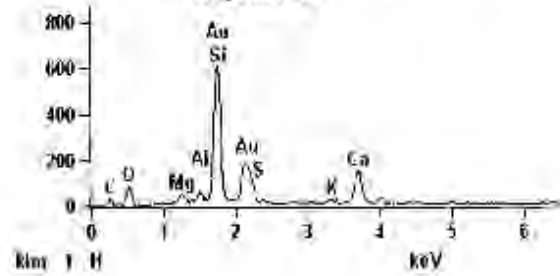
Point 3

Point 4

E.4. SEM Images and EDS Data of Light Colored Oil Shale Broken
Perpendicular to the Bedding Plane
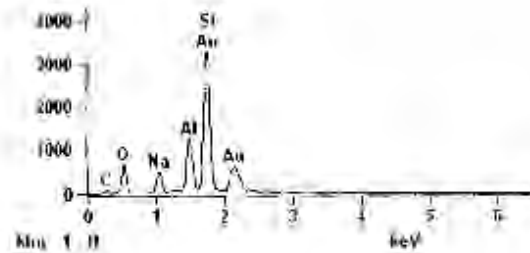
Point 1

Point 2

Point 3
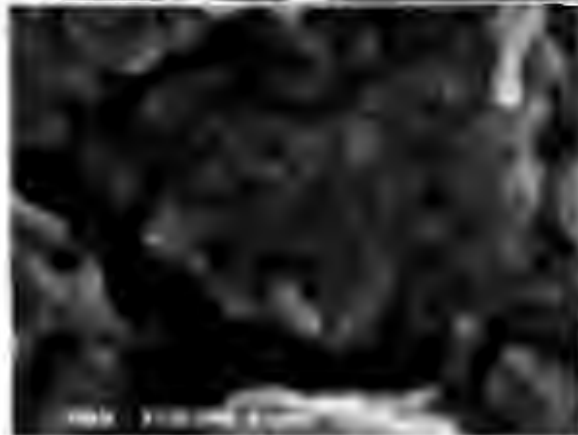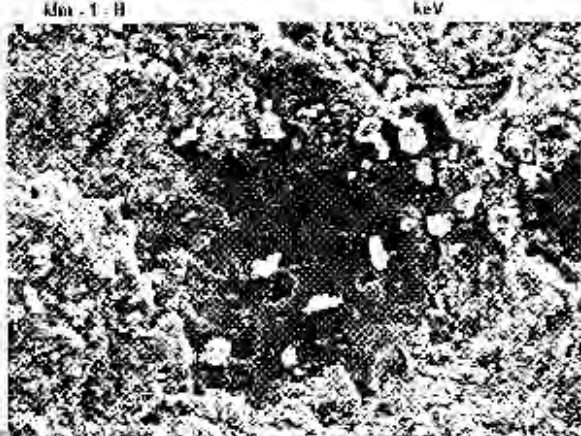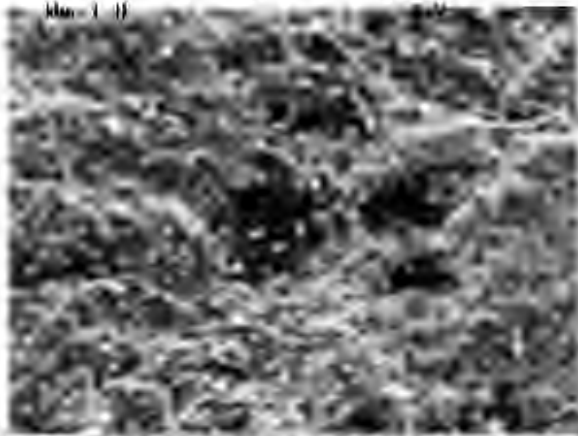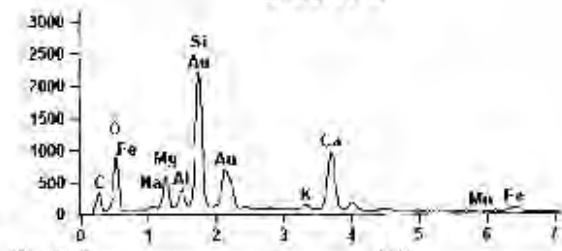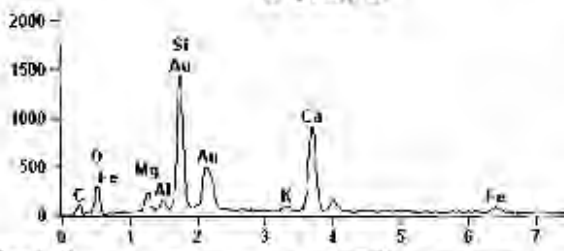
E.5. SEM Images and EDS Data of the Outside of the Oil Shale Core Perpendicular to the Bedding Plane

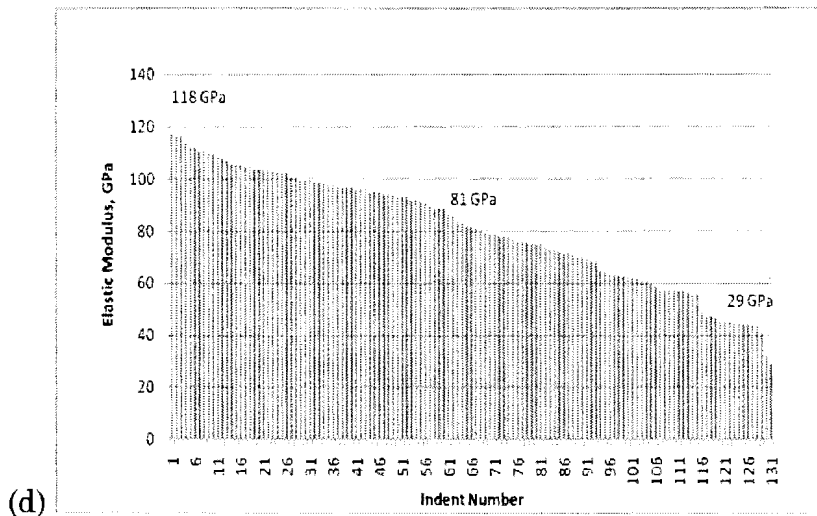**Box 1**
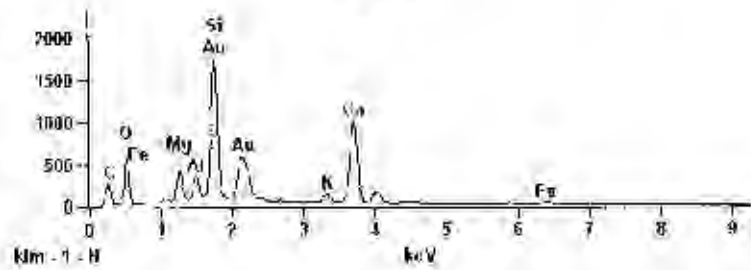
Box 2
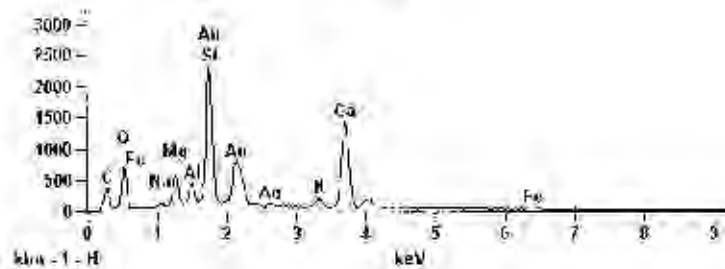
Box 3
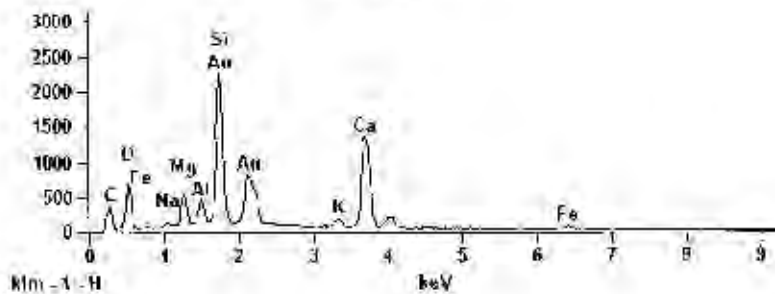
APPENDIX F. NANODINDENTATION DATA

F.1. Displacement-Controlled Nanoindentation Data of Oil Shale Indented at 150 nm. Indents were performed on (a) Light Parallel, (b) Light Perpendicular, (c) Dark Parallel and (d) Dark Perpendicular samples.
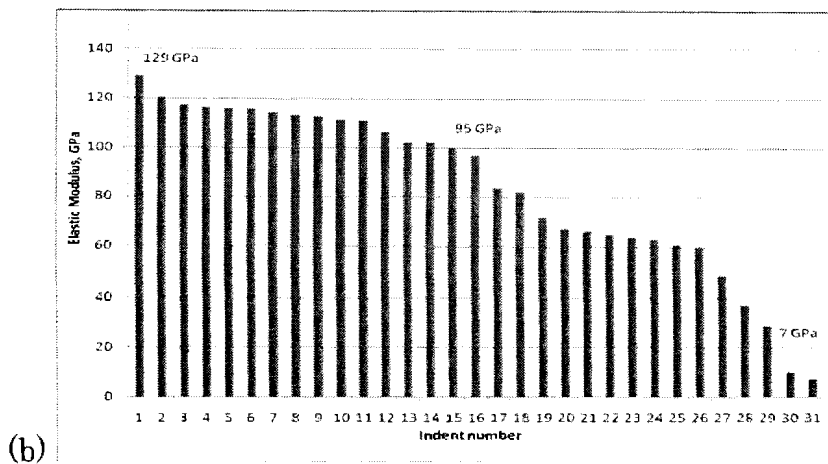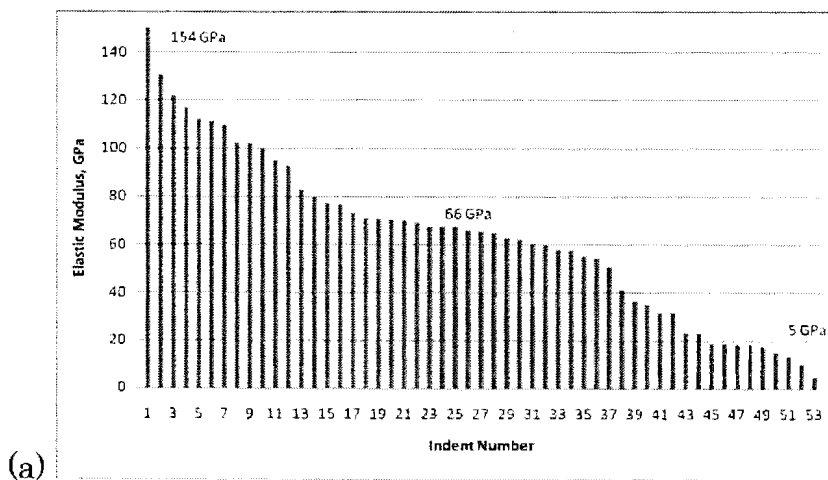

(a)

(b)

(c)

(d)
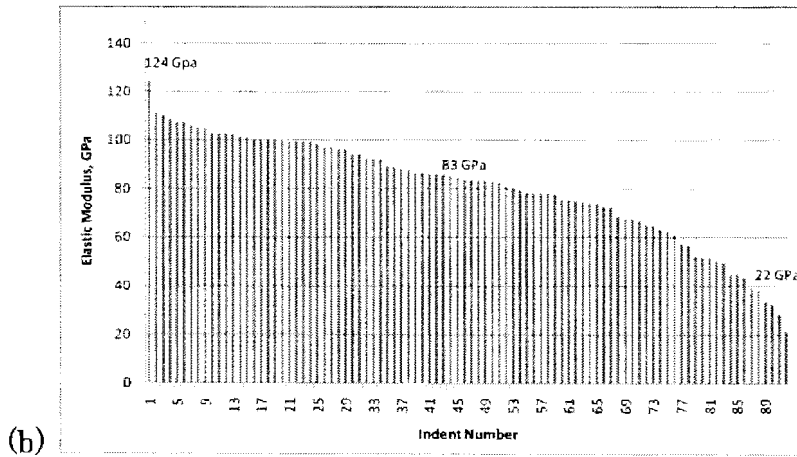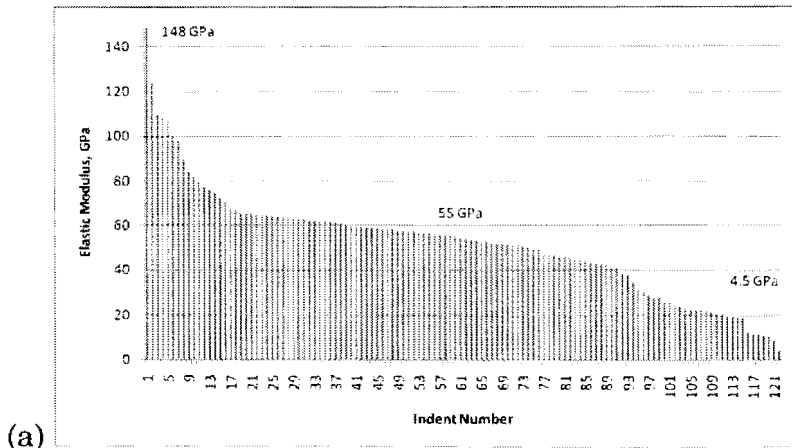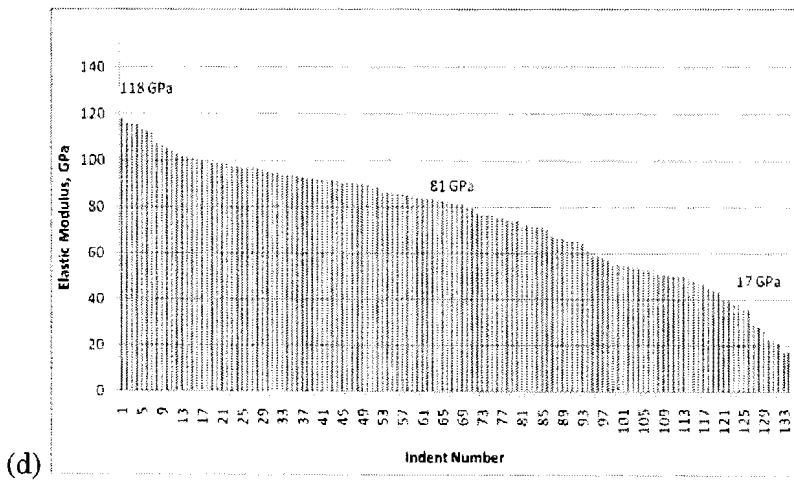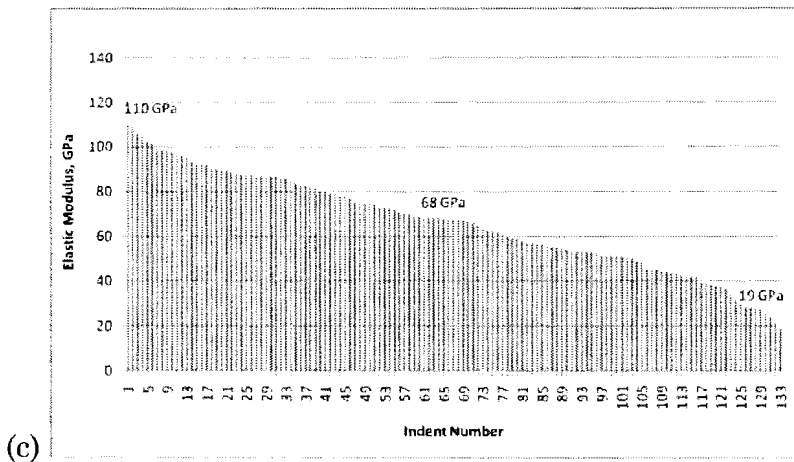
F.2. Displacement-Controlled Nanoindentation Data of Oil Shale Indented at 100 nm. Indents were performed on (a) Light Parallel, (b) Light Perpendicular, (c) Dark Parallel and (d) Dark Perpendicular samples.
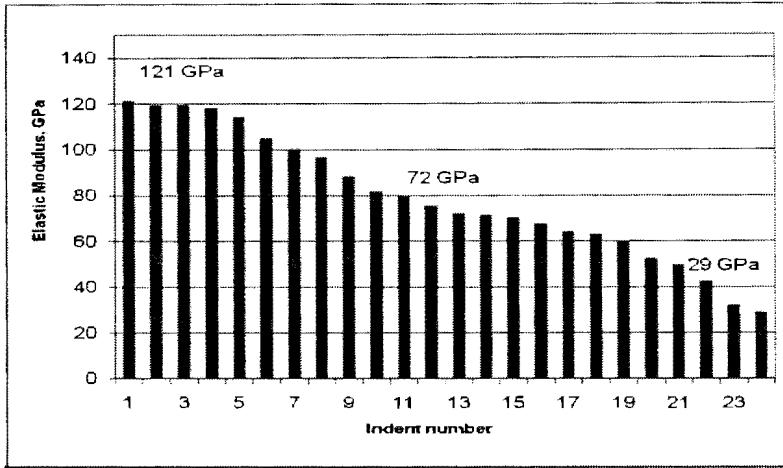

(a)

170
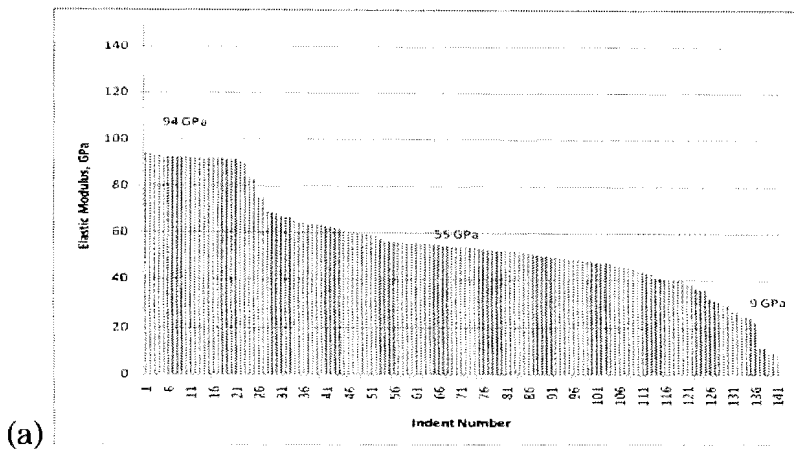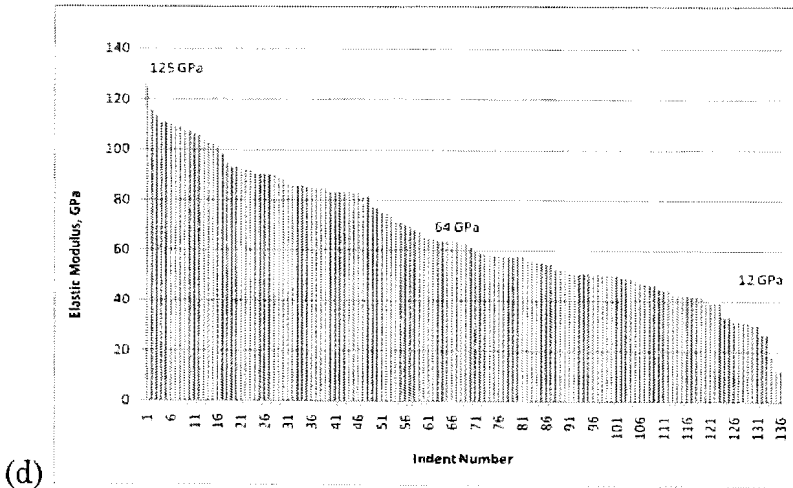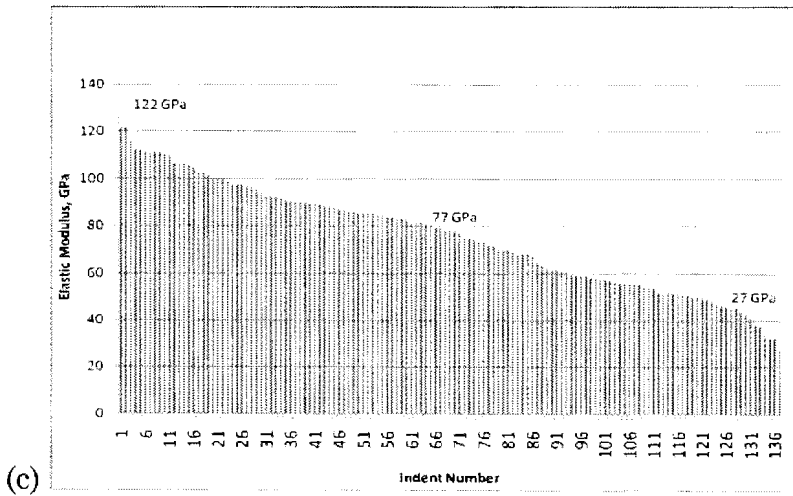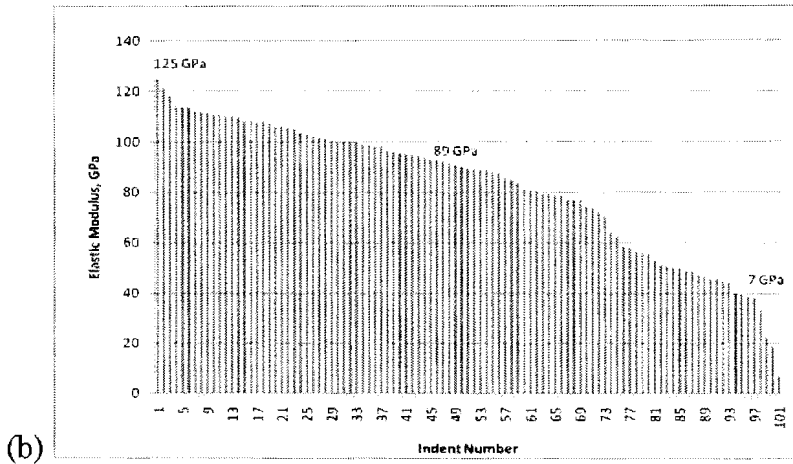
F.3. Displacement-Controlled Nanoindentation Data of Oil Shale Indented at 50 nm. Indents were performed on (a) Light Parallel, (b) Light Perpendicular, (c) Dark Parallel and (d) Dark Perpendicular samples.
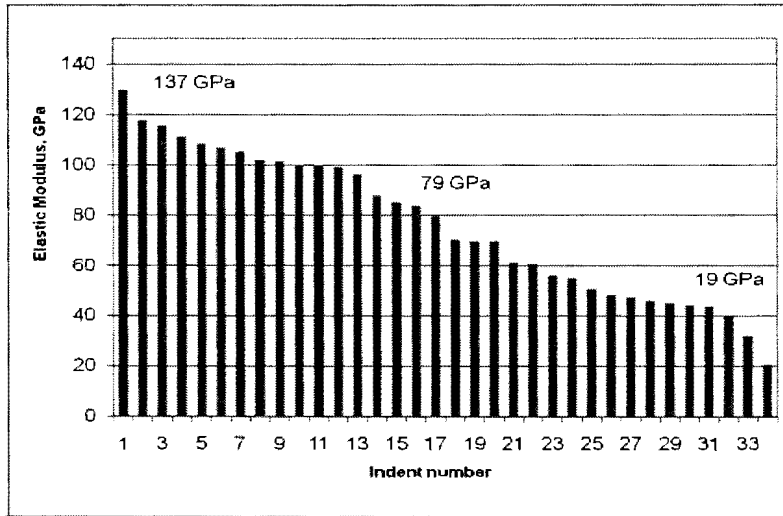
(a)

(b)

(c)

172

(d)
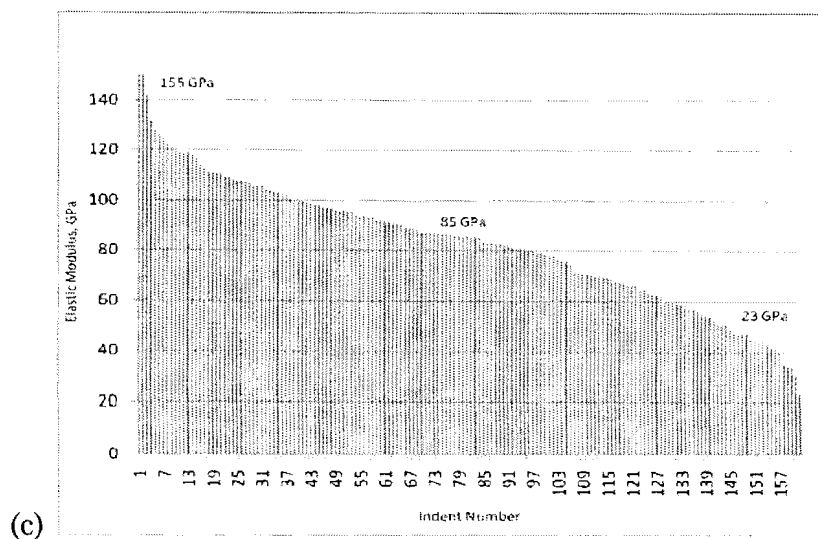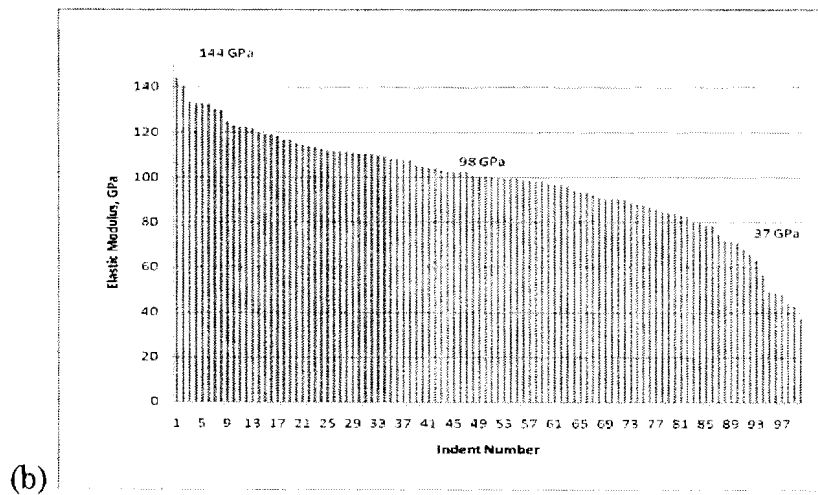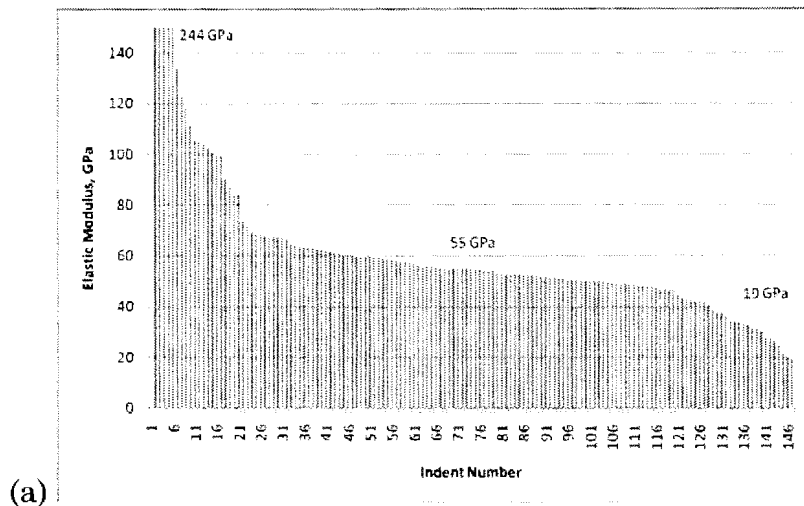
F.4. Load-Controlled Nanoindentation Data of Oil Shale. Indents were performed on (a) Light Parallel, (b) Light Perpendicular, (c) Dark Parallel and (d) Dark Perpendicular samples.

(a)

(b)

173

(c)

(d)

174